WDL-TR2949

6 JUNE 1966

# EXPERIMENTAL STUDY OF COATINGS FOR TEMPERATURE CONTROL OF SOLAR CELLS

BY DONALD C. BRIGGS



**SUBMITTED TO:**

**NATIONAL AERONAUTICS AND SPACE ADMINISTRATION**

**WESTERN OPERATIONS OFFICE**

**LOS ANGELES, CALIFORNIA**

**UNDER CONTRACT NO. NAS 7-409**



PHILCO WDL DIVISION

A Subsidiary of Ford Motor Company | 3875 Fabian Way, Palo Alto, California

WDL TECHNICAL REPORT 2949

# EXPERIMENTAL STUDY OF COATINGS FOR TEMPERATURE CONTROL OF SOLAR CELLS

6 June 1966



Submitted To The:

NATIONAL AERONAUTICS AND SPACE ADMINISTRATION
Western Operations Office
Los Angeles, California

Submitted by: Donald C. Briggs
Donald C. Briggs

Approved by: M. E. Lapides
M. E. Lapides, Mgr.,
Space Technology

Under Contract NAS 7-409

PHILCO CORPORATION
A Subsidiary of Ford Motor Company
WDL Division
Palo Alto, California

# PREFACE

This study was conducted for support of programs at the:

NATIONAL AERONAUTICS AND SPACE ADMINISTRATION
Systems Engineering Division
Ames Research Center
Moffett Field, California

The contract was awarded via the Western Operations Office and administered by Ames Research Center

TABLE OF CONTENTS


| Section | | Page |
|---|---|---|
| 1 | SUMMARY | 1 |
| 2 | INTRODUCTION | 2 |
| 3 | SYMBOLS | 4 |
| 4 | GENERAL BACKGROUND | 6 |
| | 4.1 Filter Characteristics | 6 |
| | 4.2 Reflective Coatings. | 7 |
| | 4.3 Solar Cell Equivalent Circuit | 8 |
| 5 | EXPERIMENTAL APPROACH | 9 |
| | 5.1 Filter Characteristic Measurements | 9 |
| | 5.1.1 Transmittance Measurements | 9 |
| | 5.1.2 Temperature Effects | 10 |
| | 5.1.3 Reflectivity Measurements | 10 |
| | 5.2 Coating Characteristic Measurements | 11 |
| | 5.3 Equilibrium Temperature Test | 12 |
| | 5.3.1 Test Procedure | 12 |
| | 5.3.2 Description of Test Apparatus | 13 |
| | 5.3.3 Description of Spacecraft Model | 16 |
| 6 | ANALYTICAL APPROACH | 18 |
| | 6.1 Interference Filters | 18 |
| | 6.1.1 Variation of the Filter Characteristics with Angle of Incidence. | 18 |
| | 6.1.1.1 Spectral Shift | 18 |
| | 6.1.1.2 Decrease in Transmittance | 19 |
| | 6.1.2 Variation of the Filter Characteristics with Temperature | 20 |
| | 6.2 Reflective Coatings | 21 |
| | 6.2.1 Reflective Coating Optimization Analysis | 23 |
| | 6.2.2 Coating and Filter Optimization Analysis | 24 |
| | 6.3 Equilibrium Temperature Investigation | 25 |
| | 6.3.1 Cell Temperature History | 25 |
| | 6.3.2 Cell Stack Temperature Gradiant | 26 |
| | 6.3.3 Solar Cell Performance Analysis | 27 |
| | 6.3.4 Optimization Analysis | 29 |
| | 6.3.4.1 Rotating Approximations | 29 |
| | 6.3.4.2 Solar and Solar Cell Spectral Characteristics | 31 |
| | 6.3.4.3 Temperature Effectiveness | 31 |
| | 6.3.4.4 Optical Properties | 31 |
| | 6.3.4.5 Degradation Effects | 32 |

TABLE OF CONTENTS (Continued)


| Section | | | Page |
|---|---|---|---|
| 7 | RESULTS AND DISCUSSIONS | | 33 |
| | 7.1 | Filter Characteristics Measurements | 33 |
| | | 7.1.1 Filter Representation | 33 |
| | | 7.1.2 Spectral Shift | 33 |
| | | 7.1.3 Decrease in Transmittance | 34 |
| | | 7.1.4 Variation of Filter Characteristics with Temperature | 35 |
| | 7.2 | Reflective Coatings | 36 |
| | | 7.2.1 Reflective Coating Area Fraction Prediction | 36 |
| | 7.3 | Results of Optimization Analysis | 37 |
| | 7.4 | Equilibrium Temperature Test | 38 |
| | | 7.4.1 Presentation of Results | 38 |
| | | 7.4.2 Discussion of Results | 39 |
| | | 7.4.2.1 Voltage Current Relationships | 39 |
| | | 7.4.2.2 Open Circuit Voltage | 40 |
| | | 7.4.2.3 Short Circuit Current | 40 |
| | | 7.4.2.4 Angle of Incidence | 42 |
| | | 7.4.2.5 Equilibrium Temperatures | 43 |
| | | 7.4.2.6 Reflective Coatings | 43 |
| | | 7.4.2.7 Approximate Peak Power | 43 |
| | 7.5 | Calibration Tests | 44 |
| | 7.6 | Environmental Test | 44 |
| 8 | CONCLUDING REMARKS | | 45 |
| 9 | REFERENCES | | 46 |
| TABLES | | | 47 |
| FIGURES | | | 53 |
| Appendices | | | |
| A | Blue-Red Reflecting Solar Cell Cover Spectral Specifications | | 82 |
| B | Rotating Solar Cell Transient Thermal Analysis | | 84 |
| C | Theoretical Performance Analysis | | 89 |
| D | Optimization Procedure | | 93 |
| E | Transient Time Response | | 94 |
| F | Equilibrium Temperature Analysis | | 96 |
| G | Solar Cell Cover Environmental Testing | | 100 |
| H | Spectrophotometric Measurements | | 101 |

# LIST OF ILLUSTRATIONS


| Figures | | Page |
|---|---|---|
| 1 | Perfect and Real Filter Characteristics (Silicon Solar Cells) | 53 |
| 2 | Simplified Equivalent Circuit for Solar Cell | 54 |
| 3 | 3' x 3' Vacuum Chamber and Magnetic Drive | 55 |
| 4 | Experimental Test Apparatus | 56 |
| 5 | Experimental Test Configuration | 57 |
| 6 | Instrumentation Block Diagram | 58 |
| 7 | Vacuum Chamber Controls and Instrumentation | 59 |
| 8 | OCLI Solar Simulator | 60 |
| 9 | Spectral Distribution of OCLI Solar Simulator (Model 31) Output Compared to Johnson's Curve | 61 |
| 10 | Spectral Distribution of Carbon Arc Compared with Johnson's Curve | 61 |
| 11 | Solar Cell Test Fixtures | 62 |
| 12 | Quasi-Steady-State Transient Temperature Variation | 63 |
| 13 | Spectral Response of Silicon Solar Cells | 64 |
| 14 | Calculated Spectral Shift vs Relative Wave Number | 65 |
| 15 | Franction of Light Reflected vs Angle of Incidence | 66 |
| 16 | Fraction of Light Passing Front Surface of Solar Cell Cover Glass | 67 |
| 17 | Reflective Coating Optimization(Power vs $\eta_a S$) | 68 |
| 18 | Fraction of Silicon Solar Cell Covered by Ideal Reflector as a Function of Average Solar Intensity for Maximum Average Power | 69 |
| 19 | Typical Recorder Trace(Equilibrium Temperature Test) | 70 |
| 20 | Rotating Results for Filter No. 1 | 71 |
| 21 | Rotating Results for Filter No. 2 | 72 |
| 22 | Rotating Results for Filter No. 3 | 73 |
| 23 | Rotating Results for Filter No. 4 | 74 |
| 24 | Rotating Results for Filter Nos. 5 and 6 | 75 |
| 25 | Rotating Results for Cover Glass with 20 Percent Area Covered with Coating | 76 |
| 26 | Rotating Results for Cover Glass with 40 Percent Area Covered with Coating | 77 |

## LIST OF ILLUSTRATIONS


| Figures | | Page |
|---|---|---|
| 1 | Perfect and Real Filter Characteristics (Silicon Solar Cells) | 53 |
| 2 | Simplified Equivalent Circuit for Solar Cell | 54 |
| 3 | 3' x 3' Vacuum Chamber and Magnetic Drive | 55 |
| 4 | Experimental Test Apparatus | 56 |
| 5 | Experimental Test Configuration | 57 |
| 6 | Instrumentation Block Diagram | 58 |
| 7 | Vacuum Chamber Controls and Instrumentation | 59 |
| 8 | OCLI Solar Simulator | 60 |
| 9 | Spectral Distribution of OCLI Solar Simulator (Model 31) Output Compared to Johnson's Curve | 61 |
| 10 | Spectral Distribution of Carbon Arc Compared with Johnson's Curve | 61 |
| 11 | Solar Cell Test Fixtures | 62 |
| 12 | Quasi-Steady-State Transient Temperature Variation | 63 |
| 13 | Spectral Response of Silicon Solar Cells | 64 |
| 14 | Calculated Spectral Shift vs Relative Wave Number | 65 |
| 15 | Franction of Light Reflected vs Angle of Incidence | 66 |
| 16 | Fraction of Light Passing Front Surface of Solar Cell Cover Glass | 67 |
| 17 | Reflective Coating Optimization(Power vs $\eta_a S$) | 68 |
| 18 | Fraction of Silicon Solar Cell Covered by Ideal Reflector as a Function of Average Solar Intensity for Maximum Average Power | 69 |
| 19 | Typical Recorder Trace(Equilibrium Temperature Test) | 70 |
| 20 | Rotating Results for Filter No. 1 | 71 |
| 21 | Rotating Results for Filter No. 2 | 72 |
| 22 | Rotating Results for Filter No. 3 | 73 |
| 23 | Rotating Results for Filter No. 4 | 74 |
| 24 | Rotating Results for Filter Nos. 5 and 6 | 75 |
| 25 | Rotating Results for Cover Glass with 20 Percent Area Covered with Coating | 76 |
| 26 | Rotating Results for Cover Glass with 40 Percent Area Covered with Coating | 77 |

LIST OF ILLUSTRATIONS (Continued)


| Figures | | Page |
|---|---|---|
| 27 | Current as a Function of Incident Angle for Various Loads | 78 |
| 28 | Open Circuit Voltage as a Function of Cell Temperature | 79 |
| 29 | Constant Temperature Short Circuit Current vs Intensity | 80 |
| 30 | I-V Curves Showing Effect of Series Resistance | 81 |
| F-1 | Quasi-Steady-State Equilibrium Temperatures as a Function of Solar Intensity for Various $\alpha/\epsilon$ Ratios | 99 |

# LIST OF TABLES


| Tables | | Page |
|---|---|---|
| 1 | Averaged Cut-On and Cut-Off Points from Spectrophotometer Measurements | 47 |
| 2 | List of Test Equipment | 48 |
| 3 | Optimization Results Optimum "Cut-On" and Cut-Off" Wavelengths for Ideal Filter | 49 |
| 4 | Normal Cut-On and Cut-Off Wavelengths from Transmissivity and Reflectivity Measurements (Wavelengths in Microns) | 50 |
| 5 | Calculated Spectral Shift as a Function of Incident Angle | 51 |
| 6 | Summary of Rotating Solar Cell Test Results | 52 |

## SECTION 1
## SUMMARY

An analytical and experimental program was undertaken to study the use of selective interference filters and highly reflective coatings for temperature control of solar cells. Optical characteristics of reduced bandpass filters and metallic reflective coatings as a function of angle of incidence and temperature were measured and presented. Experimental efforts included the measurement of filter-adhesive-cell composite performance under equilibrium temperature conditions at insolation levels approximately equal to those encountered at 1.0, 0.6, and 0.4 AU. These tests were performed on a model simulating a spinning spacecraft.

In addition, analytical studies were performed to determine the optimum assembly using filters and/or reflective metallic coatings and to predict solar cell temperature and performance at 1.0, 0.6, and 0.4 AU. The analysis was also conducted for the case of spinning spacecraft with solar cells bonded to, but thermally insulated from, the spacecraft.

The results of the program illustrated the importance of thermal control and confirmed that in the range of insolation considered the selective interference filters seemed to produce the best method of thermal control. The results also illustrated the importance of series resistance on solar cell performance operating at high temperature and high insolation conditions.

author

# SECTION 2

# INTRODUCTION

Space missions requiring near sun approaches have produced increased impetus for the study of advanced thermal control techniques. An examination of the properties of solar cells indicates that substantial improvement in performance can be obtained by adequate thermal control.

The use of highly selective interference filters as solar cell thermal control devices has been suggested by many sources. The purpose of this investigation is to analytically and experimentally examine the use of filters and highly reflective coatings as a means of solar cell thermal control.

This study has been directed toward predicting solar cell temperature and performance at one, three, and six times the solar intensities at one sun (140 $mw/cm^2$) air mass zero. The experimental investigation is limited to the case of a spinning spacecraft with solar cells bonded to, but thermally insulated from the spacecraft and will deal with temperature and electrical performance of a single spinning solar cell, with various types of coverglasses. The work reported includes three general areas. These are:

a. The measurement of the optical characteristics of the reduced band-pass filters and metallic reflective coatings as a function of angle of incidence and temperature.

b. The analytical determination of the optimum assembly using filters and/or reflective metallic coatings and the prediction of solar cell temperature and performance at 1.0, 0.6, and 0.4 AU.

c. The experimental measurement of the performance of solar cell assemblies with filters and with selected area fractions of reflective coatings.

These investigations were performed to establish a more complete understanding of the performance of solar cell assemblies under equilibrium temperature conditions at high solar intensities.

Thanks are extended to Optical Coating Laboratory, Inc. and particularly Dr. A. Thelen for their aid and assistance in evaluating the filters and coatings measurements. The efforts of Mr. S. Shenkman on the analytical studies and Mr. B. Mamula on the experimental tasks are acknowledged and appreciated.

## SECTION 3

## SYMBOLS

| | | |
|---|---|---|
| a | - | Semiconductor Materials Property |
| A | - | Areas, Square Meters |
| B | - | Constant |
| C | - | Thermal Capacitance, $\rho C_p V$, Joule/$^{o}$C |
| $C_p$ | - | Specific Heat, joule/kilogram $^{o}$C |
| E | - | Voltage, volts |
| $E_g$ | - | Effective Thermal Band-gap, Electron Volts |
| F | - | Fraction of Light, watts/cm$^2$ |
| $F_{ave}$ | - | Average Flux, watts/cm$^2$ |
| I | - | Current, amps |
| $I_L$ | - | Light Generated Current, Amps |
| $I_t$ | - | Energy Intensity, watts/cm$^2$ |
| $I_{rs}$ | - | Energy Reflected from Surface S, watts/cm$^2$ |
| $I_o$ | - | Incident Energy, watts/cm$^2$ |
| k | - | Boltzmann's Constants - 1.38 x $10^{-23}$ joule/$^{o}$K |
| K | - | $\epsilon A \sigma T_{ave}^3$ |
| N | - | Multiplier - Number of Suns |
| $N_\lambda$ | - | Relative Wave Number - Dimensionless |
| n | - | Index of Refraction - Dimensionless |
| P | - | Power, Watts |
| q | - | Charge of electron |
| Q | - | Heat Input, watts/meter$^2$ |
| r | - | Reflectivity - Dimensionless |
| R | - | Resistance - Ohms |
| S | - | Solar Constant (140 mw/cm$^2$) |
| s | - | Solar Distribution (mw/cm$^2$micron) |
| T | - | Temperature $^{o}$C |
| t | - | Transmittance - Dimensionless |
| V | - | Volume, cu. meters |
| $\alpha$ | - | Absorptivity, Dimensionless |
| $\beta$ | - | Incident Angle, degrees |

## LIST OF SYMBOLS (Cont'd)

| | | |
|---|---|---|
| $\epsilon$ | - | Emissivity, Dimensionless |
| $\eta$ | - | Efficiency, Dimensionless |
| $\theta$ | - | Time, Seconds |
| $\lambda$ | - | Wavelength - microns |
| $\sigma$ | - | Stefan-Boltzmann Constant - $4.88 \times 10^{-8}$ kg-cal/sq m)(hr)($^{\circ}K^4$) |
| $\lambda_1$ | - | Cut On Wavelength - microns |
| $\lambda_2$ | - | Cut Off Wavelength - microns |
| $\lambda_3$ | - | Cut On Wavelength - microns |
| $\rho$ | - | Density, kilograms/meter$^3$ |
| $\tau$ | - | Transmissivity - Dimensions |
| $\omega$ | - | Angular Velocity, radians/sec |

Subscripts

| | | |
|---|---|---|
| a | - | Area |
| B | - | Base |
| C | - | Coating |
| F | - | Filter |
| L | - | Load |
| m | - | Maximum |
| O | - | Reference Value - Normal |
| P | - | Parallel |
| r | - | Reflectivity |
| s | - | Series |
| S | - | Surface |
| sc | - | Solar Cell |
| T | - | Temperature |
| t | - | Total |

Superscripts

| | | |
|---|---|---|
| ' | - | Second |
| * | - | Normalized |

# SECTION 4
# GENERAL BACKGROUND

One of the most successful solar cell thermal control techniques is the installation of cover glass slides with spectrally selective multi-layer interference filters and anti-reflective coatings which selectively reflect wavelengths outside the range of cell response. These filters are usually applied to cover glasses made from fused silica. The cover glass mounting of these filters has the added benefit of increasing the solar array emissivity from about 0.37 for the bare cell to about 0.85 for the cover glass as well as providing protection against radiation damage.

## 4.1 FILTER CHARACTERISTICS

The most desirable filter would transmit solar radiation only in the wavelength region corresponding to the spectral response of the solar cell. Unfortunately, real filters include undesirable transmission bands in the IR regions. Throughout this study reference is made to the ideal filter which is a filter that cuts completely on and off at specified wavelengths, has perfect transmission when cut-on and has perfect energy rejection when cut-off. The region between the cut-on and cut-off is referred to as the "band pass." The portion of the spectrum which is outside the bandpass region, hence, is called the rejection band. Most earth-orbiting spacecraft which employ silicon solar cell power systems utilize a "blue" filter which rejects solar energy only on the short wavelength side of the solar cell's response bandwidth.

Suppression of both the shorter wavelengths and some of the solar energy just beyond the cell's long wavelength response can be accomplished by using a "blue-red filter." Figure 1 illustrates the transmissivity of the "blue-red filter" as well as the ideal filter approximation. The blue-red filters

generally exhibit an undesirable transmission band in the IR region. However, it has been shown that the infrared rejection can be increased by increasing the number of filter layers, as shown in Figure 1

When the filter-cell-stack is attached to a spinning spacecraft the insolation will vary according to the cosine of the angle between the normal to the cell and the spacecraft-sun line. This is the angle of incidence (β) which is illustrated below

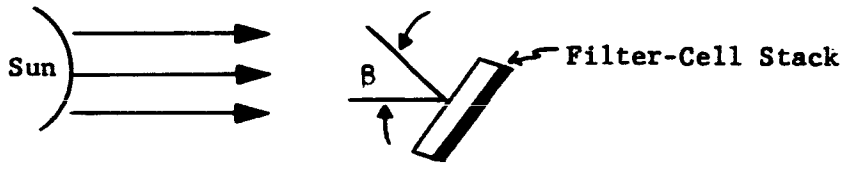


As the angle of incident illumination increases, multi-layer filters exhibit a characteristic spectral shift to shorter wavelengths accompanied by a decrease in the transmission.

Effects similar to the angle of incidence effects are also caused by increasing the filter temperature. The following sections of this report will discuss in detail the spectral shift and the transmission changes caused by both the angle of incidence and the filter temperature.

## 4.2 REFLECTIVE COATINGS

Highly reflective coatings can be used for thermal control by covering a portion of the photovoltaic cell and utilizing the high reflectivity of the coating to reduce the total energy absorbed. The reduction of the absorbed energy lowers the cell's operating temperature and can increase the maximum power output at high solar intensities even though there is a reduction in active cell area.

Series resistance can be a major problem at high solar intensities; this is generally overcome by employing high grid densities. Polishing the grid contacts to produce a highly reflecting surface can be used as a means of thermal control similar to the use of a highly reflective coating deposited on a coverglass.

Reflective coatings might also be used in conjunction with the selective interference filters. Reflective coatings offer some distinct advantages, especially in conjunction with the examination of the series resistance effects at very high insolation levels.

## 4.3 SOLAR CELL EQUIVALENT CIRCUIT

The equivalent circuit for a solar cell is generally considered to be as shown in Figure 2. The junction is represented by a diode and the circuit shows the representative power source, and lumped series and parallel resistances. The diode follows a modified classical diode equation, the interesting deviations being common on silicon solar cells. Applying Kirchhoff's Laws and taking the light generated current as positive for convenience to relate to the I-V curves used in this report, gives the following equation for the current I and the voltage V in the load:

$$I = I_L - I_o \left[ e^{\left(\frac{q}{nkT}\right)(V-IR_s)} - 1 \right] - \frac{V}{R_p} \qquad (1)$$

In general, $R_p$ is usually large enough to make the last term negligible. The dark, or saturation current, $I_o$ is given by

$$I_o = a\, T^3 e^{E_g/kT} \qquad (2)$$

The light generated current $I_L$ is approximately proportional to the light intensity incident on the solar cell. Thus, combining equations (1) and (2) allows the analysis of solar cell performance for any specific condition of insolation and temperature.

# SECTION 5

# EXPERIMENTAL APPROACH

The experimental tasks are divided into two distinct areas; one is the spectral measurements performed on the filters and coatings, the other concerns the performance testing of the filter-cell stack assemblies. The test procedure and description of the apparatus is presented in this section of the report.

## 5.1 FILTER CHARACTERISTIC MEASUREMENT

To facilitate the study of the filter characteristics applicable to solar cell covers on a spinning spacecraft, samples of six typical blue-red multilayer interference filters were obtained from Optical Coating Laboratory, Inc. Characteristics of these filters are given in Table 1.

A random sample of four was taken from each of the filter types for spectral measurements. The spectral measurements were performed over the range of wavelengths from 0.35 to 2.0 microns. This range was felt more than adequate since it covers approximately 90 percent of the solar spectrum. In addition the substrate absorbs much of the UV and far infrared so that about 95 percent of the solar spectrum is thus accounted for. The data is presented in Appendix H.

### 5.1.1 Transmittance Measurements

A special fixture was fabricated that allowed the tilting of a single filter-cover-glass with respect to the incident beam. The transmission of each sample was measured on a Perkin-Elmer Model 350 Spectrophotometer as a function of wavelength for incident angles of 0, 15, 30 and $45^{o}$.

It would be desirable to measure the spectral shift of the filters at incidence angles greater than $45^{o}$. However, the thickness of the filters (see Table 1) caused a lateral displacement of the transmitted beam so large that the beam was shifted off the detector. Thus, at increasing incident angles, the experimental uncertainity increases to a point where

the measurements are no longer valid. Special devices can be constructed to counteract this shift. However, the increased number of reflective surfaces will tend to cause other unmeasurable errors. With the present equipment, the measured transmittance of the filters is expected to have approximately a $\pm$ 2% uncertainty at normal incidence. For the thinner substrates, this uncertainty is expected to increase to about $\pm$ 5% at an incidence angle of $45^{\circ}$. With measurements at incidence angles greater than $45^{\circ}$ the results have questionable validity. The thicker filters show a noticeable drop in transmittance at an incidence angle of $45^{\circ}$. This is attributed to the fact that the beam was being shifted off the detector. The experimental uncertainty is also affected by the nonlinearity of detector response across the detector face. Section 6.1.1.1 shows a method for extrapolating the measurements to $90^{\circ}$.

### 5.1.2 Temperature Effects

Filter transmission measurements were made on the Perkin-Elmer Spectrophotometer to determine the filter characteristics as a function of temperature. To accomplish these measurements a special isothermal soak bath was built to fit the test section of the spectrophotometer. The oven was properly insulated so that the temperature inside the oven would not affect the spectrophotometer. Temperature measurements were determined by means of a laboratory precision thermometer. Spectral transmission measurements were taken at $26.7^{\circ}C$, $65.5^{\circ}C$, and $139^{\circ}C$. These measurements are confined to normal incident angles; however, the results are directly applicable to other incident angles. The experimental accuracy is expected to correspond to that of the transmission measurements described above.

### 5.1.3 Reflectivity Measurement

The samples to be used in the equilibrium temperature tests were cemented with Dow Corning XR-63488 adhesive to Hoffman type N12-CG silicon solar cells.

Reflectivity measurements were then made on the test samples with the Perkin-Elmer Spectrophotometer total integrating sphere. The resulting curves represent the portion of the incident beam reflected; however, they also allow the determination of the thermal absorptivity, since all the energy is either absorbed or reflected, from:

$$\alpha = 1 - r \qquad (3)$$

Comparison of the results shown in Table 4 between the reflectivity and transmissivity measurements showed excellent agreement except in the UV region where a noticeable increase in absorptance was observed from the reflectivity measurements. This increased absorptance in the UV region is attributed to the energy absorbed by the adhesive and not an experimental error. This is substantiated by the excellent agreement throughout the rest of the spectrophotometer traces.

## 5.2 COATING CHARACTERISTIC MEASUREMENTS

The equilibrium temperature experimental program was to consider samples with highly reflective silver deposited on fused silica substrates. The solar cell covers obtained from OCLI for these equilibrium tests were 60 mil fused silica substrates with 20 and 40 percent of the second surface area covered with the highly reflective silver coating.

To eliminate geometrical orientation effects, the characteristics of the coating and substrate were determined independently. Reflectance measurements were made on the bare coverglass cemented to the solar cells identical with this procedure described for the filters. In addition, a one inch diameter metallic disc was obtained with the silver deposited on the front surface. Reflectivity measurements were also performed on this disc. The proper combination of these two results allows the evaluation of the composite coating-cell-stack spectral characteristics (see Section 7.2).

## 5.3 EQUILIBRIUM TEMPERATURE TEST

The basic objective of the work reported in this section is to measure the performance of solar cell assemblies with filters and with selected area fractions of reflective coatings. The experiment was to simulate a spinning spacecraft with solar cells bonded to, but thermally insulated from, the spacecraft. The tests were performed at three flux levels such that the normal insolation was one, three, and six times the solar intensity of one air mass zero sun.

Tests were performed on filter-cell-stacks utilizing the six multi-layer interference filter types previously discussed. In addition, tests were performed on cover-cell-stack assemblies which employed two reflective coating area fractions. In the reflective coating tests, area fractions of 20 and 40 per cent were used. The coatings were applied completely covering the long dimension perpendicular to the cell grid lines.

The tests were conducted with the purpose of determining the performance characteristics of each type of solar cell cover with a view toward maximizing the available power at the particular solar intensities.

### 5.3.1 Test Procedure

The voltage-current relationship of each cover-cell-stack was obtained at a one sun intensity prior to the equilibrium temperature test. These calibration tests were performed on the OCLI solar simulator because of the superior spectral match to the actual solar curve as well as the uniformity and repeatability of the output. The results of these calibration tests were recorded for comparison with identical recalibration tests which were performed following the exposure to the high solar intensities. The calibration tests were performed in an effort to observe any degradation in cell performance which might occur from exposure to the high insolation and elevated equilibrium temperatures.

Following the initial calibration test each model was installed in the vacuum chamber and tested at one, three, and six times the solar intensity at air mass zero. The distance from the Strong Carbon Arc for the various solar intensities was determined by pyrheliometer measurements inside the vacuum chamber prior to the equilibrium temperature tests. The intensity was checked during the tests by observing the short circuit current from a calibrated solar cell placed inside the vacuum chamber at the test plane.

At the completion of the equilibrium test, the cells were recalibrated on the OCLI Solar Simulator as described above.

In addition to these tests, several tests were performed to support the discussion of the equilibrium tests. A series of silicon cells with fused silica coverglasses was placed at one sun position on the OCLI simulator, and the short circuit current was recorded as a function of incident angle. Also performed was a test where the short circuit currents of several typical silicon solar cells were compared to the output from the Eppley Pyrheliometer at increasing solar intensities. This test was to illustrate the short circuit current's variation with intensity at high solar intensities. The results of these tests are reported in conjunction with the equilibrium temperature tests. Several of the filter-cell-stacks were also exposed to a humidity soak for eight hours at 100°C and 100 percent relativity humidity and then retested on the OCLI solar simulator.

### 5.3.2 Description of Test Apparatus

The rotating solar cell tests were performed in a three foot diameter, three foot long vacuum chamber at a pressure of approximately $5 \times 10^{-6}$ torr. A magnetic drive was constructed which was driven by a gear reduction electric motor. The drive was equipped for rotation in either direction. The magnetic drive was accomplished by two bar magnets, one attached to the motor outside the vacuum chamber and the other attached to the central rotating shaft inside the chamber. This drive method eliminated the need for employing a mechanical feed-through which might develop vacuum leaks during testing.

The electric drive motor was geared for an output speed of 43 RPM. Transient heat transfer calculations were performed from which it was observed that any rotational speed greater than 10 RPM would have a maximum temperature variation of less than three degrees ($3^{o}C$); thus, any rotational speed greater than 10 RPM should produce identical equilibrium temperatures. The output variation of the solar cells rotating at 43 RPM was found to be well within the response of the Sanborn Recorder (Item 3 Table 2) and was therefore accepted for the test. Figure 3 shows the drive motor and magnet attached to the vacuum chamber.

The inside of the vacuum chamber is lined with a cold wall shroud which was painted with a flat black vacuum paint to provide an acceptable heat sink for the experiment. Inside the shroud, the central rotating shaft is supported in three places by teflon bearing supports which allow the shaft to rotate freely even at the very low temperatures imposed by the liquid nitrogen cooled shroud. On one end of the shaft is the mating bar magnet which drives the shaft. The spacecraft model is attached to the other end which is aligned with the Vicor window through which the radiation must pass (see Figure 4).

The electrical leads from the model pass through the shaft and are divided into four sets of two leads which come out of the shaft at four places. These leads then pass through a pulley system and are attached to springs as shown in Figure 5. From the springs the leads go to the electrical feedthroughs. The pully system allows the lead wires to be wrapped around the central shaft while the model rotates. It was found that with this technique the model could rotate approximately 120 turns before reversing the rotational direction is required. This technique proved satisfactory and eliminated the need for slip rings or other devices.

After attaching the model to the end of the shaft, the shaft and model were insulated with many layers of aluminized mylar as shown in Figure 5. This was to reduce extraneous radiation from the model as well as protect the

lead wires from the high solar intensities.

Also included inside the chamber was a fixed water cooled solar cell which was used as a means of measuring the magnitude of the incident flux. The short circuit current of this cell was calibrated against the Eppley Pyrheliometer inside the chamber. Thermistors were installed on the cold wall at the far end of the shroud and behind the water cooled solar cell. The cold wall thermistors provided a check on the sink temperatures while the one on the cooled solar cell was used as a check on the water cooling system.

The electrical wiring and instrumentation components are shown on the Instrumentation Block Diagram (Figure 6). The voltage and current output from each solar cell was recorded on a calibrated Sanborn Recorder. The cell's temperatures were obtained by measuring the respective thermistor's resistance on a Leeds and Northrup Wheatstone Bridge.

The current was measured by monitoring the voltage across a shunt resistance. The shunt resistance was obtained by the use of an EICO precision resistance decade box which allowed the use of the particular shunt resistance which would give the maximum accuracy on the recorder trace. The load resistance was also made variable between 0 and 100 ohms by the use of a Helipot Precision Potentiometer. As shown in the Instrumentation Block Diagram (Figure 6), the load resistance on the cell is the sum of the variable shunt resistance and the potentiometer resistance.

Figures 4 and 7 are photographs of the instrumentation used for the equilibrium testing. The apparatus was mounted on a cart which could easily be moved with the vacuum chamber.

The one sun calibration tests were performed using the OCLI solar simulator (Figure 8). The output of the solar simulator was established by measuring the short circuit current output from the Heliotek Standard Solar Cell. The output from each test cell was recorded on the Moseley X - Y Recorder. The short circuit current was also measured with a precision Weston

milliampmeter to provide a more accurate value for future comparisons.

Figures 9 and 10 present a comparison of the manufacturers calibration and the solar spectrum for the two solar simulators used in the experimental program. Preliminary spectral measurements were performed to check the manufacturer's data. In addition, the OCLI simulator lamps were balanced and calibrated according to the calibration procedure supplied by the manufactuerer.

Table 2 lists all the test equipment employed in the experimental tasks herein reported.

5.3.3 Description of Spacecraft Model

In evaluating the performance of solar cell assemblies which represent a spinning spacecraft with solar cells bonded to, but thermally insulated from the spacecraft, it is obvious that the only heat transfer mechanisms available for temperature control are those occuring on the front surface of the solar cell assembly. In order to experimentally approximate these conditions a model was constructed such that the heat transfer by conduction and radiation from the edges and back of the cell assembly was minimized.

The model frame was made out of .0794 cm. thick fiberglass attached to a brass tube. The cell attachment area of the frame was covered with a .0397 cm. thick piece of fiberglass. The entire vehicle model was assembled with epoxy with the intent of keeping the thermal mass as small as possible and also maintaining a minimum conduction path between the cells and the mounting structures.

The filter-cell-stacks were attached to the model with a silicon adhesive after the lead wires had been attached. Installed between the filter-cell-stacks and the support were YSI precision thermistors which permitted the determination of the filter-cell-stack temperature during testing. The

model was then wrapped with .00254 cm aluminized mylar super radiation insulation such that only the front face of the cell assembly was exposed. Figure 11 shows the final insulated assembly ready for mounting in the vacuum chamber as well as an uninsulated model illustrating the internal construction.

Estimation of the heat leak from the lead wires and model conduction paths for this final model assembly showed the heat leak to be less than 5 percent of the insolation in the worst case. When this was compared with the ±5 percent uncertainty associated with determining the incident flux, the model configuration was considered adequate for this experimental investigation.

# SECTION 6
# ANALYTICAL APPROACH

The prime objective of the analytical investigation is to determine the optimum assembly using filters and/or reflective metallic coatings and to predict solar cell temperature and performance at 1.0, 0.6, and 0.4 A.U. In addition various analytical efforts were performed to complete the investigation of the filter and coatings spectral characteristics. Supplementary analytical efforts were also executed to justify the equilibrium temperature test program.

## 6.1 INTERFERENCE FILTERS

Methods are presented which allow an approximation to the prediction of the spectral characteristics of selective interference filters. The spectral specifications for the OCLI filters are presented in Appendix A for reference and to complete the basic understanding of the multi-layer interference filters. This specification provides the reader with a measure of the manufacturing tolerances and limits involved with the respective filter characteristics.

### 6.1.1 Variation of the Filter Characteristics with the Angle of Incidence

#### 6.1.1.1 Spectral Shift

The transmittance characteristics of all interference filters shift with increasing angle of incidence towards shorter wavelengths. This shift toward shorter wavelengths can be well approximated by the relation which governs the angle shift of a single film (Ref. 3).

$$\lambda = \lambda_o \sqrt{1 - \frac{\sin^2 \beta}{n^2}} \qquad (4)$$

where n is, in the case of the single film, the refractive index and in the case of multi-layers is an "average index." From Equation 4:

$$n = \lambda_o \sin \beta \frac{1}{\lambda_o^2 - \lambda^2} \tag{5}$$

If the "n" is unknown, equation (5) with measured values of $\beta$, $\lambda_o$ and $\lambda$ allow the determination of the "average index" of refraction which, when substituted into equation (4), allows the prediction of $\lambda$ at any angle of inclination. Therefore, **transmittance measured at any two angles of incidence allows prediction of the performance at all other incident angles. Now let**

$$\frac{\lambda_o}{\lambda} = N_\lambda \tag{6}$$

where $N_\lambda$ is defined as the relative wave-number. Equation (6) allows the expression of equations (4) and (5) in terms of relative wave-numbers:

$$n = \sin \beta \sqrt{\frac{N_\lambda^2}{N_\lambda^2 - 1}} \tag{7}$$

$$N_\lambda = \frac{1}{\sqrt{1 - \frac{\sin^2 \beta}{n^2}}} \tag{8}$$

Using equations (7) and (8) with the test data allows a simple and straight forward method of predicting and evaluating the phase shift at high angles of incidence.

6.1.1.2 Decrease in Transmittance

The preceding section described the spectral shift toward shorter wavelength which occurs with increasing incident angle. As the incident angle increases, there occurs a characteristic decrease in transmittance caused mainly by the portion of light reflected by the various surfaces. The transmittance as a function of both the incident angle and wavelength can be fairly accurately calculated; however, these calculations require a complete understanding of multi-layer interference filter design techniques and

knowledge regarding the nature of the incident light. In conjunction with this study Dr. Alfred Thelen (Ref. 6) calculated the theoretical transmission for a typical blue-red multi-layer interference filter. These results presented in Appendix H were used to confirm, in a general manner, the transmittance measurements performed for this study.

In addition to the decrease in frontal area with increasing incident angle the transmittance is effected by an increased reflection from the first surface. Consider a plain cover glass which has an index of refraction of 1.523 (a good value for various cover glass materials). Assume that the incident light is natural or unpolarized light. (Unpolarized light is a mixture of waves polarized in all possible azimuths.) By symmetry, the reflectance of a surface can be determined by summing one-half of the parallel polarized light and one-half of the vertically polarized light. The reflectance of a surface is then given by

$$r = \frac{1}{2} \frac{\tan^2 (\beta - \beta^1)}{\tan^2 (\beta + \beta^1)} + \frac{1}{2} \frac{\sin^2 (\beta - \beta^1)}{\sin^2 (\beta + \beta^1)} \qquad (9)$$

The angles in equation (9) may be expressed in terms of the incident angle and the respective indices of refraction by Snell's law as follows:

$$n \sin \beta = n^1 \sin \beta^1 \qquad (10)$$

Equations (9) and (10) allow the determination of the average reflectance as a function of incident angle.

### 6.1.2 Variation of the Filter Characteristics with Temperature

Spectral measurements were made on samples of each filter type at 26.7°C, 65.5°C, and 139°C. These measurements presented in Appendix H showed effects similar to the incident angle effects; that is, there occurs a shift to the shorter wavelengths with increasing temperature accompanied by a characteristic decrease in transmittance. However, these effects are much smaller than the incident angle effects and appear to be inconsequential

for solar cell performance calculations. The temperature effects are much smaller than the uncertainty imposed upon solar cell calculations by the typical deviations in cell to cell response to the solar spectrum.

## 6.2 REFLECTIVE COATINGS

The following analysis describes an approximate method of determining the optimum area fraction of reflective coating to be used for maximum performance.

Consider a highly reflective coating applied to a defined percentage of the lower face of a solar cell cover as shown

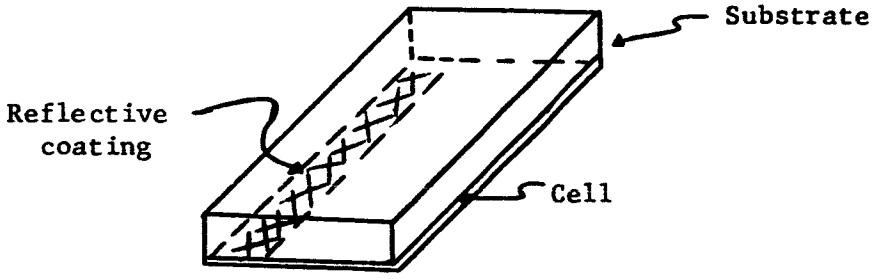


Basic Assumptions:

1. No absorption in the substrate
2. All energy transmitted to the cell is absorbed
3. No absorption in the adhesive
4. Isothermal solar cell
5. No edge effects.

The energy reflected from the top surface can be determined by

$$I_{r_S} = I_o r_S \tag{11}$$

from which the transmitter energy is obtained

$$I_t = I_o (1 - r_s). \tag{12}$$

Now the energy reflected by the reflective coating is determined by

$$I_{r_c} = \frac{A_c}{A_T} r_c I_t \tag{13}$$

and the energy reflected by the solar cell is

$$I_{r_{sc}} = \frac{A}{A_T} r_{sc} I_t \tag{14}$$

Neglecting second order reflections the total reflected energy can be obtained from equations (11), (13) and (14) as

$$I_{r_t} = I_{r_s} + I_{r_c} + I_{r_{sc}} \tag{15}$$

or

$$I_{r_t} = I_o \left[ r_s + \frac{A_c}{A_t} r_c (1 - r_s) + \frac{A}{A_t} r_{sc} (1 - r_s) \right]. \tag{16}$$

Defining a total reflectivity such that

$$I_{r_t} = I_o r_t \tag{17}$$

the expression for $r_t$ follows

$$r_t = r_s + \frac{A_c}{A_t} r_c (1 - r_s) + \frac{A}{A_t} r_{sc} (1 - r_s). \tag{18}$$

The absorptivity is now determined as

$$\alpha_t = 1 - r_t = 1 - \left[ r_s + \frac{A_c}{A_t} r_c (1 - r_s) + \frac{A}{A_t} r_{sc} (1 - r_s) \right] \quad (19)$$

and the total energy absorbed per unit area is

$$I_a = \alpha_t I_o \quad (20)$$

Now consider an ideal case where the coating is totally reflecting and the substrate is totally nonreflecting; hence, the total energy absorbed per unit of area is given by

$$I_a = \frac{A}{A_t} \alpha_{sc} I_o \quad (21)$$

Comparison of equation (20) to equation (21) indicates that for area fractions of reflective coatings between 20 and 60 percent the simplified equation (21) gives very good results. The use of equation (21) allows for a very general optimization analysis, and hence, with the stated restrictions it is used in the following analysis.

### 6.2.1 Reflective Coating Optimization Analysis

The "non-rotating" energy balance for the ideal coating is given as

$$\alpha_{sc} \frac{A}{A_t} S - \epsilon \sigma T^4 - P = 0 \quad (22)$$

where the power can be expressed in terms of efficiency factors as

$$P = \eta_o \eta_a \eta_t S = \eta_o \left[ 1 - .00303 (T - 544) \right] \frac{A}{A_t} S \quad (23)$$

Combining equations (22) and (23)

$$\alpha\eta_a S - \epsilon \sigma T^4 - \eta_o \left[1 - .00303\ (T - 544)\right] \eta_a S = 0. \qquad (24)$$

Now similar to the following analytical analysis for the quasi-study state rotating spacecraft where the following equation is obtained the incident solar flux and the power output are assumed to vary as the cosine of the incident angle now one half of each revolution

$$\alpha\eta_a S \int_o^{\pi} \frac{\cos\theta\, d\theta}{2\pi} - \epsilon \sigma T^4 - \eta_o \left[1 - .00303\ (T - 544)\right] \eta_a S \int_o^{\pi} \frac{\cos\theta\, d\theta}{2\pi} = 0 \qquad (25)$$

which can be simplified to

$$\frac{\alpha\eta_a S}{\pi} - \epsilon \sigma T^4 - \eta_o \left[1 - .00303\ (T - 544)\right] \frac{\eta_a S}{\pi} = 0. \qquad (26)$$

Hence it is noted that equations (24) and (26) are identical if the solar intensity is defined as the average solar intensity incident on the photovoltaic cell.

### 6.2.2 Coating and Filter Optimization Analysis

An obvious extension of the above analysis is to consider an ideal blue-red filter with a cut-on at 0.4 microns and a cut-off at 1.2 microns. Following the development of the filter analysis presented in Appendix C the energy balance for the non-rotating filter coating combination can be expressed as

$$\alpha\eta_a S \int_{\lambda_1}^{\lambda_2} S^* d\lambda - \epsilon \sigma T^4 - \eta_a \eta_o \eta_T S \frac{\int_{\lambda_1}^{\lambda_2} \tau R^* S^* d\lambda}{\int_o^{\infty} R^* S^* d\lambda} = 0 \qquad (27)$$

and from the above analysis for the rotating vehicle, equation (27) is applicable (with the assumed cosine variation of solar intensity) simply be defining S as the average over a complete revolution.

## 6.3 ROTATING SOLAR CELL INVESTIGATION

The goal of the analytical investigation is to determine the optimum assembly using filters and/or reflective metallic coatings and to predict solar cell temperature and performance at 1.0, 0.6, and 0.4 A.U. The analysis is to be conducted for the case of a spinning vehicle with solar cells bonded to but thermally insulated from the space vehicle.

A complete analysis involves knowledge of many parameters which affect both the cell performance and temperature. Almost all factors which effect cell performance can be considered as degradation factors. For example, ultra-violet irradiation, particle bombardment, temperature cycling have degrading effects on solar cell performance. In addition, the case being considered requires knowledge of the optical effects of the selected cover glass which can become very important at large angles of incidence.

This analysis presents a method of calculation which allows the use of any combination of degradation coefficients and physical data to obtain the cover-cell-stack properties that produces the maximum power output at any given space location.

In addition to the prediction of optimum filters, evaluation of the performance of cells with known filters was desired to back up the experimental program.

### 6.3.1 Cell Temperature History

The degree of complexity of the analysis of solar cell performance is a function of the transient temperature response of the cell. For a solar cell in space with constant insolation, the equilibrium temperature is a constant and can readily be determined. A solar cell rotating about an axis perpendicular to the insolation vector receives a sinusoidally varying heat flux (neglecting optical effects of the coverglass at high angles of incident) for one half of each revolution and nothing during the second

half of the revolution. The cell also radiates to space for the entire revolution.

Appendix B presents the derivation of the equations which describe the temperature history for a body heated in this manner. The basic equations are:

For $0 \leq \omega\theta \leq \pi$

$$T = \frac{\alpha Q_{max}}{\omega C} \left[ \frac{1}{1 + \left(\frac{K}{\omega C}\right)^2} \right] \left[ \frac{K}{\omega C} \sin(\omega\theta) - \cos(\omega\theta) \right] + Be^{(K/C)\theta} \qquad (28)$$

and for $\pi \leq \omega\theta \leq 2\pi$

$$T = T_{(\omega\theta = \pi)} e^{(-K/C)\theta} \qquad (29)$$

The analysis shows that the temperature extremes, for $K/\omega C \ll 1$ occur at $\sin(\omega\theta) = \frac{1}{\pi}$ and $\pi - \frac{1}{\pi}$. The results indicate that a filter-cell-stack having a total thickness of 0.190 cm (0.154 cm thick coverglass and 0.036 cm thick cell) will have about $2^{\circ}C$ maximum temperature variation at rotational speeds of 43 RPM. Figure 12 presents the calculated transient temperature for a typical unfiltered cell with a clear coverglass ($\epsilon = .8$, $\alpha = .7$) exposed to six suns and rotating at 43 RPM. It is apparent that for the cases considered in this study the results of this analysis tends to justify the assumption of constant temperature. This assumption greatly reduces the complexity of the analytic effort. The fact that the temperature variation determined from this analysis was so small, was used to simplify the design of the rotating solar cell experiment by allowing the use of thermistors to read the mean solar cell temperature.

### 6.3.2 Cell Stack Temperature Gradient

The coverglass itself is beneficial to solar cell performance in that it provides an effective way to lower the temperature of the solar cell

operating in space. A bare cell (without a silicon monoxide coating) has an emissivity between 0.3 and 0.4. When a cover glass is applied to the cell the emissivity is raised to approximately 0.9. The coverglass is also used for radiation protection when the cell is to be exposed to high radiation doses such as solar probe missions.

The filters and coatings used for the experimental efforts were deposited on 0.153 and 0.306 cm coverglasses. To evaluate the effect of these relatively thick coverglasses on the cell temperature, an investigation of the thermal gradient across the filter-cell-stack was performed.

The thermal gradient analysis of a fixed position filter-cell-stack indicates that the heat conduction rate through a 0.153 cm thick coverglass is large enough that the thermal gradient can be neglected. In addition, the rotation of the cell stack causes the front surface to be alternately heated and cooled. Thus, it can be concluded that the total filter-cell-stack can be assumed to be isothermal during equilibrium operation. This assumption further reduces the complexity of the analytical analysis.

### 6.3.3 Solar Cell Performance Analysis

The solar cell conversion efficiency at standard temperature, $\eta$, is defined as the ratio of the maximum power output to the incident solar flux. For silicon solar cells the conversion efficiency is primarily a function of temperature and is effected very little by the magnitude of the insolation. Since the solar cell conversion efficiency, $\eta$, generally decreases with increasing temperature, the purpose of adding a filter is to transmit only the solar energy in the spectral range where the solar cell response will tend to maximize the potential power output.

Another method of thermal control to be investigated is the use of highly reflective opaque coatings. Highly reflective coatings reduce the ratio between the absorptance and the emittance which reduces the cell's

temperature. The coating also reduces the active cell area; however, as previously shown, at very high irradiation intensities the decrease in output caused by the reduction of active cell area is more than offset due to the increase in conversion efficiency caused by the temperature reduction.

Appendix C presents the derivation of the power equation incorporating the filter and coating characteristics. The slight increase in absorptance caused by the coverglass and adhesive has been omitted; however, the increased absorptance can be accounted for by proper scaling of the absorptivity coefficient. The coating is assumed distributed over the cell surface so that it will not introduce thermal gradients in the cell. Thus, the assumption of the isothermal cell is still valid.

Appendix C presents the power equation for a non-rotating solar cell; the extension to the rotating case with changing irradiation is discussed in the Optimization Section of this report.

Appendix C illustrates the development of the energy balance equation used in the solar cell performance analysis. Combining the terms the energy equation can be presented as:

$$\left(\frac{A_B}{A_T}\right) NS \left[\frac{\int_{\lambda F_1}^{\lambda F_2} \tau_{\lambda_F} r_\lambda s_\lambda \, d\lambda}{\sum_{\lambda=0}^{\infty} r_\lambda s_\lambda \, \Delta\lambda}\right] \eta = \frac{NS}{\sum_{\lambda=0}^{\infty} s_\lambda \, \Delta\lambda} \left[\frac{A_B}{A_T}\left\{\int_{\lambda F_1}^{\lambda F_2} \tau_{TF} (\alpha_B)_F s_\lambda \, d\lambda + \right.\right.$$

$$\left.\left. \int_{\lambda R_1}^{\lambda R_2} \tau_{\lambda_R} (\alpha_B)_R s_\lambda \, d\lambda\right\} + \left(1 - \frac{A_B}{A_T}\right)\left\{\int_{\lambda F_1}^{\lambda F_2} \tau_\lambda (\alpha_C)_F s_\lambda \, d\lambda + \int_{\lambda R_1}^{\lambda R_2} \tau_{\lambda e} (\alpha_C)_R s_\lambda d\lambda\right\}\right]$$

$$- \epsilon (T) \sigma A_r T^4 \qquad (30)$$

### 6.3.4 Optimization Analysis

The non-linearity and complexity of the power and energy balance equations prohibits a closed form solution for the optimum solar cell cover parameters. An iterative numerical approach was determined to be the most expedient method of solution. The optimization analysis presented in Appendix D provided the basic approach to determination of the parameters which would optimize the solar cell power output for the particular cases considered.

An electronic computer program was prepared using several previously developed Philco programs as subroutines which incorporated the method of analysis presented in Appendices C and D to provide the optimum values of the "cut-on" and "cut-off" wavelengths as well as the optimum percentage of coating required to obtain the maximum power output for each case. This program requires that all basic data be fit with appropriate polynominal equations. The results of this program were used as initial values for the performance evaluation program. This program uses the same equations developed in Appendix C but the basic data is used in numerical form which increases the accuracy of the results. This program then allows iterations of $\lambda_1$ and $\lambda_2$ to check for the point of maximum power. The results of this analysis are presented in Table 3. These results are for ideal filters and the qualifications will be discussed in the following sections. The ramifications of these results are apparent and show the requirement of decreasing bandpass with increasing intensity.

#### 6.3.4.1 Rotating Approximations

The performance analysis presented above has been developed for non-rotating solar cells with constant intensity. It has been shown that the assumption of constant temperature eliminates the time dependance of temperature from the analysis. Consideration of the instanteous response of the cell would require inputs of the filter optical effects as a function of incident angle, the power output as a function of incident angle, and the filter-cell-stack absorptivity as a function of incident angle. The resulting computer program

would be beyond the scope of the effort herein reported. As a result, the incorporation of "average values" allows the simplification of the rotating consideration and provides a direct comparison to the non-rotating analysis.

The major problem involved in such an analysis is the variation of optical properties as a function of incident angle. Since the wavelength shift is consistantly towards the ultra-violet as the angle of incidence increases, the resulting optimized values of the wavelengths are to be interpreted as applicable for an intermediate incident angle.

The incident solar flux varies with the cosine of the incident angle. The average flux incident on the filter cell stack is then determined by averaging the integrated flux per revolution. The average flux is then given by

$$F_{ave} = \frac{NS}{\pi} \tag{31}$$

Utilizing this assumption the absorbed energy for the rotating case can be determined from the non-rotating analysis simply by dividing by $\pi$.

The light generated current is directly proportional to the incident solar flux intensity and thus for power output where the external current is approximately equal to the light generated current, the power can be assumed to vary with the cosine of the incident angle. (At increasing load resistances the power output tends to vary as the cosine square.) In the analysis the difference in the power relationship has a relatively minor effect and the assumption that the output power varies as the cosine of the incident angle allows the same analogy between rotating and non-rotating case as was used for the energy absorbed. This assumption also allows the non-rotating analysis to be used directly in evaluating the rotating cases. The only change that is required is that the solar intensity be divided by $\pi$ and considered as the average solar intensity throughout the analysis.

6.3.4.2 Solar and Solar Cell Spectral Characteristics

The basic data for the solar spectrum used in this analysis was taken from the solar spectrum as reported by Johnson. In addition to the solar spectrum, data was required for the solar cell spectral response. Figure 13 presents a typical silicon solar cell response curve from Reference 1 which was used as input to the computer program.

6.3.4.3 Temperature Effectiveness

The solar cell maximum power can be empirically represented as a simple function of temperature. The program uses a linear function; however, the functional relationship can be modified to fit basic data as it becomes available. The program used the temperature effectiveness as a multiplier to the conversion efficiency to account for the effect of temperature on the maximum power output.

6.3.4.4 Optical Properties

The general analysis allows the use of typical filter and coating properties as a function of wavelength. The results obtained initially assumes an ideal filter having a square bandpass region. The filter cell stack is assumed to absorb apportionately to the absorptivity $\alpha$, and reflect the amount $(1 - \alpha)$ in the bandpass regions as well as reflect all the insolation in the rejection bands. For further efforts, the program also allows for absorption as a function of wavelength in the rejection bands.

The optical properties used in the optimization analysis reflect an optimum type filter. Once optimum cut-on and cut-off wavelengths are determined from this analysis, real filter and coating affects should be investigated; however, the ideal approximations are expected to yield useful results.

### 6.3.4.5 Degradation Effects

The parameters which affect solar cell performance, such as radiation effects, electrical properties of the cell, and adhesive degredation are not considered in the initial optimization analysis. These effects can be accounted for by appropriately altering the solar cell conversion efficiency to reflect the desired effect. It is expected that future uses of this program will be made by which its versatility can be explored.

# SECTION 7
# RESULTS AND DISCUSSION

## 7.1 FILTER CHARACTERISTIC MEASUREMENTS

Appendix H presents the spectrophotometer traces for a typical example of each filter type. For purposes of calculation and presentation, the values for the four samples of each type were averaged and the average values are presented in the discussions. It was noted, however, that very little difference was observed between the traces for the same filter type. The averaged results are presented in Table 4.

### 7.1.1 Filter Representation

The filter types obtained from Optical Coating Laboratory Incorporated can be identified by the cut-on and cut-off wavelengths, presented in Table 1. They are identified by their respective cut-off and cut-on points for a normal incident angle. These values are the result of averaging the 50 percent transmission points from measurements made on the four samples of each filter type.

Filter types 1, 2, and 3 have a bandpass narrower than the total solar cell response bandwidth. Filter 4 is essentially a "blue" filter while filter types 5 and 6 closely approximate a bandpass over the entire silicon solar cell response bandwidth.

It is apparent that the above six filters are representative of the types which would be considered for solar cell thermal control, with the possible exception of the increased infrared rejection which would be beneficial at extremely high solar intensities.

### 7.1.2 Spectral Shift

The method described in Section 6.1.1.1 was used with the test data to predict the transmittance shift at large angles of incidence. Measured

values of transmittance for incidence angles of 0 and 30 degrees were used for the calculations. These angles provided a means of calculating the average index of refraction for the various filters. The calculated values are presented on Figure 14. The predicted values of spectral shift for 15 and 45 degrees show very good agreement with the measured values and tend to substantiate the above described analysis. Figure 14 shows the calculated spectral shift for the various filters as a function of the relative wave-number. Table 5 compared with Table 1 illustrates the agreement of these calculations to the actual measured cut-on points for the six filters. These results show that for solar cell calculations the transmittance shift, as a function of incidence angle, can be adequately approximated with measurements at any two incident angles.

### 7.1.3 Decrease in Transmittance

The method of approximating decrease in transmittance was used to predict the decrease in transmittance for a typical solar cell cover.

The results for light from a vacuum to the cover glass is presented in Figure 15. These results only consider one surface while in the filter-cell-stack the light transmitted by the first surface encounters several other changes of materials; however, the subsequent surfaces can be shown to be made less significant by matching the indices of refraction.

Most solar cell calculations using multi-layer interference filters assume an average constant transmittance across the principle bandpass regions. With a view toward this type of calculations measured values of transmittance were averaged over the bandpass region and compared to the theoretical curve. The results showed very good agreement and the agreement can be made closer by using improved value for the index of refraction of the coverglass.

As a further check, the theoretical calculations on transmittance were also averaged over the bandpass region. These results are presented in Figure 15.

The results of both the theoretical calculations and the spectrophotometer test seem to indicate that the above described equations should provide an adequate method for determining the average transmittance. Figure 16 illustrates the combined effect of the decrease in area by the cosine factor and the reflectance at the front surface.

### 7.1.4 Variation of Filter Characteristics with Temperatures

Examination of the general equations suggested for filter calculations indicates that the temperature effect is generally predictable if the temperature effects on the index of refraction are included. Check calculations were performed and the results further confirmed the use of this technique for predicting the magnitude of the temperature effects on multilayer interference filters.

The elevated temperature measurements indicated one problem which tends to complicate the understanding of the temperature effect. Spectral measurements were made on selected samples at 26.7°C following both the 65.5°C and the 139°C tests. No apparent difference was observed between the original 26.7°C measurements and the 26.7°C spectral characteristics following the 65.5°C measurements. However, when the spectral characteristics were measured following the 139°C test, the spectral shift did not return to the original value while the transmittance appeared to return to its original value. If the filter did not remain at the elevated temperature for a prolonged period, the filter returned to the original characteristic which seems to indicate a time dependence upon this parameter.

It thus appears that some additional oxide is formed in the filter as a result of the elevated temperature. As a part of the manufacturing process, the filters are heated to 177°C ± 5°C and retained at this elevated temperature for a period of one hour. The spectral measurements seemed to indicate that this environmental test should eliminate the above described effect. Unfortunately, a complete investigation of this effect could not be accomplished within the scope of effort herein reported. Furthermore, as

stated above, this effect is small enough so that it is inconsequential to basic solar cell power calculations. Further research seems advisable in view of a more complete understanding of multi-layer filter characteristics.

In conjunction with the work herein reported, OCLI duplicated the transmittance measurements on a typical blue-red filter which provided an independent check on the magnitude of these results. These results further confirmed the fact that the temperature effects on multi-layer filters are so small that it can justifiably be eliminated from the solar cell output calculations.

## 7.2 REFLECTIVE COATINGS

The reflectivity measurements of the coatings are presented in Appendix H. These traces show that the reflective coating has a mean reflectivity of approximately 0.8 and the reflectivity of the substrate is approximately 0.2. Assuming all the light reflected from the substrate is reflected by the front surface and assuming that all the light reflected by the coating is also reflected from the substrate, the percentage of incident light can be calculated for various area fractions of coatings. Thus using mean values for the 20 percent area fraction approximately 36 percent of the incident energy would be reflected and 52 percent would be reflected for the 40 percent area fraction.

### 7.2.1 Reflective Coating Area Fraction Prediction

The approximate method of determining optimum area fractions of coatings and the simplified method of calculating filter and coatings was used to evaluate the usefulness of coatings as a means of thermal control.

For given solar cell properties and assuming an ideal filter, the mean operating temperature was determined as a function of $\eta_a S$ for both the coating alone and the coating with an 0.4 to a 1.2 micron bandpass filter. These results now allow the determination of power as a function of $\eta_a S$ which is presented in Figure 17. This figure shows the optimum value of

$\eta_a S$ to maximize power. These values of $\eta_a S$ are now used to determine the optimum ratio of reflective coating as a function of average solar intensity. These results are presented in Figure 18.

These figures show the relative advantage of using the ideal filter as well as the percentage coating required. For example, at an average solar intensity of two suns (AMZ), 48 percent of the cell is covered without an ideal filter while only 15 percent of the cell is covered when the ideal filter is used. The use of the filter also results in approximately 50 percent increased power output because of the increase in active cell area.

## 7.3 RESULTS OF OPTIMIZATION ANALYSIS

The results of the filter optimization analysis developed in Section 6.4 are presented in Table 3. These results show that to obtain maximum power, under equilibrium temperature conditions, the filter bandpass is significantly narrower for high intensity solar flux than for the smaller intensities. The results also show that the bandpass region is not symmetrical about the peak of the solar cell response curve but shifted toward the longer wavelengths. This is caused by the trade-off between incoming flux and generated power output.

The results represent an idealized approach to filter optimization. The filters are ideal filters absorbing only in the bandpass region. No attempt is made to account for real filter effects such as the UV absorption and the transmittance in the far IR region. The results are for a solar cell having an overall conversion efficiency of 10 percent at standard conditions. Additionally, the absorptivity and emissivity are assumed to be constants rather than functions of wavelengths. The values used for the initial results were $\alpha = 0.7$ and $\epsilon = 0.8$; both values tend to be a little low for real filters.

Similar results were obtained for ideal filters and reflective area coatings combined. In all cases considered the use of any reflective coating caused

a decrease in optimum power. These results indicate that, with the initial conditions considered, the interference filters provide the best means of thermal control. However, the results seemed to indicate that the combination of coatings and filters might show some definite advantages as a thermal control device, when the solar intensities are higher than those considered in this presentation.

## 7.4 EQUILIBRIUM TEMPERATURE TEST

### 7.4.1 Presentation of Test Results

During each test the load resistance was increased in incremental steps up to 100 Ω. The output of both current and voltage, for each test cell, was recorded on the Sanborn Recorder producing traces of cell output which resemble the expected pulsating direct current. Figure 19 shows a typical output obtained from the recorder.

The peak values of current and voltage were obtained from these traces and plotted in the usual form for solar cell characteristics. Each test cell was tested at the three designated flux levels. The results for each cover type are plotted on the same figure for direct comparison. Figures 20 to 26 present the results from the tests performed. The extrapolated short circuit currents and open circuit voltages are presented in Table 6 along with the recorded cell temperatures of each test.

Initial examination of the recorder traces seemed to indicate that at very low load resistances the current output, as a function of incident angle, varied approximately with the cosine of the incident angle, while at higher load resistances the output appeared to be almost of square wave form. Figure 27 is a typical plot of current as a function of incident angle for various load resistances obtained from a typical recorder trace. Only the current is present here, but from Ohm's law, the voltage output is similar. The extrapolated open circuit voltage from the presented data as well as some additional open circuit voltage tests were plotted as a function of

cell temperature and the results are presented in Figure 28. It is observed that regardless of the cell cover types used, data appears to be consistant and illustrates the expected linear relation.

The extrapolated short circuit current results did not appear to be as orderly and will be discussed in the next section. A preliminary test showed that at high solar intensities the short circuit current dropped appreciably with increasing temperature. In an attempt to explain these results a series of cells were tested at various solar intensities at constant temperature, and the results are presented in Figure 29. These tests were performed on cells from the same lot as those used for the rotating test and compared with other readily available silicon solar cells, including the Heliotek standard cell used for calibration in this report. The total intensity of the source was measured by the Eppley Pyrheliometer These results show the expected linear relation as well as the unusually good agreement between the different types of solar cells.

### 7.4.2 Discussion of Test Results

The plotted peak values of the rotating solar cell always appeared to a normal incident angle. The I-V curves determined from the one sun test were compared with corresponding I-V curve obtained during the one sun calibration test. This comparison showed that the short circuit currents were identical and the open circuit voltages exhibited the expected temperature dependence. This comparison confirmed the very short response time for the cells even with the very narrow bandpass filters as well as illustrated that the peak values can be predicted from the non-rotating one sun calibration.

#### 7.4.2.1 Voltage - Current Relationship

It has been shown that open circuit voltage is not a prime function of intensity but is linearly related to temperature (Ref. 1, 2, etc.). Similarly, the short circuit current is assumed to be linearly related to

intensity and relatively unaffected by temperature. Basic references generally show a slight increase in short circuit current with increasing temperature; however, implied in the presentation of these characteristics are the assumptions of constant flux intensity and negligible series resistance. From these basic considerations the test results might be expected to show a decrease in open circuit voltage with the increasing equilibrium temperature caused by the increased insolation and similarly a proportional increase in short circuit current caused by the linear dependence of short circuit current on intensity.

7.4.2.2 Open Circuit Voltage

Figure 28 illustrates that the open circuit voltage varied as predicted above. Also presented on this figure is the similar curve from Evans (Ref 1) as typical of silicon solar cells. The agreement of these curves illustrates that these results appear consistant enough to suggest that the open circuit voltage can be used as a rough check on the cell's temperature measurement in the temperature ranges herein considered.

7.4.2.3 Short Circuit Current

Continued examination of the characteristic curves (Figures 20 to 26) show that the short circuit current does not necessarily follow the simple prediction suggested above. Figure 29 is the result of a series of tests performed at constant temperature at various intensities. This test verifies the approximate linear dependence of short circuit current with intensity. This appears contradictory to the results reported for the rotating tests; however, the combined effects of increasing temperature and increasing insolation as well as the effect of the cell's series resistance has not been discussed.

The results presented herein can be readily explained by referring to the discussion of series resistance presented by Wolf and Raushenbach (Ref. 9). The solar cells tested have a typical series resistance of approximately

one ohm (Ref 12). It is also to be noted that the leads from the rotating fixture and the associated electrical contacts necessarily cause approximately one ohm of equivalent series resistance. Wolf states that at light intensities where the product of internal series resistance and terminal current exceeds 250 mv, the short circuit current can no longer be considered identical to the light generated current. This statement is substantiated by the results of the rotating tests. Assuming a two ohm series resistance, the maximum short circuit current which can be obtained and still follow the linear relationship is 125 ma. It is also expected that as the cell temperature rises this value will drop significantly. The test results verified that if the one sun short circuit current was less than 20 ma, the one, three, and six sun tests would yield results that conform to the linear relationship. However, if the short circuit current exceeded the limiting value the short circuit current not only showed a deviation from the linear relationship but showed a decrease with increasing cell temperature. The decrease is not caused directly by the insolation but by the resulting increase in cell temperature.

Figure 30 from Reference 9 illustrates the photovoltaic output characteristics of two different solar cells taken at five values of solar irradiance between 50 $mW/cm^{-2}$ to 400 $mW/cm^{-2}$. One of these solar cells is a gridded solar cell with a series resistance of 0.38 $\Omega$ while the other solar cell is a nongridded solar cell having a series resistance of about 3.5 $\Omega$. This figure clearly illustrates that at light intensities high enough so that the product of internal resistance and terminal current exceeds 250 mV, the short circuit current can no longer be considered identical to the light generated current. The light generated current for cases where the terminal current exceeds this value can only be obtained by employing a negative bias on the cell.

An increase in cell temperature has the effect of translating the characteristic curve in the direction of decreasing voltage. Translating the curves in Figure 30 illustrate the temperature effect on short circuit current and power. It is noticed that for curves which have a very sharp knee (low series resistance) the short circuit current will remain almost constant with

increasing temperature (up to some limiting temperature) while for high series resistance cells the short circuit current can drop significantly with increasing temperature.

The results of the equilibrium temperature tests clearly illustrate this phenomenon; however, a complete experimental evaluation of these parameters exceeds the scope of the present effort. It is apparent from these results that at high solar intensities the series resistance becomes very important in the analysis of solar cell outputs. These results also confirm the fact that the cells with the smallest series resistance are preferable for high fluxes; however, optimization analyses must not lose sight of the fact that lowering the series resistance of the cells tends to increase the susceptibility to radiation damage.

7.4.2.4 Angle of Incidence

Figure 27 is a plot of current output as a function of incident angle for various load resistances obtained from the recorder trace for filter #5. This curve is typical of the results observed for all solar cell assemblies tested. The shape of these curves can be expected by examination of the basic solar cell equation.

$$I = I_L - I_o \left[ e^{\frac{q}{nkT}(V + IR_S)} - 1 \right] \qquad (32)$$

From this equation it is observed that if the exponent of the exponential is approximately equal to zero, the current varies identically with the light generated current; however, for high load resistance this does not hold. From these results it is apparent that determination of the cell output for a rotating satellite requires a complete investigation of the solar cell. It is observed that the current output remains rather flat, at high load resistances, over a wide range of incidence angles which indicate that the variation of power output from a tilted or rotating solar array is a function of the load resistance as well as the intensity incident on the cell.

### 7.4.2.5 Equilibrium Temperatures

Table 6 presents the extrapolated short circuit current, the open circuit voltage, and the corresponding equilibrium temperatures obtained on the rotating tests. The temperatures reported deviated somewhat from the predicted values which can be contributed to the many variables such as unknown thermal properties, UV absorption, IR transmission bands, heat leak through the mounting fixture, heat leak from the conduction leads, and insulation properties, and uncertainty in flux intensity. It is apparent, however, that the narrow bandpass filters provided substantial thermal control. Examination of the bandpass regions of the filters shows that filters 1, 2, 3, and 4 pass approximately equal energy levels, especially when including the IR bandpass. The wide bandpass filter, filters 5 and 6 show much higher temperatures as well as much lower output at six suns. All the filters tested show approximately a three-fold increase in short circuit current from one to three suns. However, the effects of series resistance, temperature, and bandpass intensity cause severe deviations as the insolation was increased from three to six suns. The results clearly illustrate the advantage of selective interference filters as a thermal control device as well as the importance of solar cell thermal control.

### 7.4.2.6 Reflective Coatings

The results from the reflective coating area fraction tests show results similar to those reported for the filters and verified the possibility of their use as a thermal control device.

### 7.4.2.7 Approximate Peak Power Points

Table 6 shows the approximate peak power points calculated from the I-V characteristic curves. These values indicate that for rotating solar cells a clear coverglass with an AR coating would produce the best results for a normal solar intensity of one sun (AMZ). At three suns, the reflective

coating with 20 percent area fractions showed the highest available power, and from the reflective coating analysis it is expected that again a clear coverglass with an AR coating might still improve the peak power output. When the solar intensity was increased to six suns, the selective interference filters (particularly filter #3) appeared to give the best output power. From these results, it is expected that at solar intensities less than three suns, an ideal filter with a bandpass range matched to the entire solar cell response curve and having maximum IR suppression would produce the best results. At increasing solar intensities, narrowing of the bandpass range is indicated. These results determined from tests using only the one type of silicon solar cells but should be generally applicable.

## 7.5 CALIBRATION TESTS

In addition to the results from the rotating experiments, the one sun calibration tests showed that no apparent degradation occurred to the cells as a result of the exposure to the elevated temperatures and high solar intensities. The one sun I-V curves obtain following the rotating test showed excellent agreement with the original calibration curves. Following all tests, several test filter-cell-stacks were exposed to a high humidity soak (100 percent humidity at 100°C) for a period of eight hours followed by eight hours on the laboratory shelf; the cells were re-calibrated at the one sun condition with no noticeable deviation in performance.

## 7.6 ENVIRONMENTAL TEST

All solar cell covers supplied by Optical Coating Laboratory, Incorporated, are subjected to the environmental tests as delineated in Appendix G. These tests seemed to negate the need for further environmental testing and supplied confidence in the durability and adaptability of the filter for solar cell power systems. Additional humidity tests were performed following the equilibrium temperature experiment and confirmed the fact that the filters are insensitive to basic environmental effects. It would be desirable to extend this testing to include the effect of radiation damage such as might be encountered in spacecraft missions.

# SECTION 8
# CONCLUDING REMARKS

The results of this investigation indicated that filter spectral characteristics can be adequately predicted, for most applications, from the elementary analysis presented. Also, the elementary analysis performed for highly reflective coatings appears to agree with the experimental results.

Both the experimental and the analytical efforts indicate that selective interference filters were superior to reflective coatings as a means of thermal control where the objective is to maximize the available power output.

The analytical optimization analysis illustrated the expected trend of reducing the bandpass region for close sun approach. These results illustrate that if the bandpass region could be made variable, the power output would show an increase with increasing insolation; however, filter optimized for a one sun intensity would exhibit a continuous decrease due to the rapidly rising cell temperature.

The equilibrium temperature tests substantiated the analytical efforts. These tests also showed that spinning solar cell performance can be predicted from average temperature and specific insolation consideration. The experimental tasks did illustrate the importance of series resistance on solar cell output at high temperatures and high insolation. Analysis of the experimental data indicated the need for detailed solar cell testing at high temperature and high levels of insolation to complete the investigation of solar cell performance as a function of various temperature control devices.

## SECTION 9

## REFERENCES


1. Evans, W.; and Menetry, W.R.: Energy Conversion Systems Reference Handbook. Vol. V. Direct Solar Conversion. WADD Technical Report, 60-699, September 1960.

2. Baker, J.K.: Temperature Control Techniques for Solar Energy Converters. ASD-TR-689, February 1962.

3. Thelen, A.: An Infrared Multilayer Monochrometer Optical Coating Laboratory Internal Report.

4. Thelen, A.: Multilayer Filters with Wide Transmittance Bands. Journal of the Optical Society of America. Vol. 53, no. 11, 1963.

5. Thelen A.: The Use of Vacuum Deposited Coatings to Improve the Conversion Efficiency of Silicon Solar Cells in Space. Progress in Astronautics and Rocketry, Vol. 3. Academic Press, New York, New York, 1962.

6. Thelen, A.: Private Communication. Optical Coatings Laboratory, Inc.

7. Generate Specification Guide for Solar Cell Covers. Optical Coating Laboratory, Inc. Effective January 1, 1966.

8. Cobb, M. W.; Cummings, W. S.; and Fairbanks, J.W.: The Feasibility of a Programmed Heat Shield for Solar Cell Performance Control. Philco WDL-TR-2623, October 15, 1965.

9. Wolf, M.; and Rauschenbach, H.: Series Resistance Effects on Solar Cell Measurements. Advanced Energy Conversion. Vol. 3, 1963, pp 455-499.

10. Ralph, E.L.; and Wolf, M.: Effects of Antireflection Coatings and Coverglass on Silicon Solar Cell Performance. Presented at the Photovoltaic Specialists Converence, Cleveland, Ohio, June 2, 1964.

11. Johnston, P.A.: Laboratory Experiments on the Performance of Silicon Solar Cells at High Solar Intensities and Temperatures. NASA TN D-2733, March 1965.

12. Pearson, J.: Private Communication. Hoffman Electronics, Inc.

13. Sears, F.W.: Optics. Addison-Wesley Press, Inc., 1949.

14. McAdams, W.H.: Heat Transmission. Third ed. McGraw-Hill Book Co., Inc., 1954.

Table 1 Averaged Cut-On and Cut-Off Points from Spectrophotometer Measurements

(Wavelengths in Microns)

| Incident Angle | | Filter #1 | Filter #2 | Filter #3 | Filter #4 | Filter #5 | Filter #6 |
|---|---|---|---|---|---|---|---|
| Cut On $\lambda_1$ | 0° | .405 | .590 | .701 | .810 | .390 | .405 |
| | 15 | .403 | .584 | .694 | .799 | .389 | .404 |
| | 30 | .397 | .572 | .679 | .777 | .385 | .401 |
| | 45 | .390 | .562 | .660 | .754 | .378 | .394 |
| Cut Off $\lambda_2$ | 0° | .583 | .694 | .810 | — | 1.09 | 1.09 |
| | 15 | .577 | .687 | .800 | — | 1.08 | 1.09 |
| | 30 | .564 | .668 | .777 | — | 1.06 | 1.07 |
| | 45 | .534 | .629 | .737 | — | 1.01 | 0.02 |
| IR Cut On $\lambda_3$ | 0° | 1.21 | 1.23 | 1.28 | — | 1.47 | 1.49 |
| | 15 | 1.195 | 1.22 | 1.27 | — | 1.46 | 1.48 |
| | 30 | 1.16 | 1.19 | 1.21 | — | 1.41 | 1.44 |
| | 45 | 1.12 | 1.17 | 1.19 | — | 1.33 | 1.38 |
| Substrate Thickness | | .304 cm | .304 cm. | .304 cm | .304 cm | .152 cm | .152 cm |

Table 2 List of Test Equipment

1. Strong Arcomatic Solar Simulator
   Type 75000-2 Serial No. 54943

2. Optical Coating Laboratory, Incorporated Solar Simulator
   Model 31

3. Sanborn Multi-Channel Recorder
   Model 350-100B Serial No. 1170

4. Simpson Direct Current Milliampmeter
   Model 373

5. Weston Direct Current Milliampmeter
   Model 931 Serial No. 65245

6. Helipot Precision Potentiometer
   Laboratory Model T-10-A

7. EICO Resistance Decode Box
   Model 117

8. Leeds and Northrup Wheatstone Bridge
   Model No. 4735

9. Moseley X-Y Recorder
   Model 135

10. Eppley 180 degree Pyrheliometer (Calibration 8.65 millivolts/cal $cm^{-2}$ $min^{-1}$) Model 50 Serial No. 4311

11. Heliotek Standard Solar Cell
    Cell Serial No. 170

12. Perkin-Elmer Spectrophotometer
    Model 350 Serial No. 197

13. Perkin-Elmer Spectrophotometer
    Model 13U Serial No. 192

14. Bausch & Lomb Grating Monochrometer
    Model 33-86-25

15. Vacuum Chamber with Instrumentation

16. Hoffman (type N:20 C G) Solar Cells - Efficiency 58 ma @ 400 mv
    (1 x 2 centimeter N/P silicon cells with grid lines on the short dimension)

Table 3 Optimization Results

Optimum "Cut On" and "Cut Off" Wavelengths for Ideal Filter

Non-Rotating Solar Cell

| $N_S$ | $\lambda_1$ | $\lambda_2$ | $P^1_{ave}$ | T |
|---|---|---|---|---|
| -- | Microns | Microns | $MW/CM^2$ | $^oK$ |
| 1 | 0.49 | 1.025 | 12.47 | 301 |
| 3 | 0.62 | 0.98 | 18.45 | 352 |
| 6 | 0.73 | 0.96 | 19.95 | 364 |

Rotating Solar Cell

| $N_S$ | $\lambda_1$ | $\lambda_2$ | $P^1_{ave}$ | T |
|---|---|---|---|---|
| -- | Microns | Microns | $MW/CM^2$ | $^oK$ |
| 1 | 0.44 | 1.08 | 5.93 | 231 |
| 3 | 0.48 | 1.025 | 12.16 | 300 |
| 6 | 0.56 | 1.005 | 16.45 | 336 |

[1] $P_{ave}$ - average power output per revolution

Table 3 Optimization Results

Optimum "Cut On" and "Cut Off" Wavelengths for Ideal Filter

Non-Rotating Solar Cell

| $N_S$ | $\lambda_1$ | $\lambda_2$ | $P^1_{ave}$ | T |
|---|---|---|---|---|
| -- | Microns | Microns | $MW/CM^2$ | $^oK$ |
| 1 | 0.49 | 1.025 | 12.47 | 301 |
| 3 | 0.62 | 0.98 | 18.45 | 352 |
| 6 | 0.73 | 0.96 | 19.95 | 364 |

Rotating Solar Cell

| $N_S$ | $\lambda_1$ | $\lambda_2$ | $P^1_{ave}$ | T |
|---|---|---|---|---|
| -- | Microns | Microns | $MW/CM^2$ | $^oK$ |
| 1 | 0.44 | 1.08 | 5.93 | 231 |
| 3 | 0.48 | 1.025 | 12.16 | 300 |
| 6 | 0.56 | 1.005 | 16.45 | 336 |

[1] $P_{ave}$ - average power output per revolution

Table 4 Normal Cut-On and Cut-Off Wavelengths From Transmissivity and Reflectivity Measurements (Wavelengths in Microns)

| Filter Type | Cut-on - $\lambda_1$ | | Cut-off - $\lambda_2$ | | Cut-on - $\lambda_3$ | |
|---|---|---|---|---|---|---|
| | $\tau$ * | r * | $\tau$ | r | $\tau$ | r |
| 1 | .405 | .403 | .583 | .579 | 1.21 | 1.20 |
| 2 | .590 | .588 | .694 | .693 | 1.23 | 1.22 |
| 3 | .701 | .692 | .810 | .799 | 1.28 | 1.24 |
| 4 | .808 | .815 | - | - | - | - |
| 5 | .390 | .390 | 1.09 | 1.09 | 1.47 | 1.47 |
| 6 | .405 | .404 | 1.095 | 1.09 | 1.49 | 1.48 |

* $\tau$ - results obtained from transmittance measurements

r - results obtained from reflectivity measurements

Table 5 Calculated Cut-On Points ($\lambda_1$) as a Function of Incident Angle
(Wavelengths in Microns)

| Incident Angle | Filter #1 | Filter #2 | Filter #3 | Filter #4 | Filter #5 | Filter #6 |
|---|---|---|---|---|---|---|
| 0° (known) | .405 | .590 | .701 | .810 | .390 | .405 |
| 15 | .403 | .585 | .695 | .801 | .389 | .404 |
| 30 | .397 | .5715 | .679 | .777 | .385 | .401 |
| 45 | .390 | .553 | .656 | .744 | .379 | .396 |
| 60 | .382 | .532 | .633 | .707 | .375 | .392 |
| 75 | .376 | .517 | .614 | .681 | .371 | .389 |

Table 6 Summary of Rotating Solar Cell Test Results

| Filter Number | Number of Suns | $T_{sink}$ °K | $T_{cell}$ °K | $I_{sc}$ Amp. | $E_{oc}$ Volts | $P_{peak}$ m W |
|---|---|---|---|---|---|---|
| 1 | 1 | 231 | 271 | .017 | .59 | 4 |
| | 3 | 218 | 291 | .051 | .55 | 12.8 |
| | 6 | 233 | 325 | .076 | .475 | 17.8 |
| 2 | 1 | 231 | 267 | .015 | .595 | 3.44 |
| | 3 | 218 | 282 | .045 | .56 | 13.1 |
| | 6 | 233 | 328 | .069 | .48 | 16 |
| 3 | 1 | 228 | 276 | .015 | .575 | 3.2 |
| | 3 | 228 | 280 | .046 | .560 | 13.6 |
| | 6 | 236 | 323 | .095 | .490 | 22.5 |
| 4 | 1 | 228 | 272 | .021 | .580 | 4.8 |
| | 3 | 228 | 284 | .060 | .550 | 16.2 |
| | 6 | 236 | 324 | .105 | .480 | 21.55 |
| 5 | 1 | 231 | 276 | .056 | .600 | 17.2 |
| | 3 | 230 | 291 | .145 | .565 | 29.25 |
| | 6 | 230 | 352 | .128 | .335 | 10.85 |
| 6 | 1 | 231 | 276 | .056 | .600 | 17.2 |
| | 3 | 230 | 287 | .145 | .565 | 29.25 |
| | 6 | 279 | 348 | .128 | .335 | 10.85 |
| 20% Coating | 1 | 218 | 267 | .058 | .610 | 17.2 |
| | 3 | 231 | 285 | .168 | .540 | 37.8 |
| | 6 | 221 | 342 | .076 | .370 | 13.0 |
| 40% Coating | 1 | 218 | 265 | .047 | .625 | 14.95 |
| | 3 | 231 | 283 | .128 | .580 | 26.3 |
| | 6 | 221 | 322 | .088 | .425 | 15.25 |

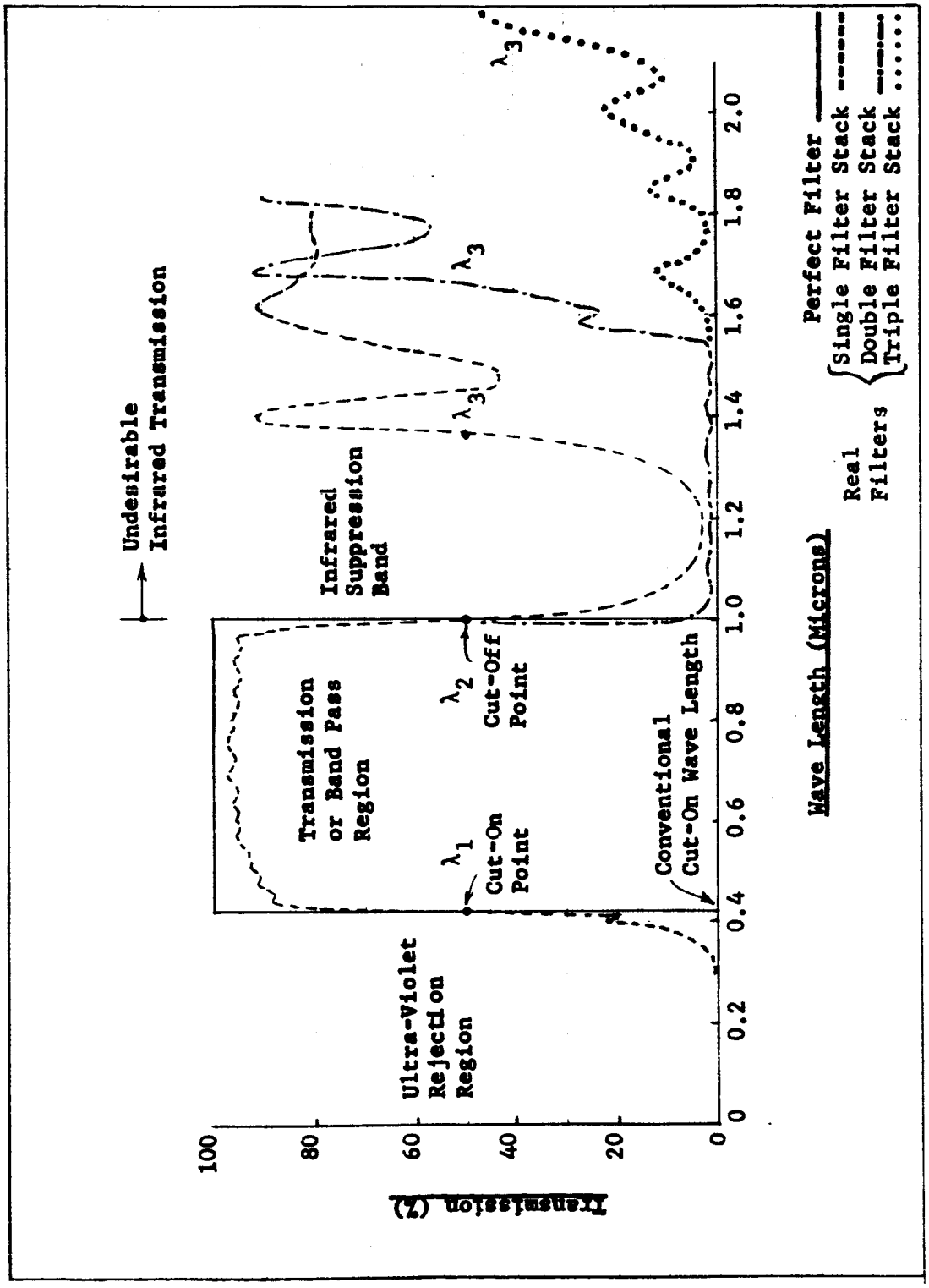


Figure 1 Perfect and Real Filter Characteristics

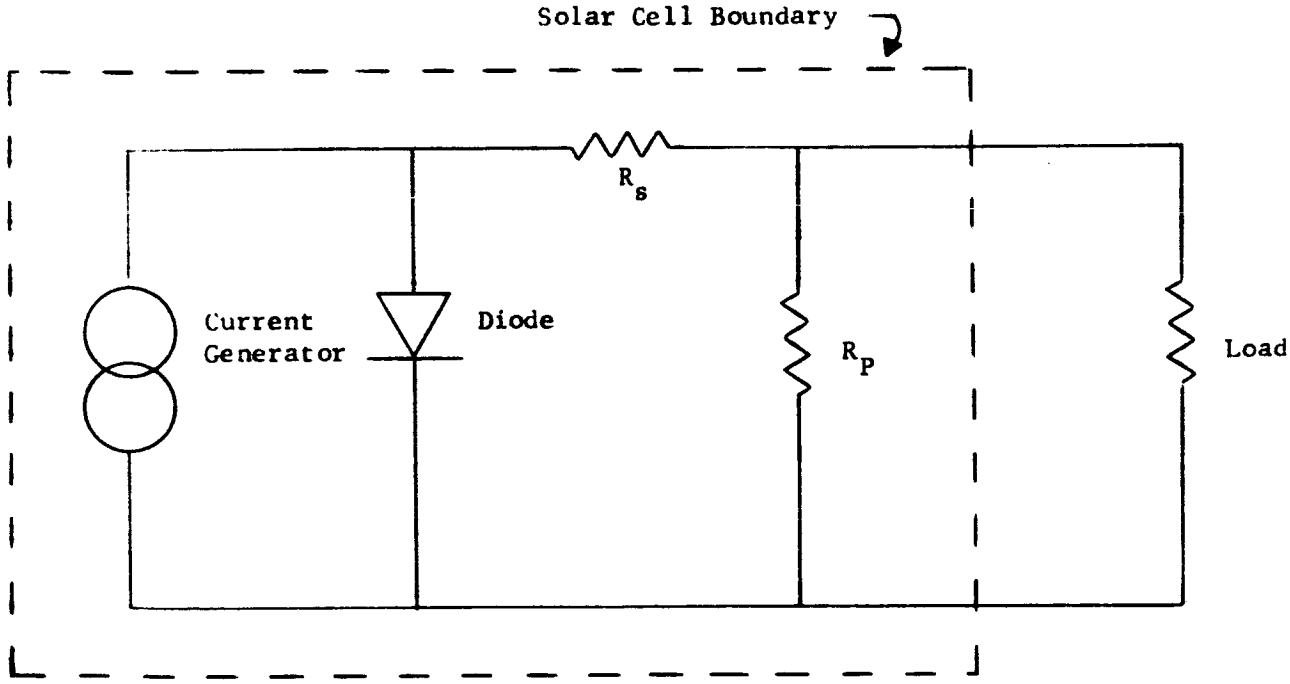


Figure 2 Simplified Equivalent Circuit for Solar Cell

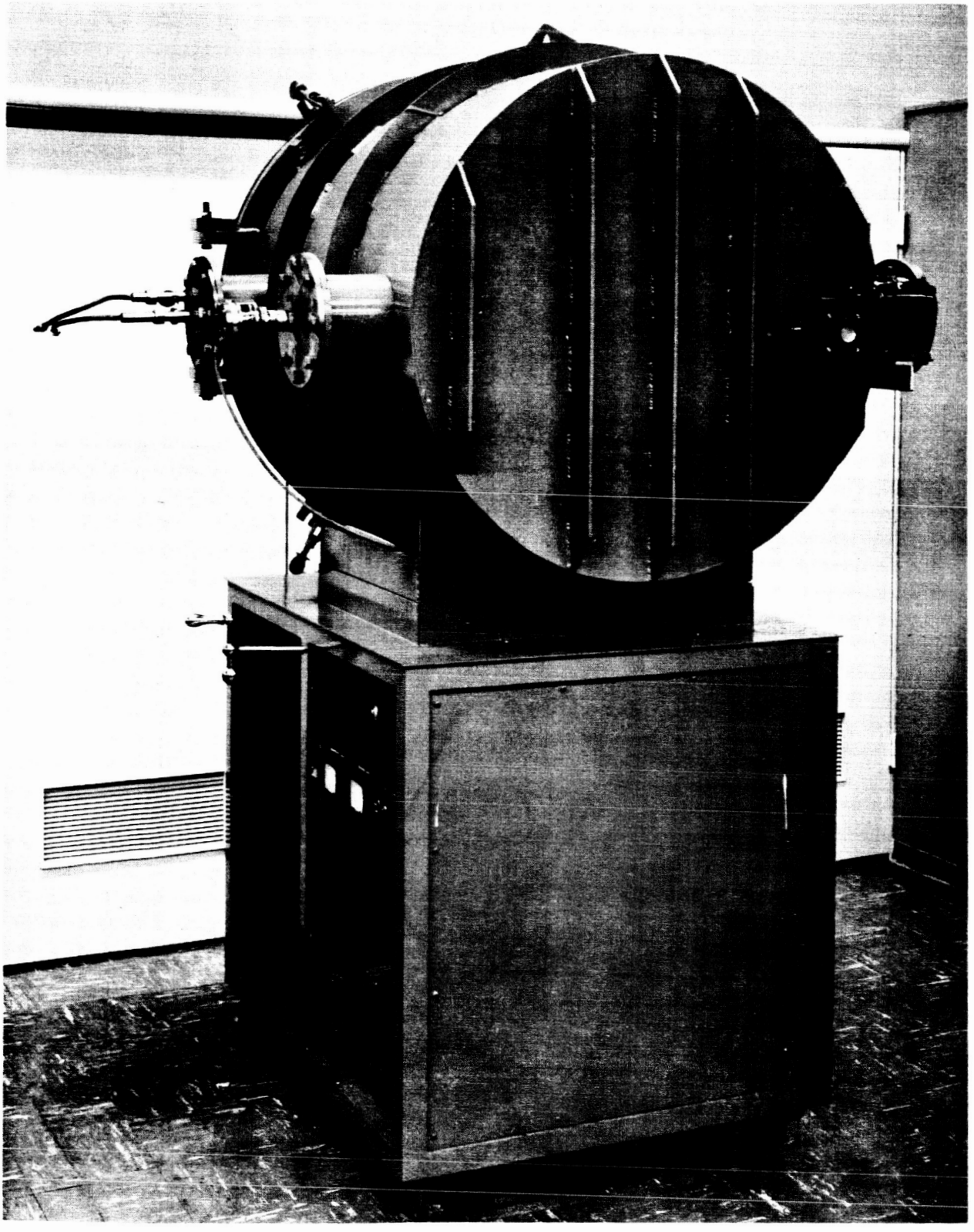

Figure 3 - 3' x 3' Vacuum Chamber and Magnetic Drive

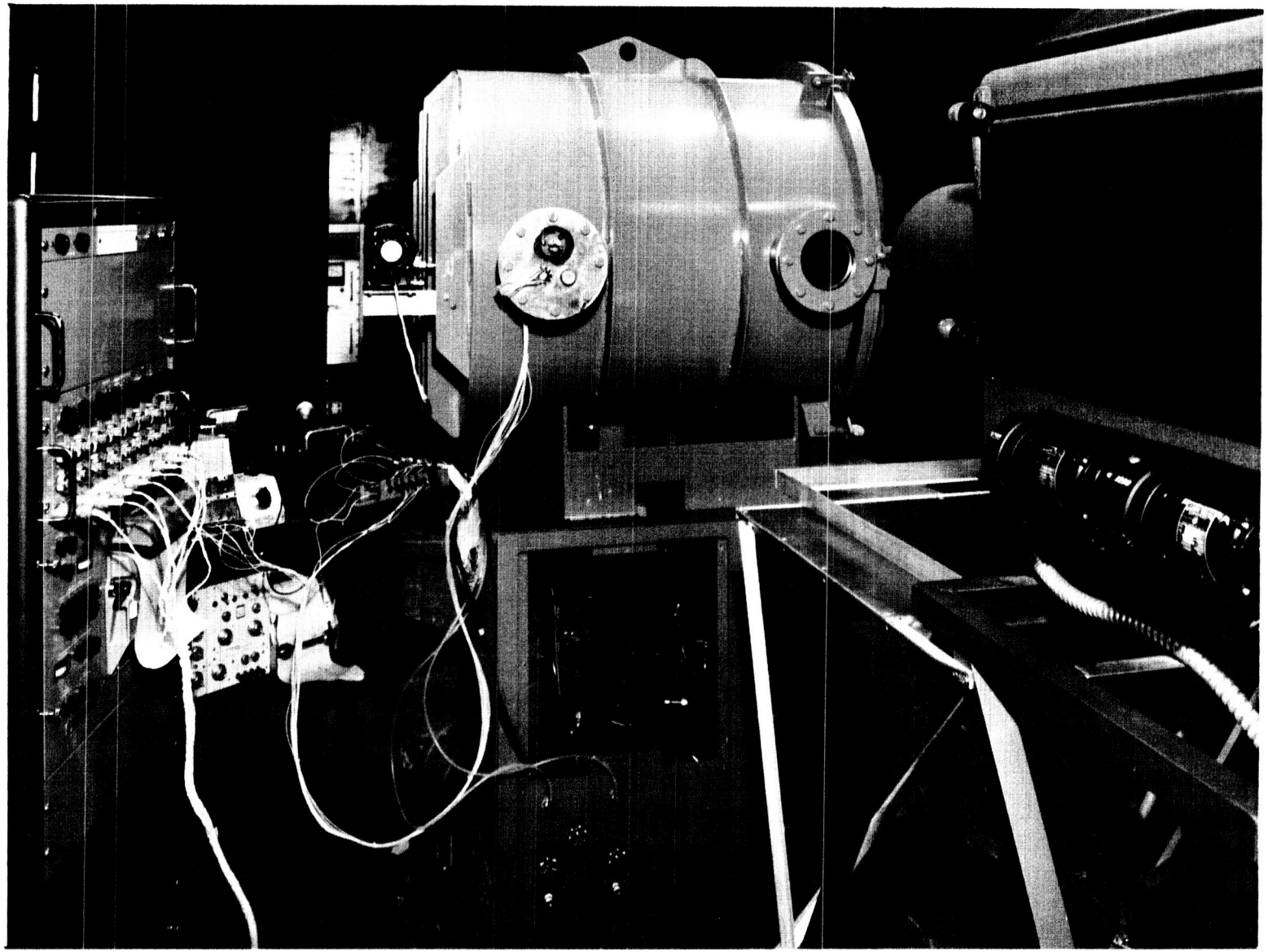

Figure 4 Experimental Test Apparatus

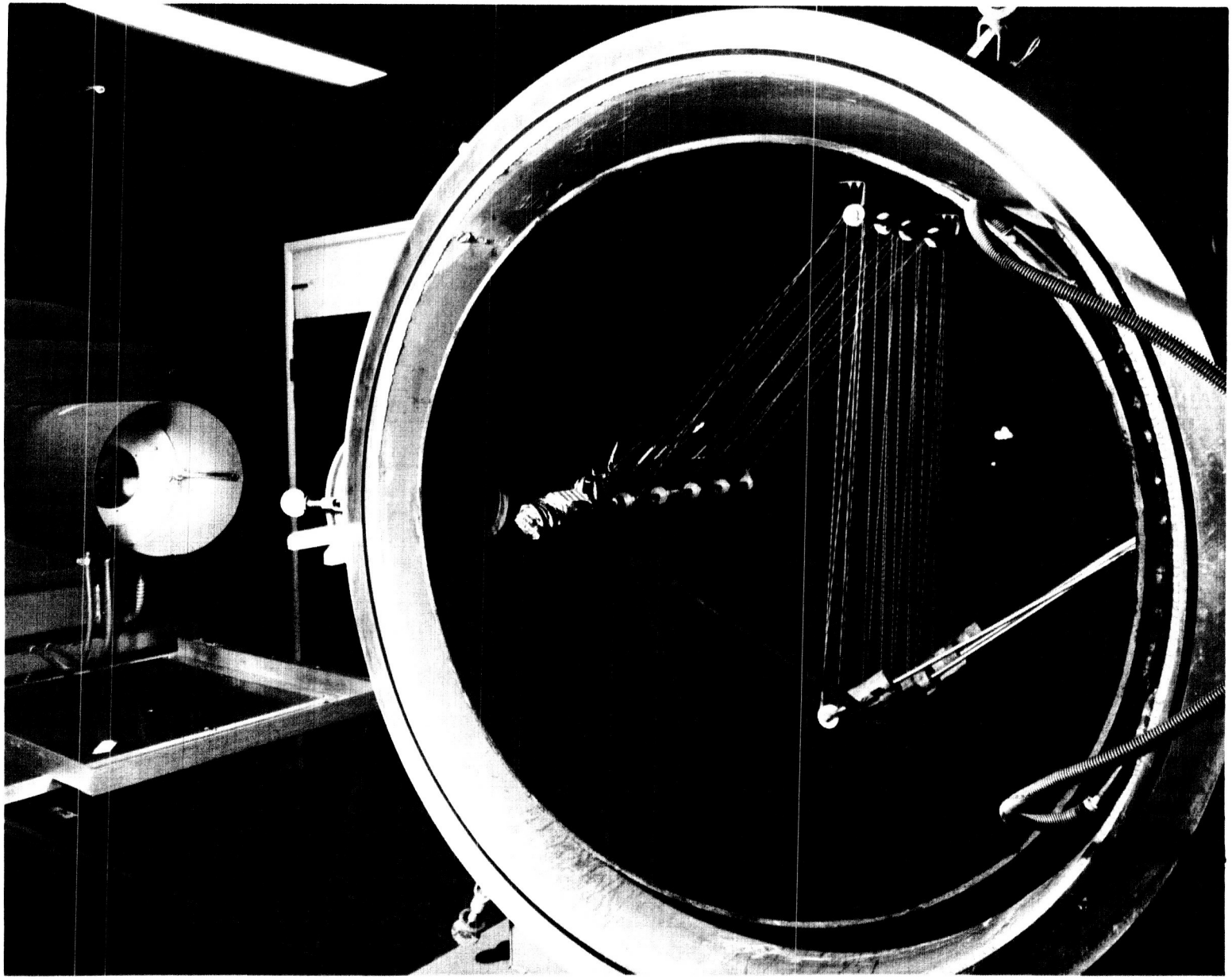

Figure 5 Experimental Test Configuration

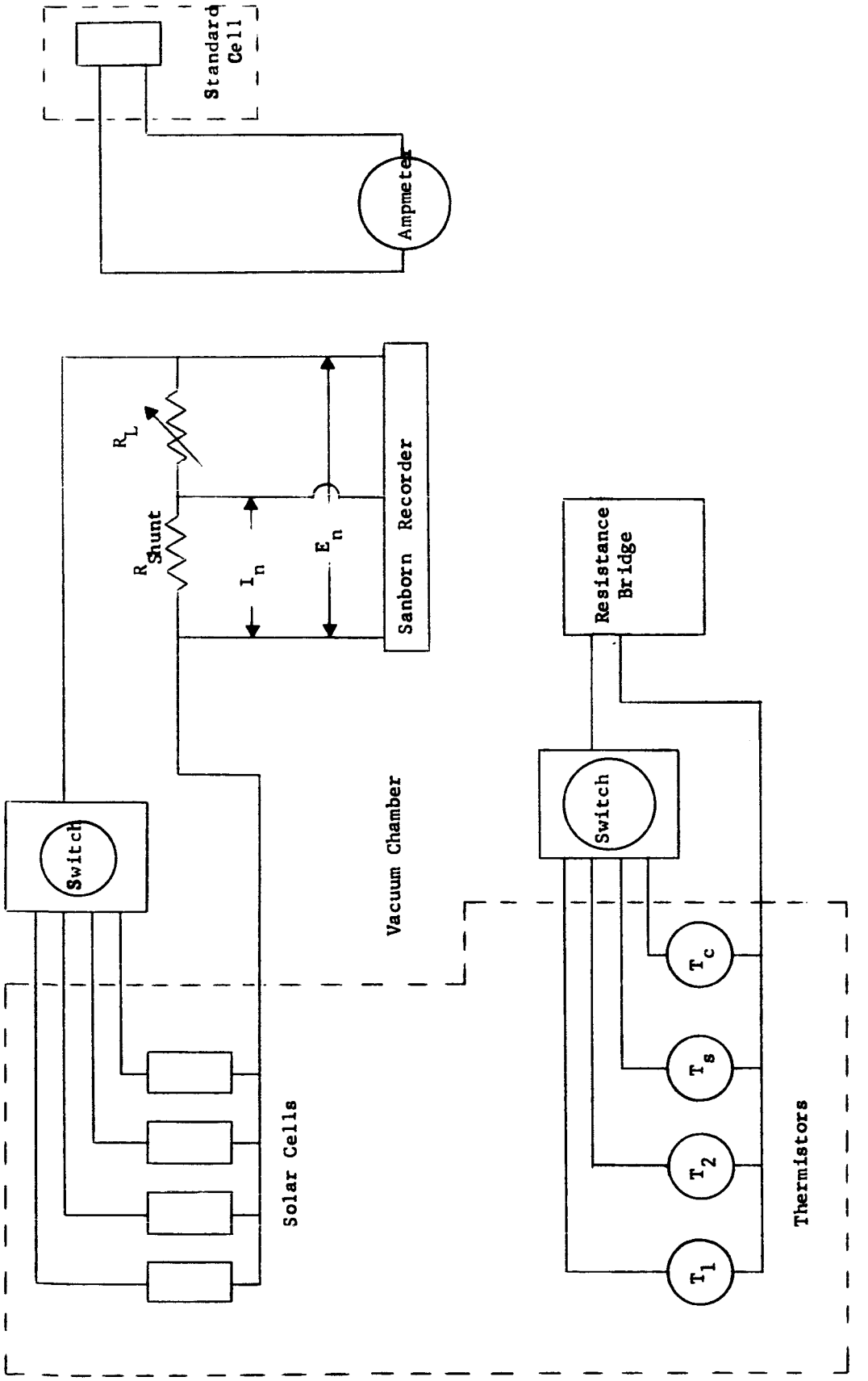


Figure 6 Instrumentation Block Diagram

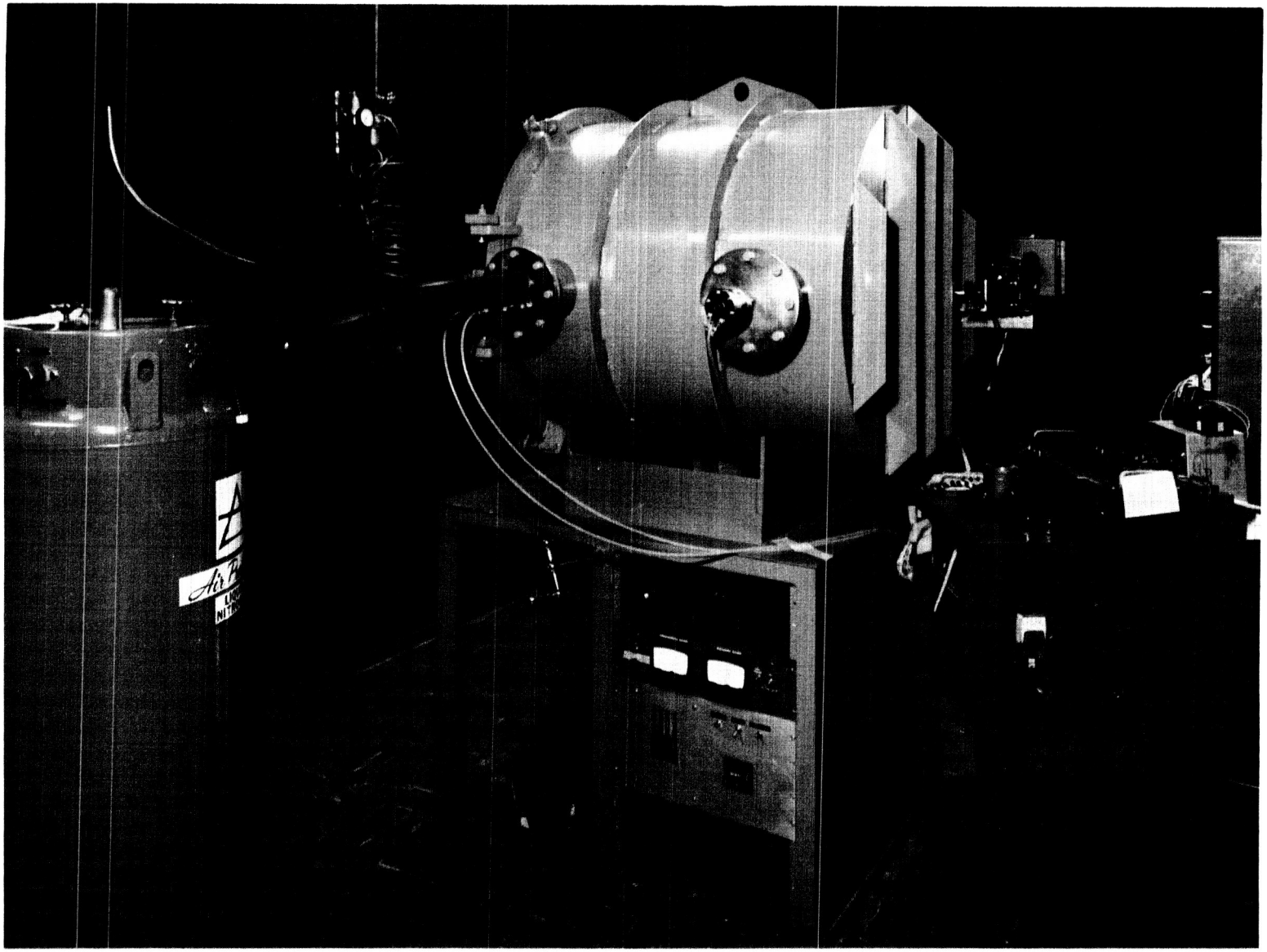

Figure 7 Vacuum Chamber Controls and Instrumentation

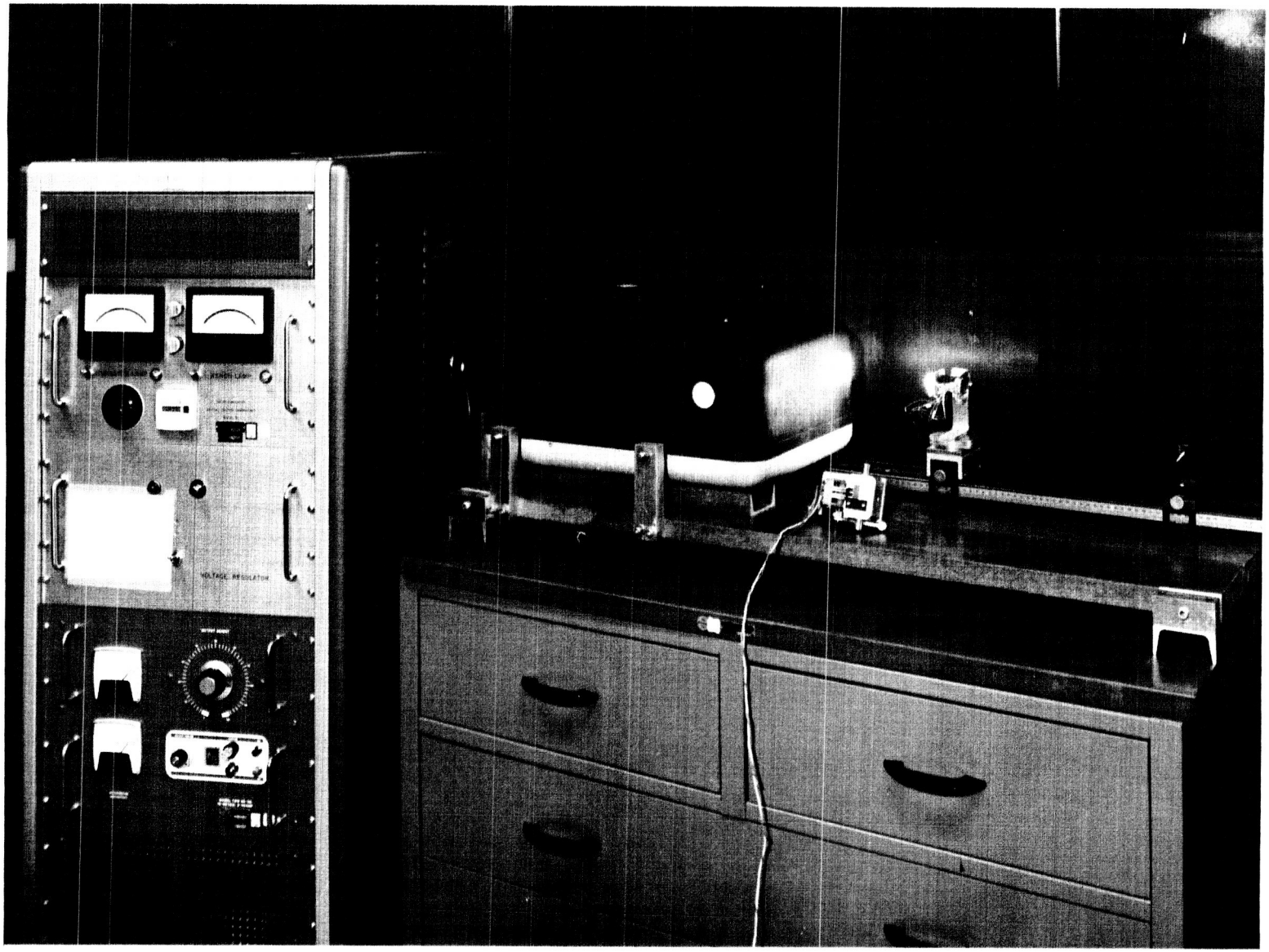

Figure 8 OCLI Solar Simulator

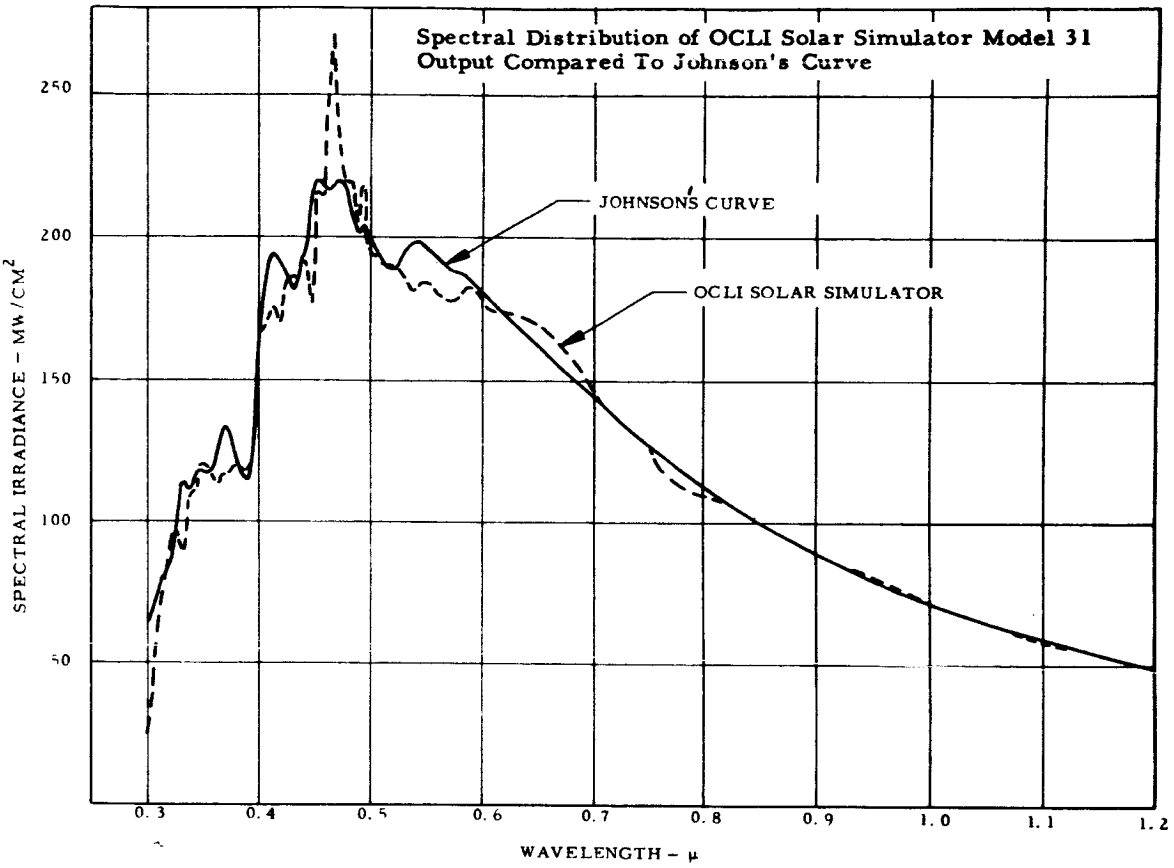


Figure 9 Spectral Distribution of OCLI Solar Simulator (Model 31) Output Compared to Johnson's Curve

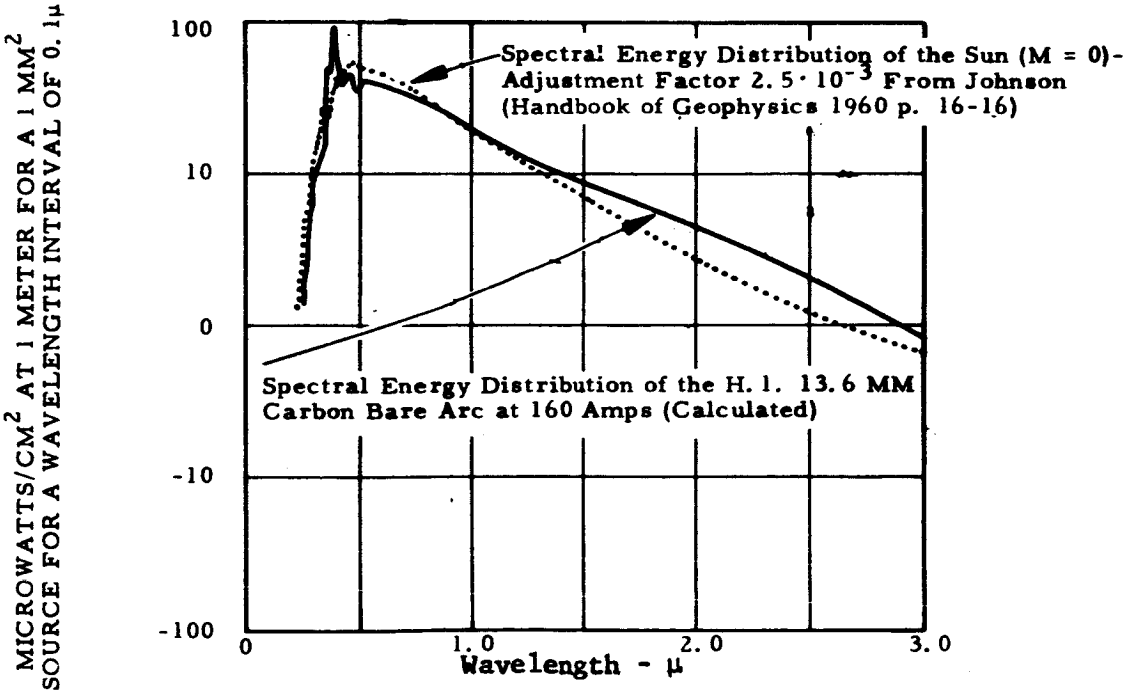


Figure 10 Spectral Distirbution of Carbon Arc Compared with Johnson's Curve

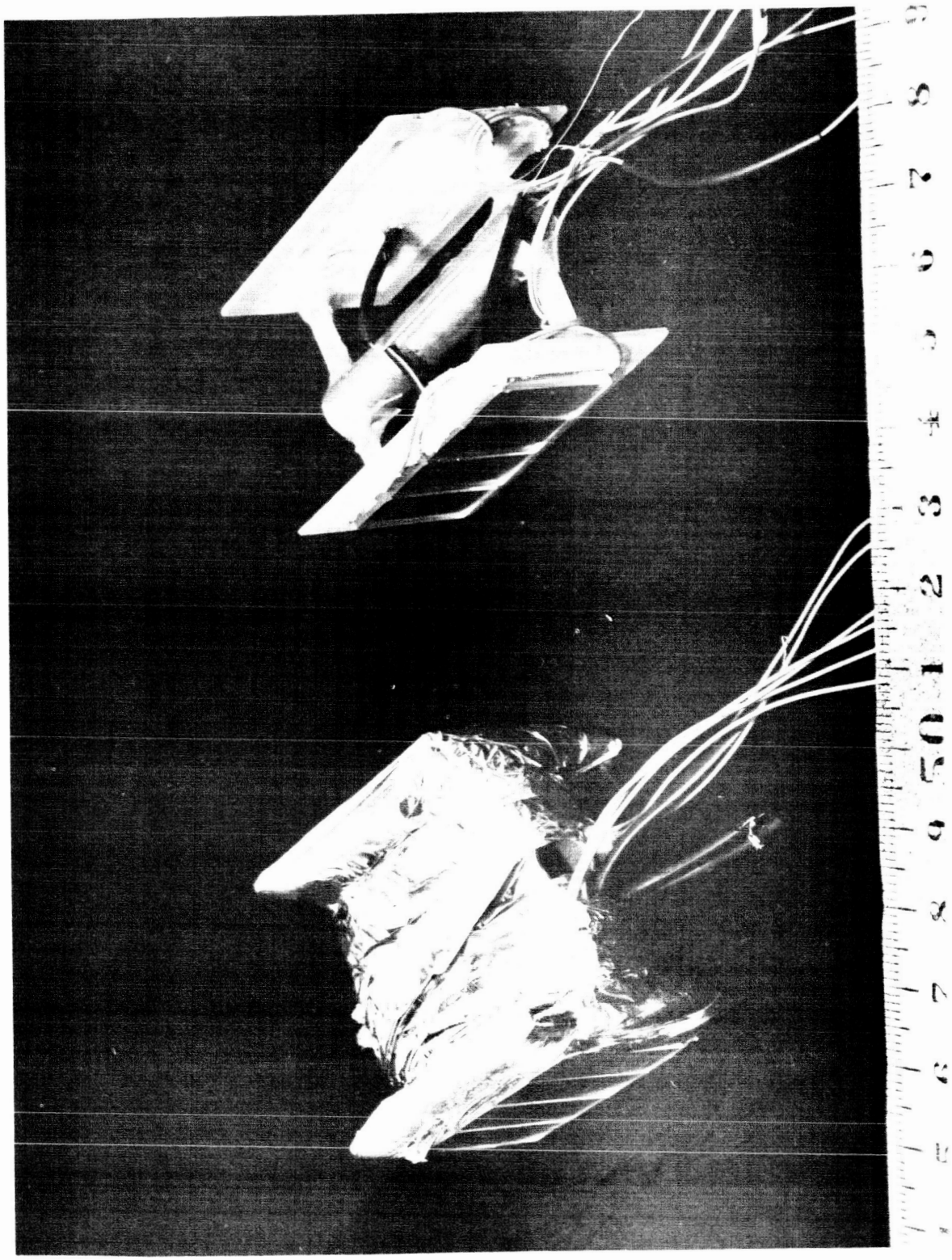

Figure 11 Solar Cell Test Fixtures

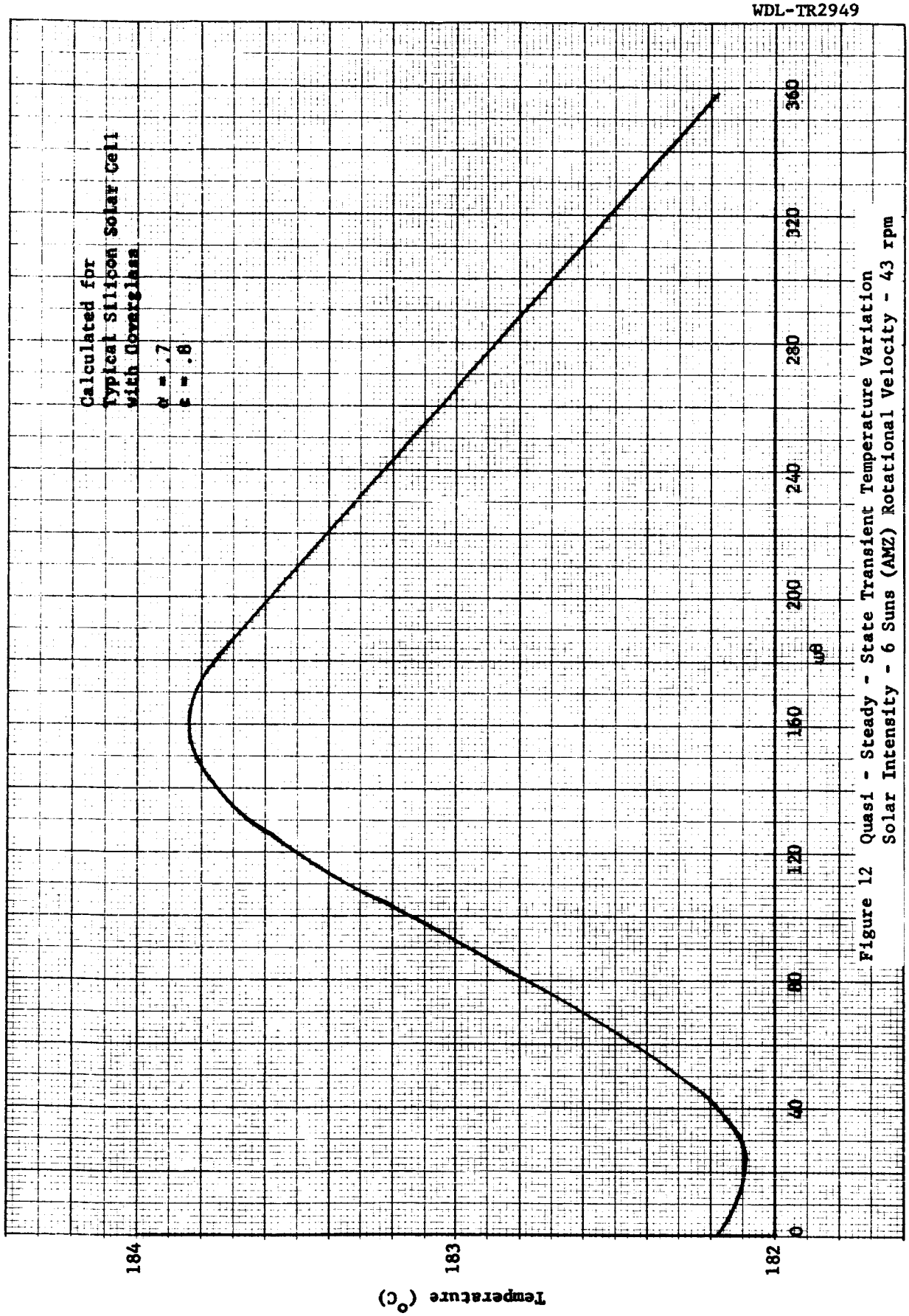


Figure 12 Quasi - Steady - State Transient Temperature Variation
Solar Intensity - 6 Suns (AMZ) Rotational Velocity - 43 rpm

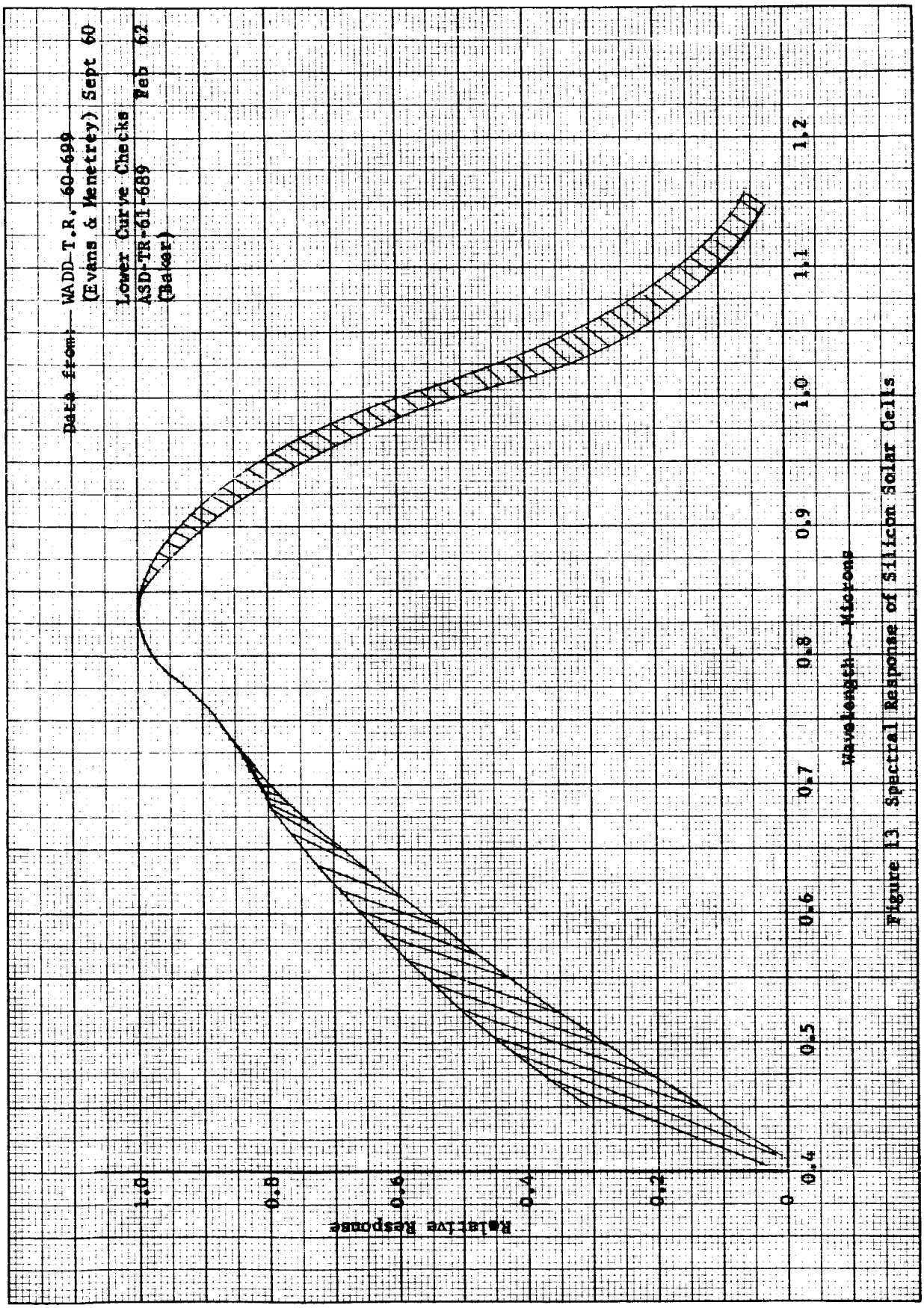


Figure 13 Spectral Response of Silicon Solar Cells

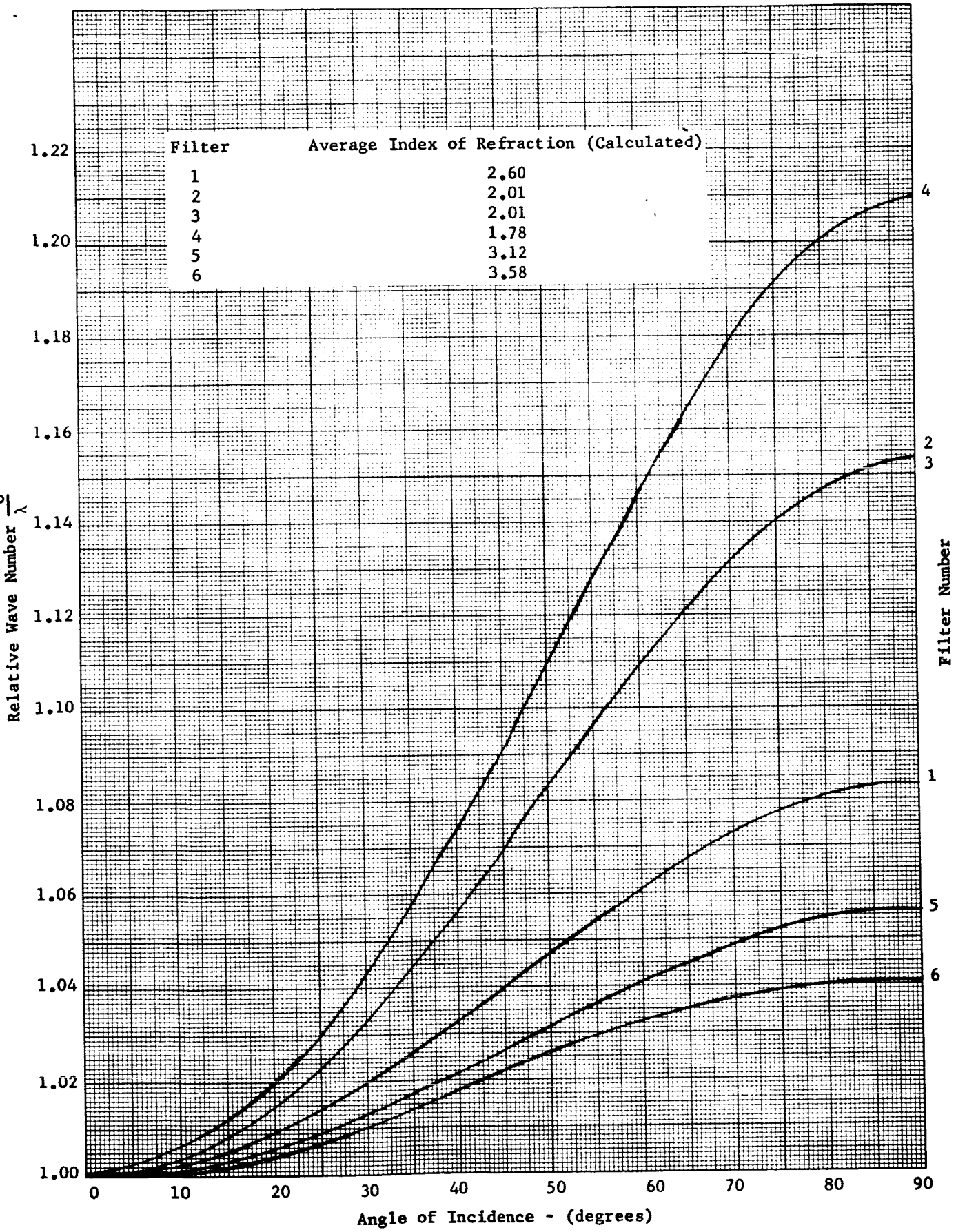


Figure 14 Calculated Spectral Shift vs Relative Wave Number

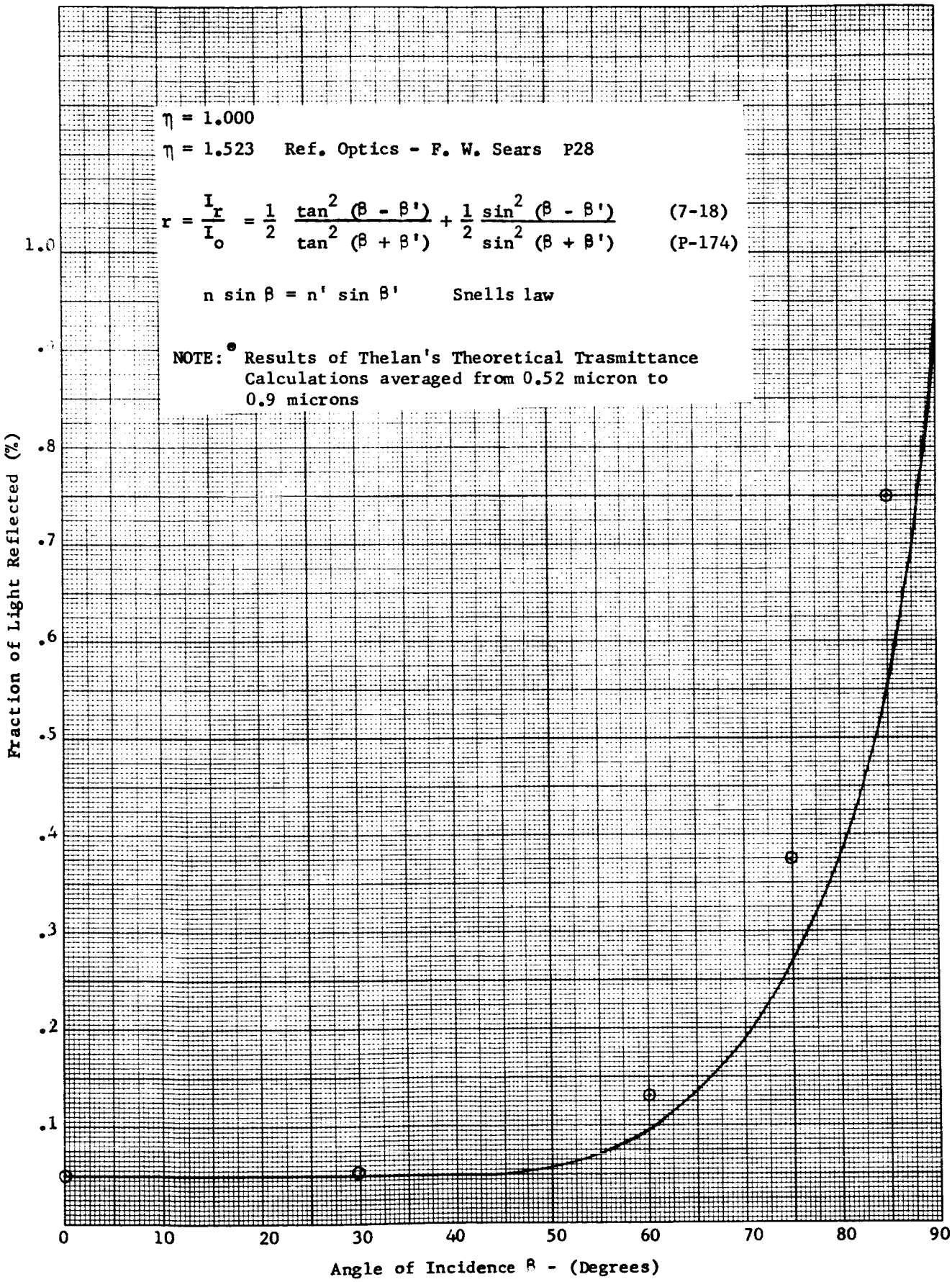


Figure 15 Fraction of Light Reflected vs Angle of Incidence

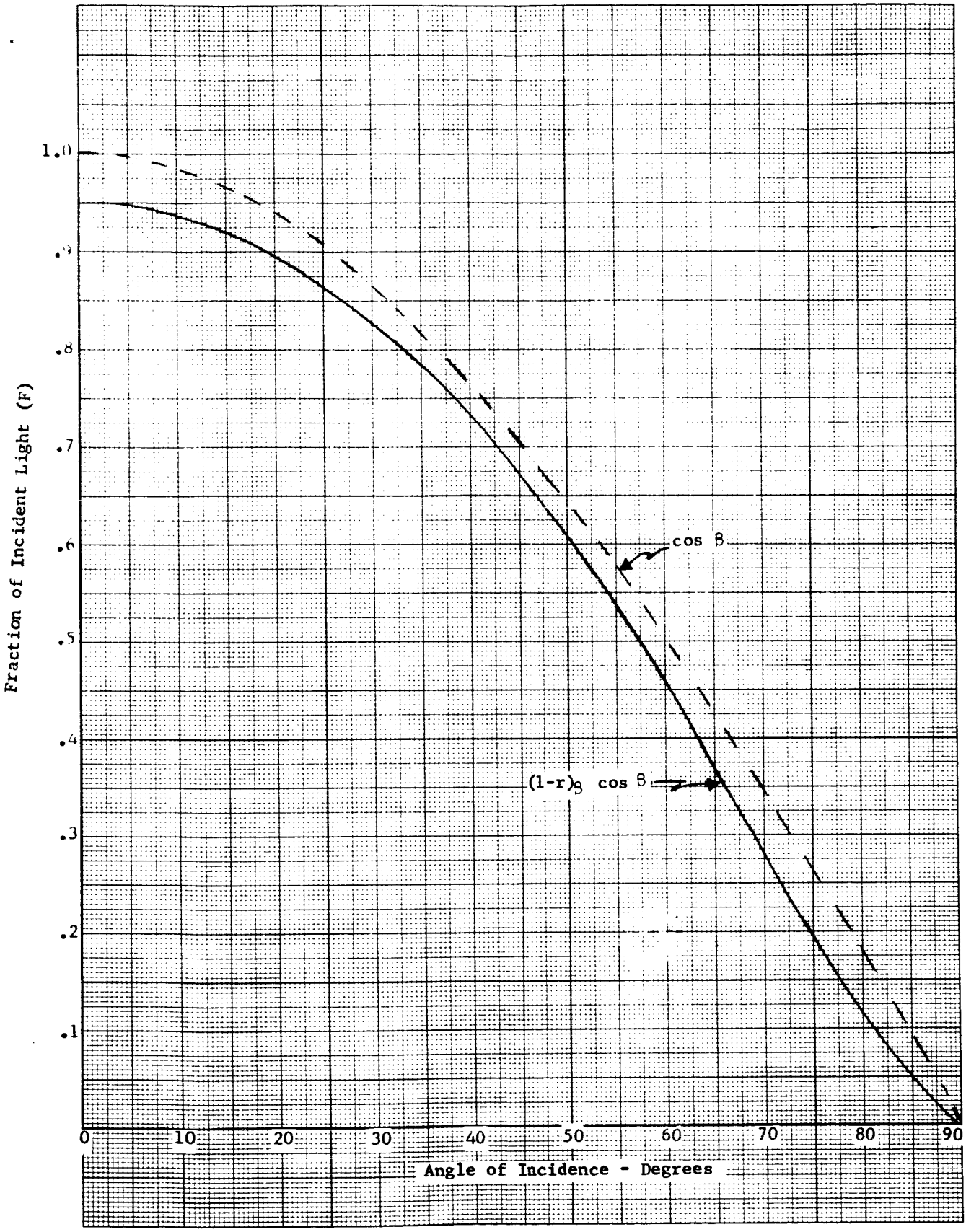


Figure 16 Fraction of Light Passing Front Surface of Solar Cell Cover Glass
$F = (1 - r)_\beta \cos \beta$

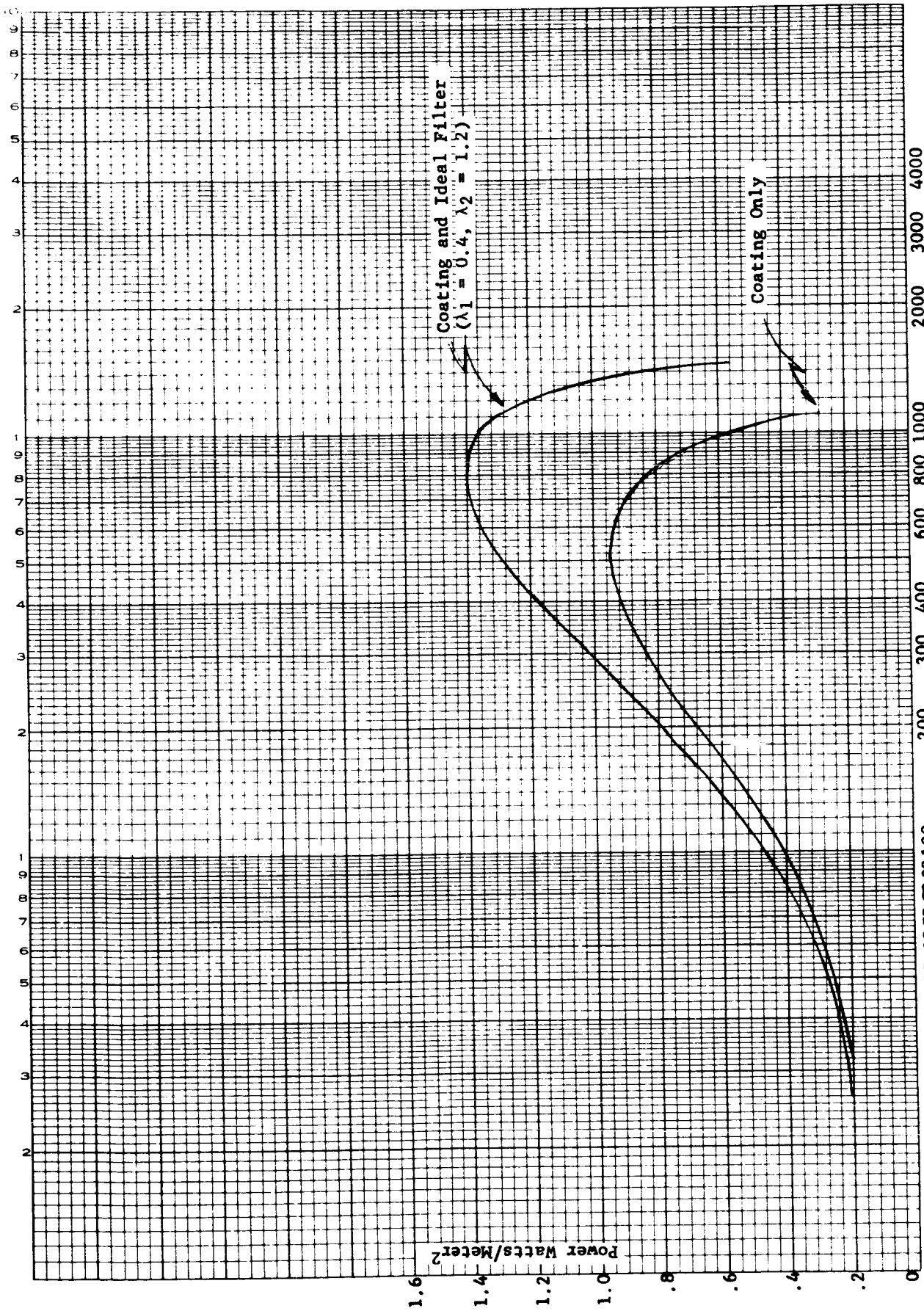


Figure 17 Reflective Coating Optimization Power vs $\eta_a S$

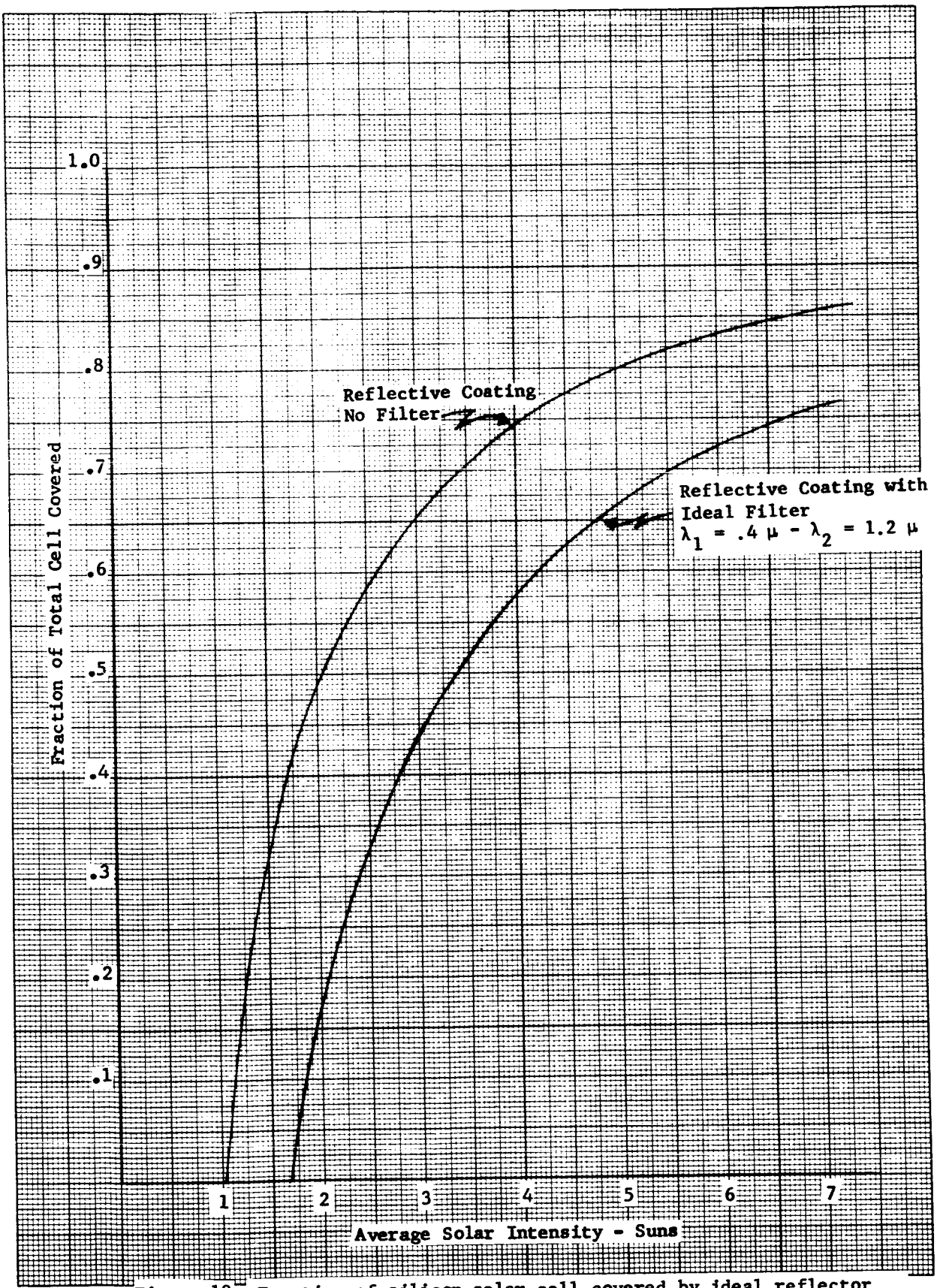


Figure 18 Fraction of silicon solar cell covered by ideal reflector as a function of average solar intensity for maximum average power

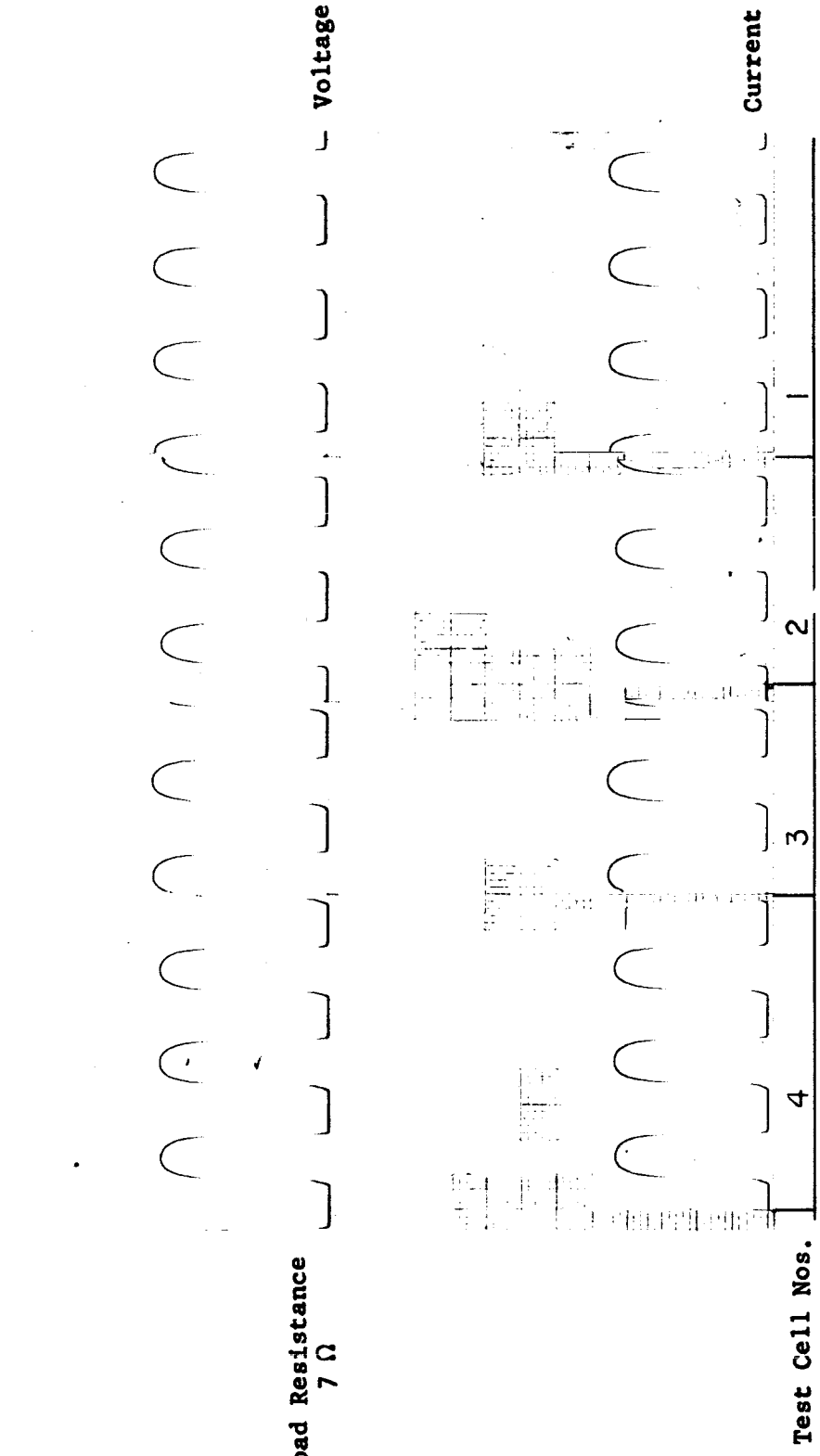


Figure 19 Typical Recorder Trace
(Output of Rotating Solar Cells)

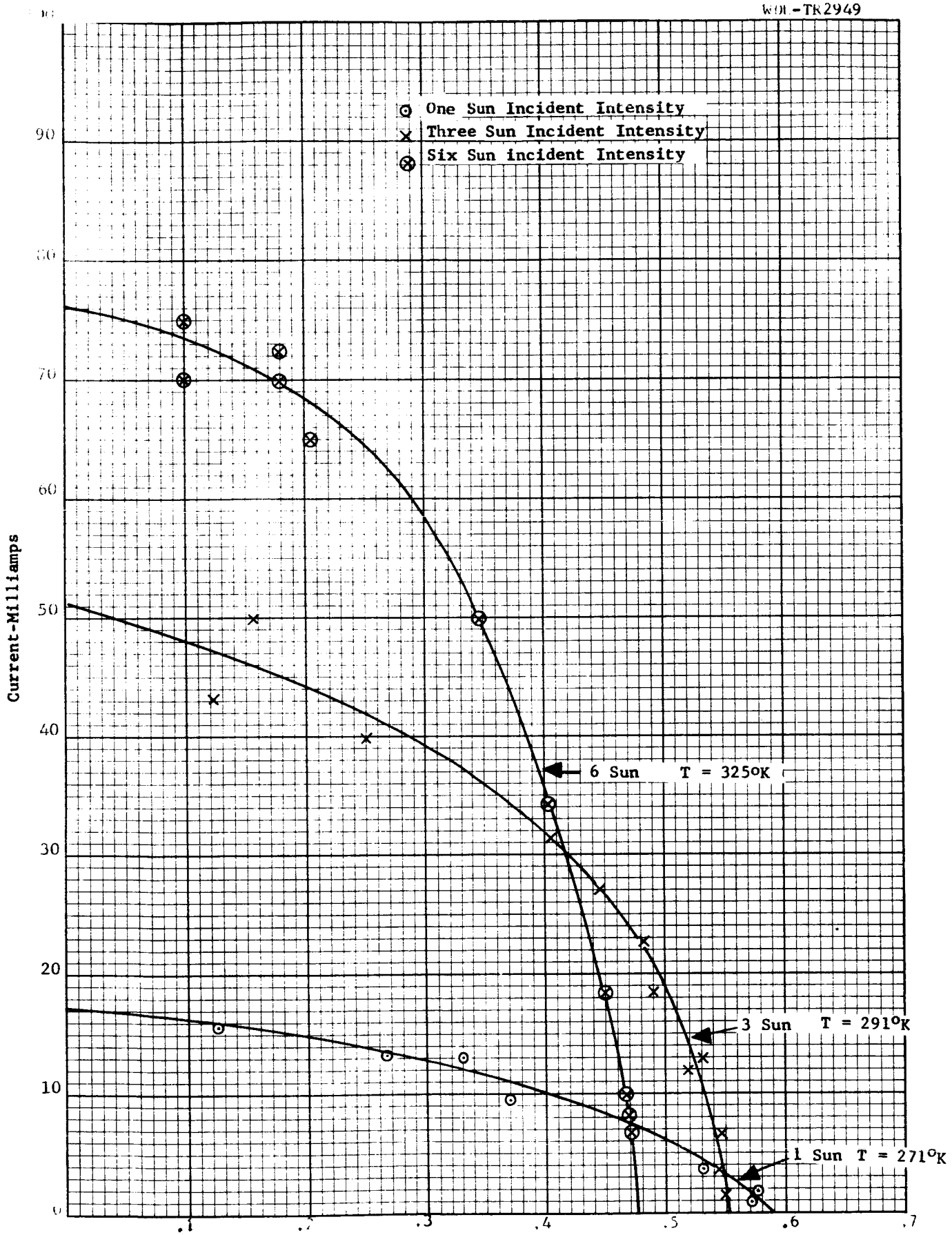


Figure 20 Rotating Results For Filter No. 1

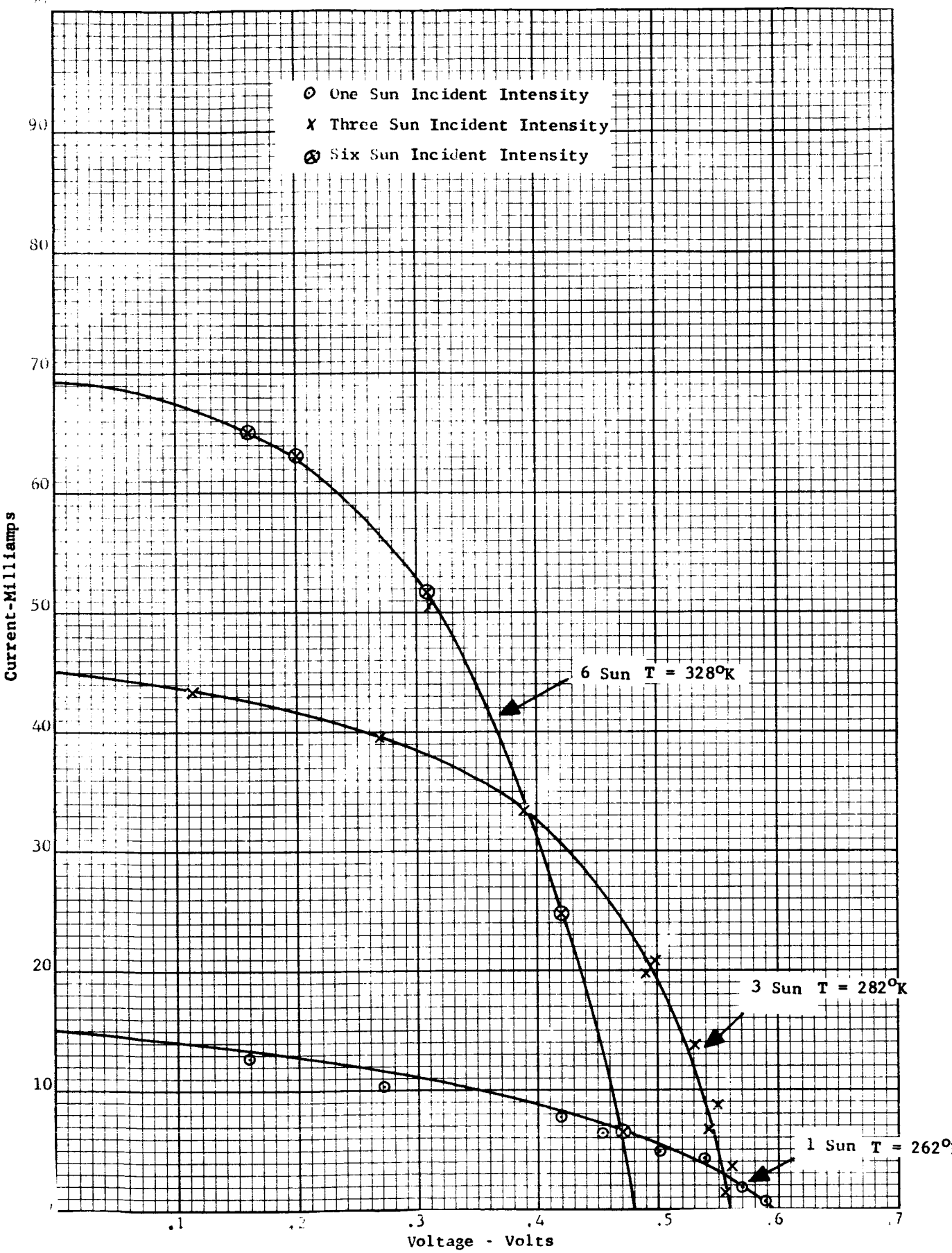


Figure 21 Rotating Results For Filter No. 2

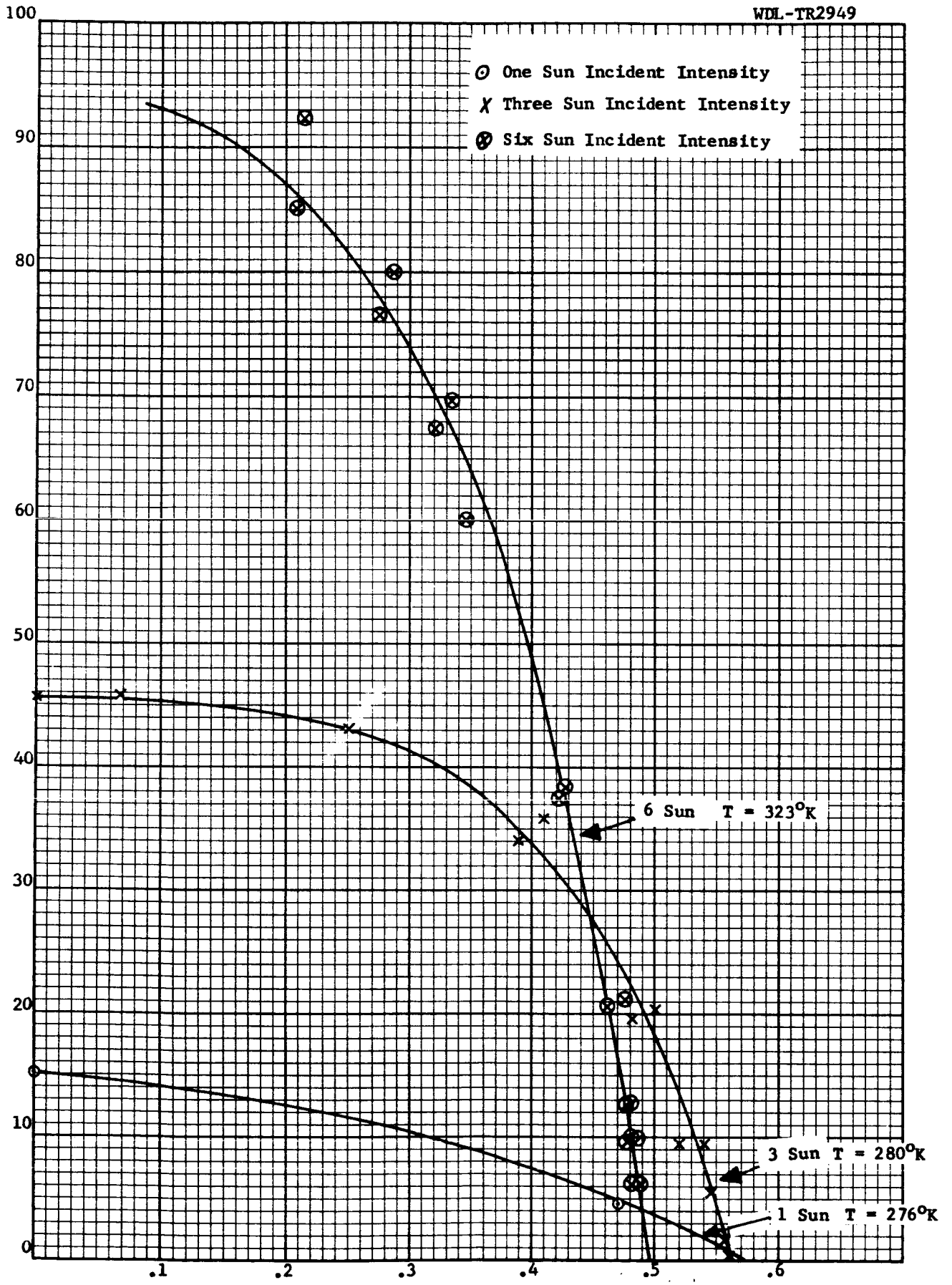


Voltage - Volts

Figure 22 Rotating Results For Filter No. 3

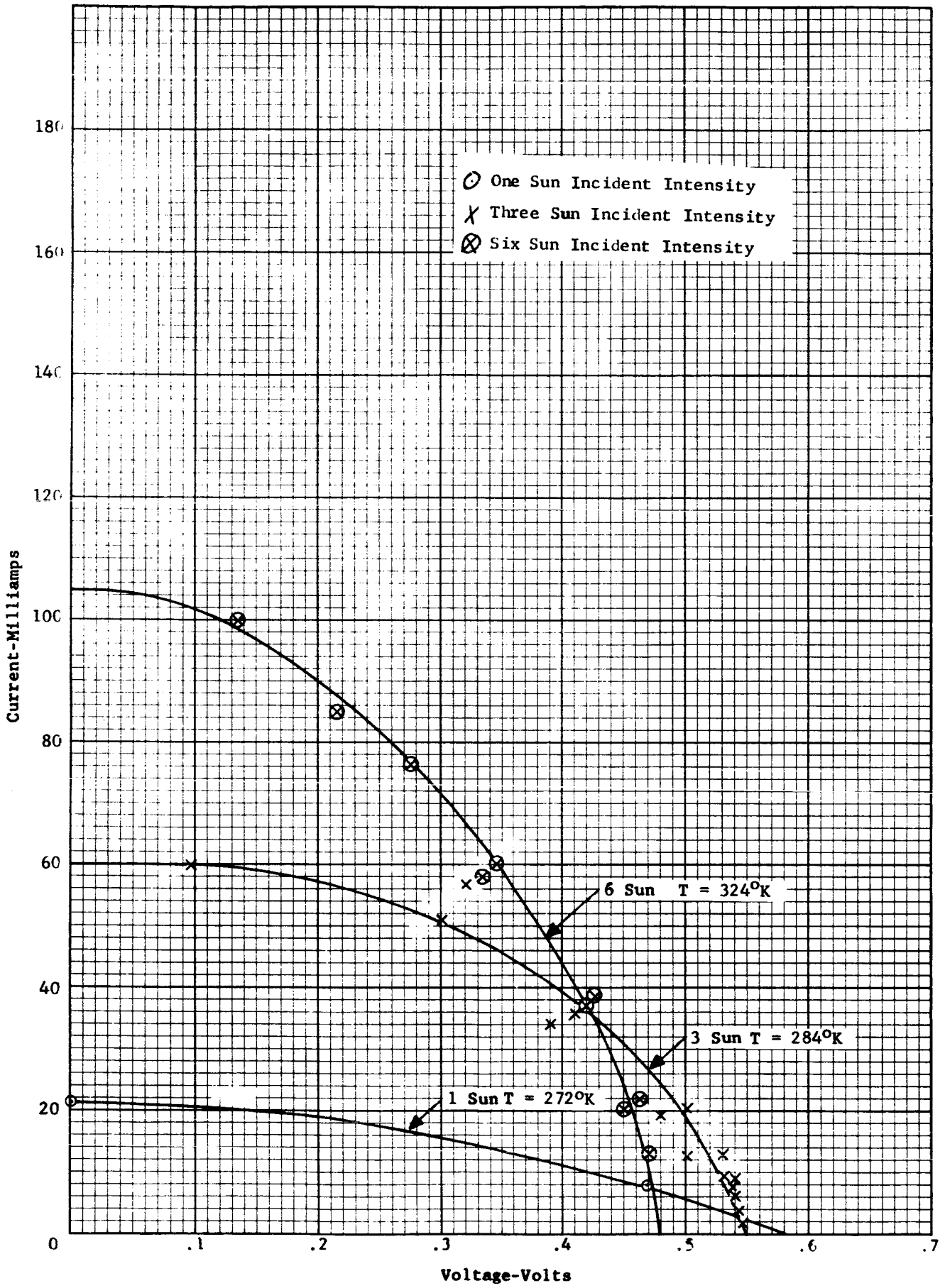


Figure 23 Rotating Results For Filter No. 4

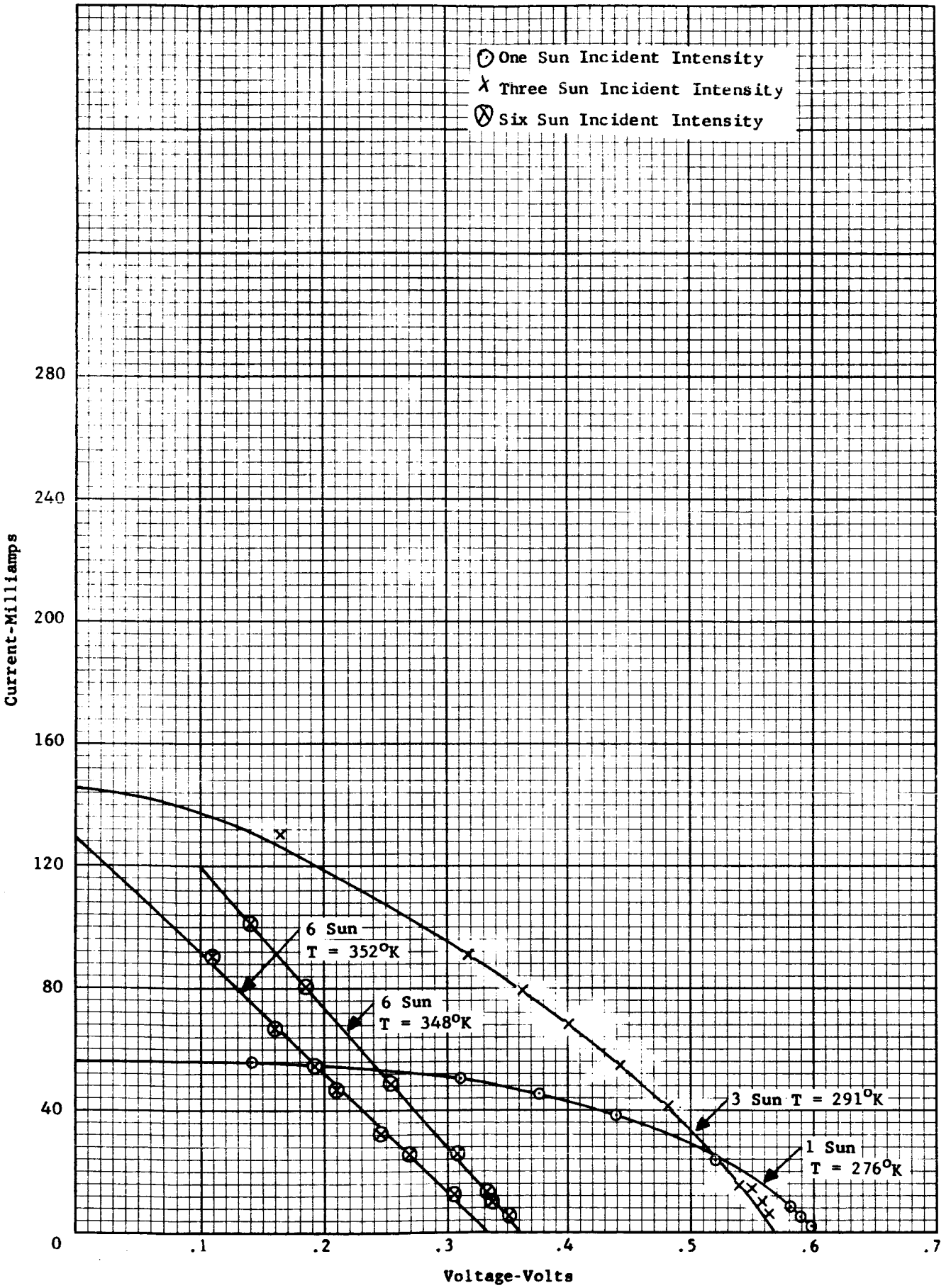


Figure 24 Rotating Results For Filter Nos. 5 and 6 (Reporting Two Runs At Six Suns)

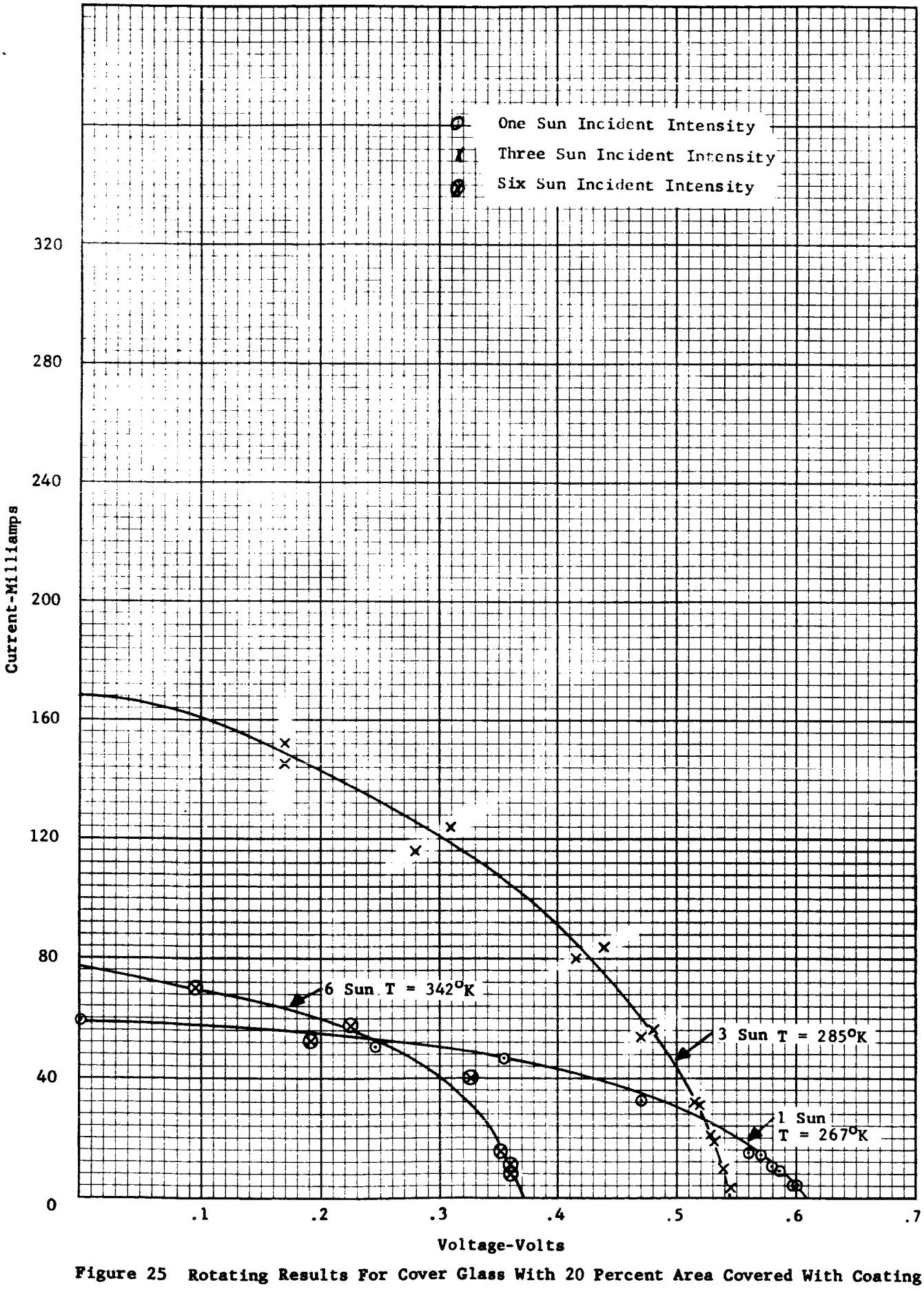


**Figure 25 Rotating Results For Cover Glass With 20 Percent Area Covered With Coating**

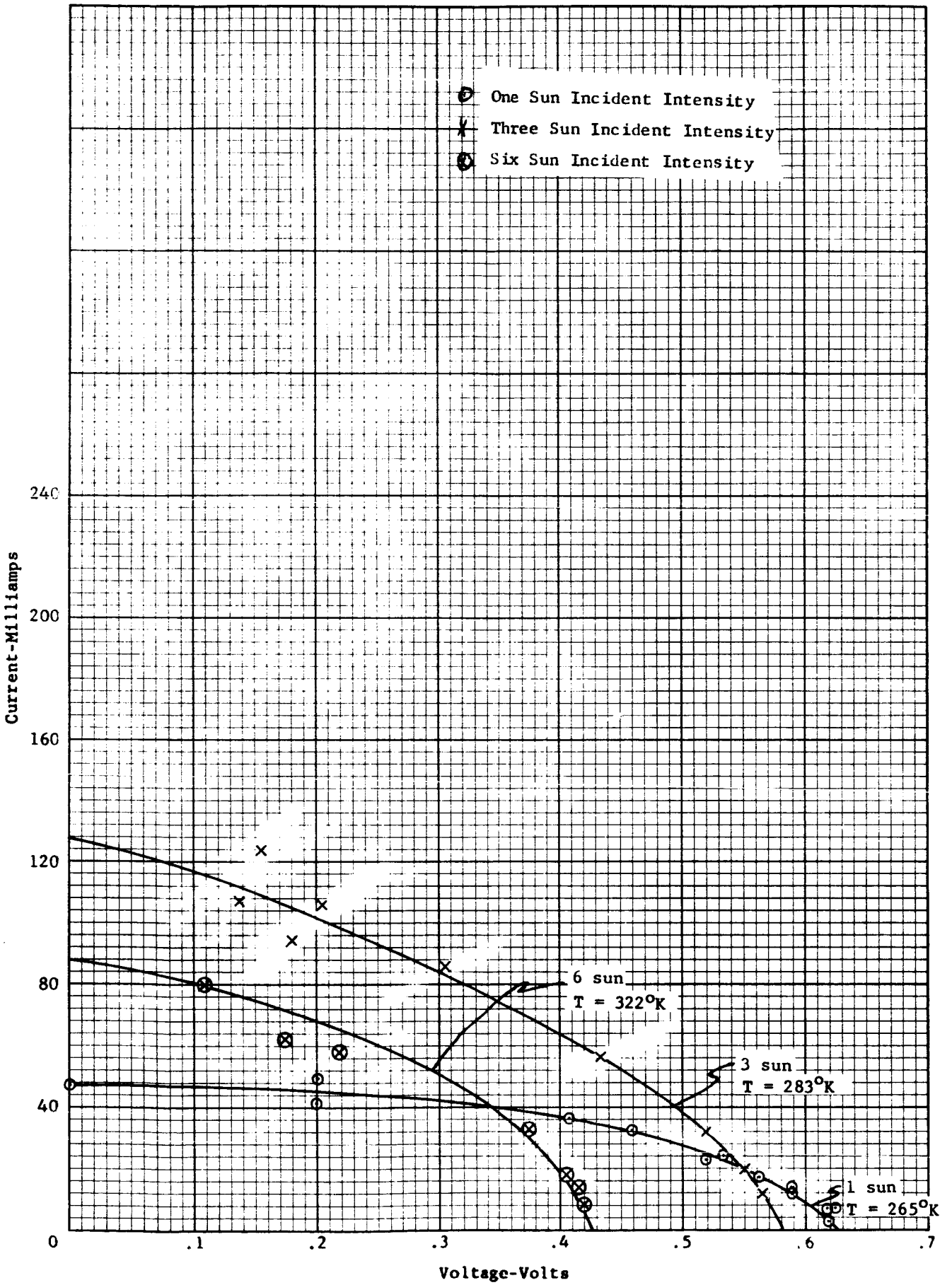


Figure 26 Rotating Results For Cover Glass With 40 Percent Area Covered With Coating

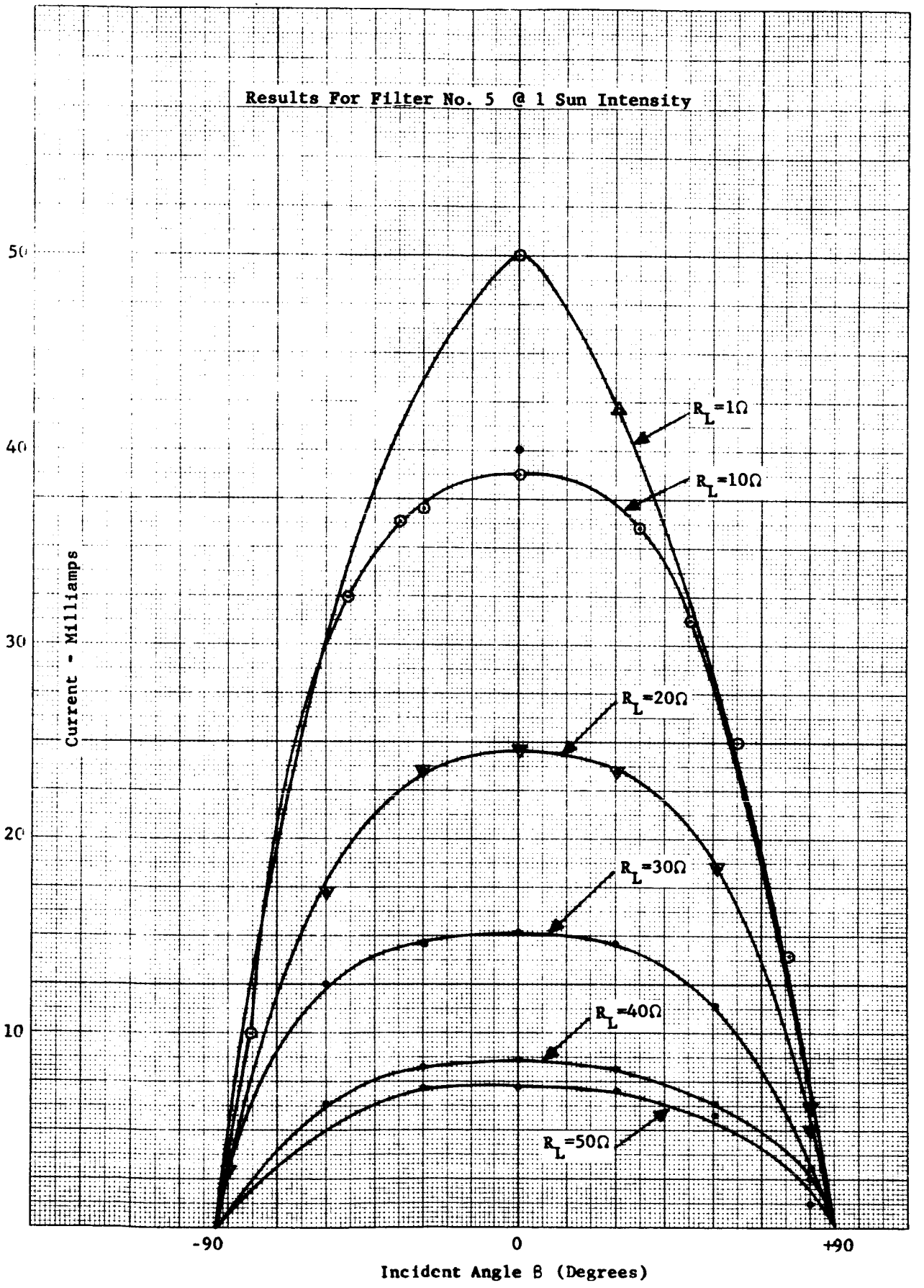


Figure 27 Current As A Function Of Incident Angle For Various Loads

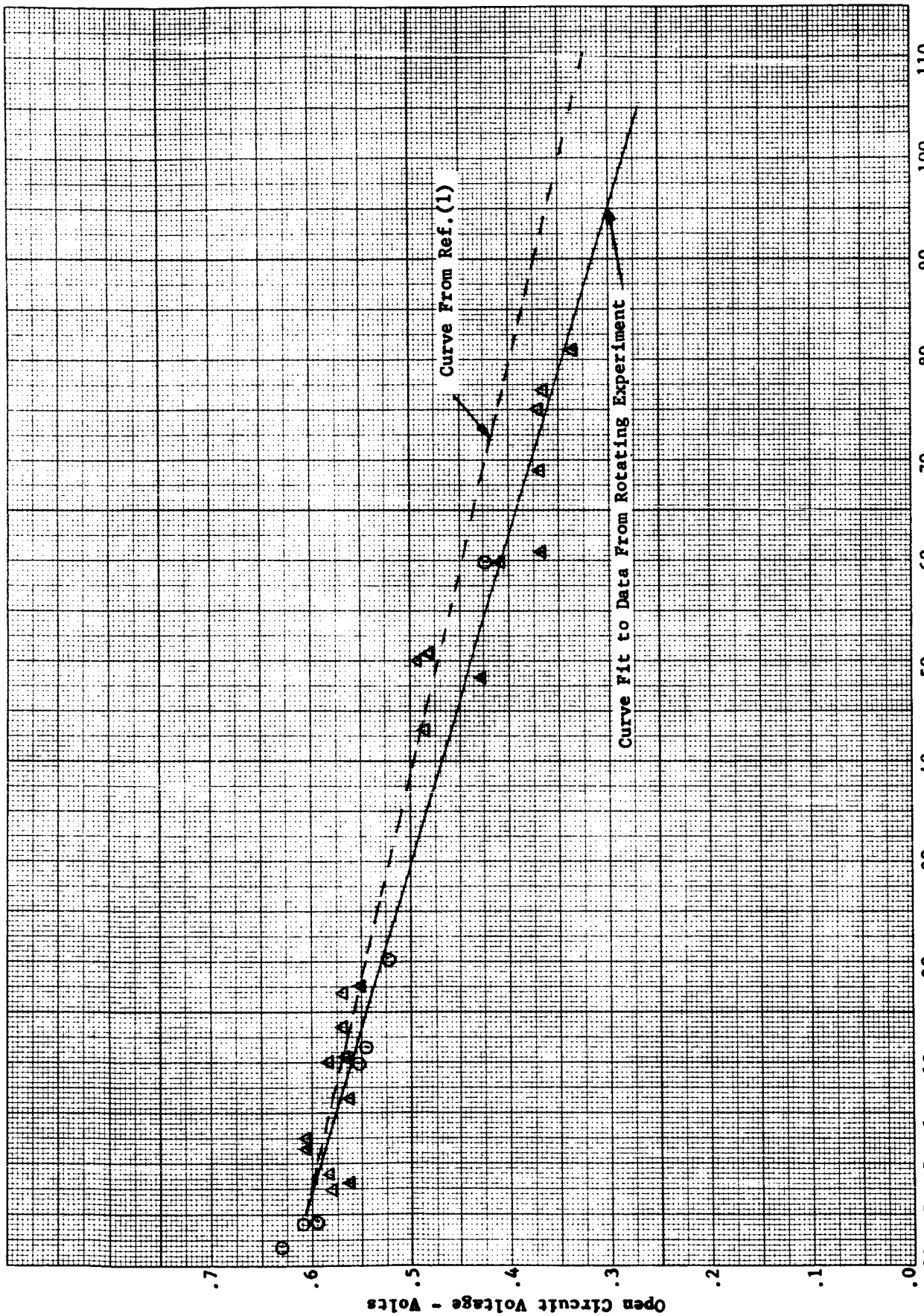


Figure 28 Open Circuit Voltage as a Function of Temperature

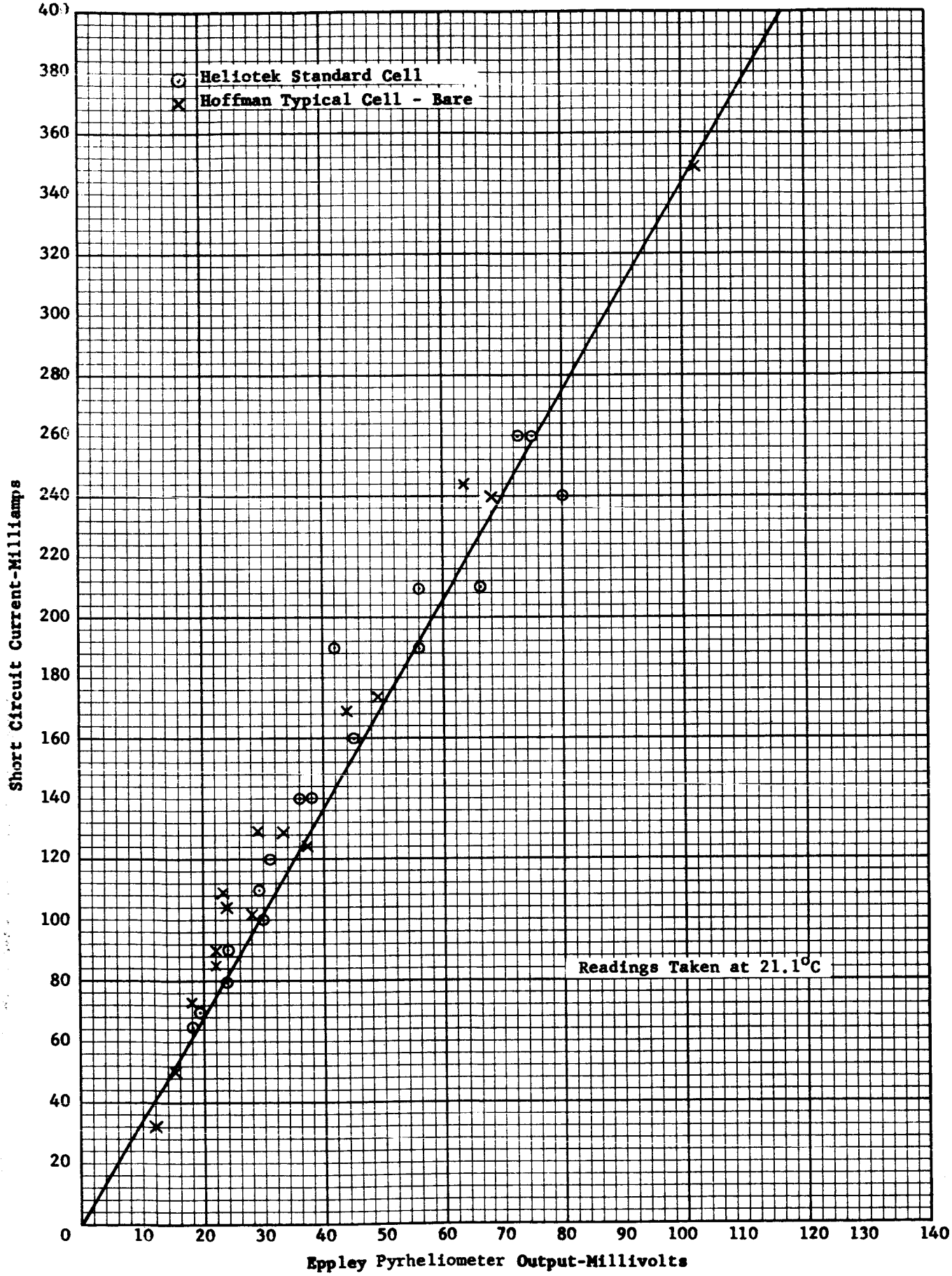


Figure 29 Constant Temperature Short Circuit Current Vs. Intensity

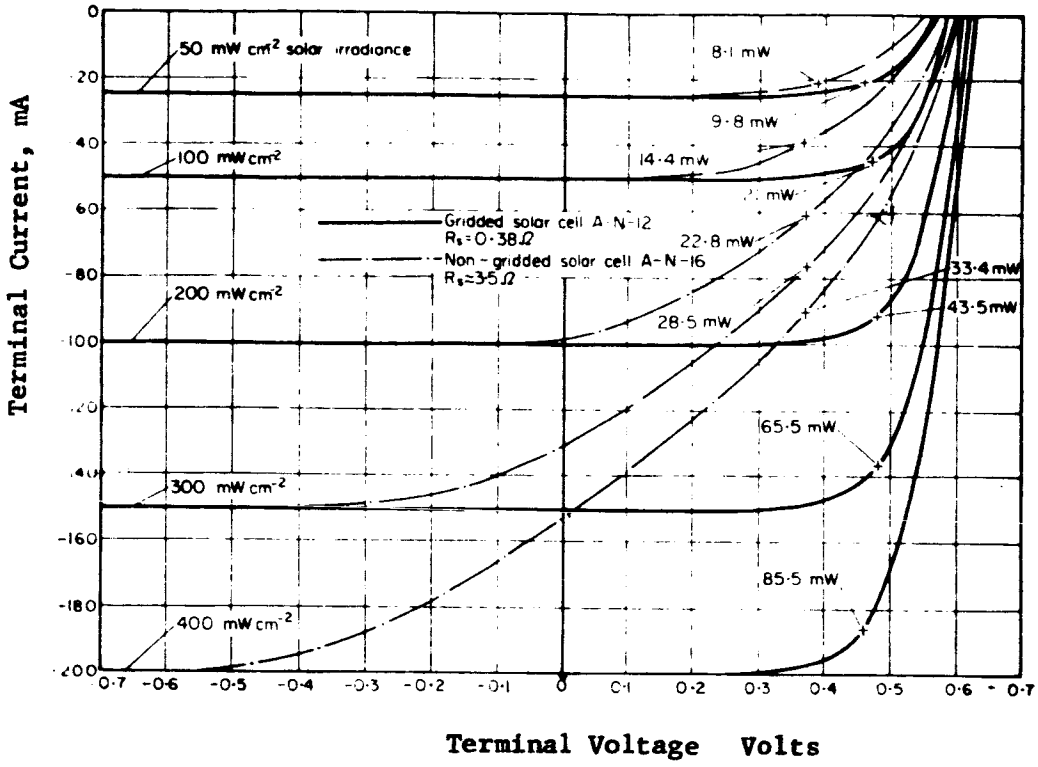


Figure 30 I-V Curves Showing Effect of Series Resistance (From Reference 9)

## APPENDIX A

## BLUE-RED REFLECTING SOLAR CELL COVER SPECTRAL SPECIFICATIONS

The spectral specifications for the OCLI are included for reference and to complete the basic understanding of the multi-layer interference filters. This specification provides the reader with a measure of the manufacturing tolerances involved with the respective filter characteristics.

### Antireflection Coating

OCLI solar cell covers are produced with silicon-monoxide antireflection coating on one surface which is designed to enhance the transmission of energy to the solar cells in the region of peak spectral response. A single layer coating is applied to produce reflections less than two percent in the wavelength region from 600 to 800 millimicrons.

### Cut-On Tolerance

The cut-on ($\lambda_1$) of the blue-red solar cell cover filter is defined as the point in transmission characteristics where the slope of the curve from the blue reflective region to the high transmission region is at 50 percent. Standard tolerance for the filter cut-on is ±15 mμ. The location of the 50 percent point in transmission (cut-on) of the filter, which should be optimized to the spectral response characteristics of the particular solar cells selected, shall be defined by the user.

### Ultraviolet Rejection

This is the region where the transmission of the filter is less than one percent, providing the protection from ultraviolet damage to the adhesives normally used to bond the covers to solar cells. Ultraviolet rejection also serves to reduce the operating temperatures of the solar cells, thereby increasing their efficiency. The following ultraviolet rejection will result as a function of the location of the cut-on point:

($\lambda_1$) - 400mμ to 425mμ - Less than one percent average transmission from 300mμ to 370mμ.

($\lambda_1$) - 430mμ or above - Less than one percent average transmission from 300mμ to 400mμ.

Cut-Off Tolerance

The cut-off of a blue-red solar cell filter ($\lambda_2$) is defined as the point in the transmission characteristics where the slope of the curve from the high transmission region to the infrared rejection region is at 50 percent. Standard tolerance for the filter cut-off is ±40mμ.

Transmission Characteristics

The following are the transmission values, measured at normal incidence in air, of a blue-red filter deposited on either microsheet or fused silica:

a. From 600mμ to 800mμ - Not less than 92 percent average

b. From ($\lambda_1$) + 50mμ to ($\lambda_2$) - 80mμ - Not less than 92 percent average

Infrared Rejection

In the blue-red filter, energy in the infrared region outside the spectral response of the solar cells is rejected by reflection. This results in lower operating temperatures of solar cells, thereby increasing their efficiency. A cut-off point within one of the following ranges should be specified with the following rejection bandwidths:

a. ($\lambda_2$) from 1100mμ to 1125mμ = 300mμ minimum bandwidth.

b. ($\lambda_2$) from 1130mμ to 1160mμ = 340mμ minimum bandwidth.

c. ($\lambda_2$) from 1165mμ to 1200mμ = 350mμ minimum bandwidth.

The maximum transmission at peak rejection of the above rejection bands shall be five percent maximum.

# APPENDIX B

## ROTATING SOLAR CELL TRANSIENT THERMAL ANALYSIS

The purpose of this appendix is to describe the method employed in determining the temperature variations for a rotating solar cell. The transient response can be characterized by the following equation

$$\rho VC_p \frac{dT}{d\theta} = -\epsilon A \sigma T^4 + \alpha Q \qquad \text{(B-1)}$$

where

$\rho VC_p$ - the system thermal capacity joules/$^oK$

$A$ - the geometric area meter$^2$

$\epsilon$ - solar cell emissivity - dimensionless

$\alpha$ - solar cell absorptivity - dimensionless

$\omega\theta$ - angular displacement - dimensionless

$Q$ - heat input - watts/meters$^2$

Assuming that the temperature variations are small (eq. $T - T_{ave} \ll T_{ave}$) allows the following linearization and simplification:

$$C \frac{dT}{d\theta} + KT = Q \qquad \text{(B-2)}$$

where

$$C = \rho C_p V$$

$$K = \epsilon A \sigma T_{ave}^3$$

$$Q = \alpha Q_{max} \sin(\omega\theta) \qquad 0 \leq (\omega\theta) \leq \pi$$

$$Q = 0 \qquad \pi \leq (\omega\theta) \leq 2\pi$$

The differential equation has been linearized for cases $T-T_{ave} \ll T_{ave}$.

For $0 \leq (\omega\theta) \leq \pi$

$$T = \frac{\alpha Q_{max}}{\omega C} \frac{1}{1+\left(\frac{K}{\omega C}\right)^2} \left[\frac{K}{\omega C} \sin(\omega\theta) - \cos(\omega\theta)\right] + Be^{-(K/C)\theta} \quad \text{(B-3)}$$

For $\pi \leq (\omega\theta) \leq 2\pi$, or $0 \leq (\omega\theta_R) \leq \pi$

$$T = T_{\theta_{R=0}} \left(e^{-(K/C)\theta_R}\right) \quad \text{(B-4)}$$

At $\theta = 0$

$$T_{\theta=0} = \frac{\alpha Q_{max}}{\omega C} \frac{1}{1+\left(\frac{K}{\omega C}\right)^2} \left[-1\right] + B \quad \text{(B-5)}$$

$$B = T_{\theta=0} + \frac{\alpha Q_{max}}{\omega C} \frac{}{1+\left(\frac{K}{\omega C}\right)^2} \quad \text{(B-6)}$$

I Quasi-Steady State

1. When quasi-steady state conditions have been achieved, and $(k/\omega C) \ll 1$,

   (1) The sin $(\omega\theta)$ term is negligible, and

   (2) $e^{-(K/C)\theta}$ may be linearized.

   Under these conditions,

   $0 \leq (\omega\theta) \leq \pi$,

$$T = \frac{\alpha Q_{max}}{\omega C} \left[-\cos(\omega\theta)\right] + B\,(1 - (K/C)\theta) \quad \text{(B-7)}$$

$$= \frac{\alpha Q_{max}}{\omega C} \left[-\cos(\omega\theta)\right] + B \left(1 - \frac{\alpha Q_{max}}{\pi T_{ave} C}\right) \theta \quad \text{(B-8)}$$

$0 \leq (\omega\theta_R) \leq \pi$

$$T = T_{\omega\theta_p} = 0\left[1 - (K/C)\theta_R\right] \quad \text{(B-9)}$$

In general, a complete solution would be accomplished by assuming $T_{\theta=0}$, solving for $T_{\omega\theta=2\pi}$, and then substituting and reiterating until convergence has been obtained. An initial estimate is achieved by the following:

Since the sin ($\omega\theta$) term may be neglected, and the exponential term is linear, thermal symmetry may be assumed, i.e., $T_{ave}$ occurs at $\omega\theta = \pi/2$ and $3\pi/2$. From Equation(B-9), using $T_{ave}$ for an initial condition instead of $T_{\omega\theta = \pi}$,

$$T_{\theta=0} = T_{ave}\left[1 - \left(\frac{K}{C}\right)\frac{\pi}{2\omega}\right] = T_{ave}\left[1 - \frac{\alpha Q_{max}}{2T_{ave}C\omega}\right] \qquad \text{(B-10)}$$

From Equation (B-6)

$$B = T_{ave}\left[1 - \frac{\alpha Q_{max}}{2T_{ave}\omega C}\right] + \frac{\alpha Q_{max}}{\omega C}\,\frac{1}{1+\left(\frac{K}{\omega C}\right)^2} \qquad \text{(B-11)}$$

Since $(K/\omega C) \ll 1$

$$B = T_{ave} + \frac{1}{2}\,\frac{\alpha Q_{max}}{\omega C} = \alpha Q_{max}\left[\frac{1}{\epsilon A\pi} + \frac{1}{2\omega C}\right] \qquad \text{(B-12)(B-12a)}$$

$$T_{0\le\omega\theta\le\pi} = \frac{\alpha Q_{max}}{\omega C}\left[-\cos(\omega\theta)\right] + \left[T_{ave} + \frac{1}{2}\,\frac{\alpha Q_{max}}{\omega C}\right]\left[1 - \frac{\alpha Q_{max}}{\pi T_{ave}C}\,\theta\right] \qquad \text{(B-13)}$$

$$= \frac{\alpha Q_{max}}{\omega C}\left[-\cos(\omega\theta)\right] - \left[\frac{\alpha Q_{max}}{\pi C} + \frac{1}{2\pi\omega T_{ave}}\left(\frac{\alpha Q_{max}}{C}\right)^2\right]\theta$$

$$+ \left[T_{ave} + \frac{1}{2}\,\frac{\alpha Q_{max}}{\omega C}\right] \qquad \text{(B-14)}$$

$$\frac{dT}{d\theta} = \frac{\alpha Q_{max}}{C}\left[\sin(\omega\theta)\right] - \frac{\alpha Q_{max}}{\pi C}\left[1 + \frac{\alpha Q_{max}}{2\omega C T_{ave}}\right] = 0 \qquad \text{(B-15)}$$

$$\sin(\omega\theta) = \frac{1}{\pi}\left[1 + \frac{\alpha Q_{max}}{2\omega C T_{ave}}\right] = \frac{1}{\pi} + \frac{1}{2}\left(\frac{K}{\omega C}\right) \qquad \text{(B-16)}$$

Equation (B-16) shows that for $(K/\omega C) \ll 1$, the thermal symmetry assumption used to evaluate B is valid, i.e.,

$$T_{ave} = \frac{\alpha Q_{max}}{\epsilon A \pi} \tag{B-17}$$

occurs at $(\omega\theta) = (\omega\theta)_R = \pi/2$, and that the maximum and minimum temperatures of a cycle occur at

$$\sin^{-1}\left(\frac{1}{\pi}\right) \simeq 18.5^{\circ},\ 161.5^{\circ} \tag{B-18}$$

$$\simeq 0.973\ \pi,\ 0.897\ \pi \text{ radians.}$$

Using these values of $\omega\theta$ in Equations (B-19) or (B-20) will provide the temperature extremes

$$T_{0\le\omega\theta\le\pi} = \frac{\alpha Q_{max}}{\omega C}\left[-\cos(\omega\theta) - \frac{1}{\pi}\left(1 + \frac{\alpha Q_{max}}{2\omega C T_{ave}}\right)\omega\theta + \left(\frac{T_{ave}}{\alpha Q_{max}/\omega C} + \frac{1}{2}\right)\right] \tag{B-19}$$

$$= \frac{\alpha Q_{max}}{\omega C}\left[-\cos(\omega\theta) - \frac{1}{\pi}\left(1 + \frac{\epsilon A\pi}{2\omega C}\right)\omega\theta + \left(\frac{\omega C}{\epsilon A\pi} + \frac{1}{2}\right)\right] \tag{B-20}$$

Calculations are simplified by assuming unit area (A) in calculating $Q_{max}$ and V, from which Q, K, and C follow.

Since $\epsilon\sigma A\, T_{ave}^{4} = \alpha Q_{max}/\pi$, T will rise and fall when Q is greater and smaller, respectively, than $\alpha Q_{max}/\pi$. This occurs when $\sin(\omega\theta) = 1/\pi$.

2. If $(K/\omega C) \gg 1$

$$T = \frac{\alpha Q_{max}}{\omega C}\ \frac{1}{1+\left(\frac{K}{\omega C}\right)^2}\left[\frac{K}{\omega C}\sin(\omega\theta) - \cos(\omega\theta)\right] + Be^{-(K/C)\theta} \tag{B-21}$$

$$= \frac{\alpha Q_{max}}{K}\ \frac{1}{1+\left(\frac{\omega C}{K}\right)^2}\left[\sin(\omega\theta) - \left(\frac{\omega C}{K}\right)\cos(\omega\theta)\right] + Be^{-(K/C)\theta} \tag{B-22}$$

When (K/C) is also very small (negligible mass), the solution approaches

$$T = \frac{\alpha Q_{max}}{K} \left[ \sin (\omega\theta) \right] \qquad \text{(B-23)}$$

which is an instantaneous response to the input heat, Q, function. The linear approximation of K is not applicable here.

3. When $K/\omega C$ is not $\gg$ or $\ll 1$, the times and angular positions of temperature ext mes are obtained from

$$(K/\omega C) \cos (\omega\theta) + \sin (\omega\theta) = \left[ \frac{B (1 + K/\omega C)^2}{\left( \alpha Q_{max} / \epsilon A \right)} \right] e^{-(K/C)\theta} \qquad \text{(B-24)}$$

# APPENDIX C
## THEORETICAL PERFORMANCE ANALYSIS

This appendix describes the method employed for solar cell performance analysis used in the optimization analysis. A single solar cell is considered isolated from its surroundings except on the face of the cell. The cell can have any combination of interference filters and area fraction of highly reflective coating. The cell is assumed to be at constant temperature. The basic energy balance can now be characterized by the following equation.

$$Q_{in} - Q_{rad} - P = 0 \qquad \text{(C-1)}$$

Each term of Equation (C-1) is now investigated individually in an effort to establish the final equation for computation.

The energy absorbed is composed of two parts, that absorbed by the filtered portion of the cell and that absorbed by the area fraction of reflective coating; thus,

$$Q_{in} = \left[ \frac{NS}{\sum_{\lambda=0}^{\infty} s_\lambda \Delta\lambda} \right] \left[ \frac{A_A}{A_T} \int \alpha_F s\, d\lambda + \left( 1 - \frac{A_A}{A_T} \right) \int \alpha_C\, s\, d\lambda \right] \qquad \text{(C-2)}$$

The integrals were evaluated by obtaining functional representation of the values and numerically integrating. For the present study, an ideal filter was assumed and the integrals were evaluated accordingly. It was further assumed that the filtered area and the reflective coating portion of the cell were at the same temperature. The ratio of $(NS/\Sigma\, s_\lambda \Delta\lambda)$ is a convenient method by which different values of solar intensity can be included. The value of N is a multiplier which accounts for the average flux per unit of time.

The second term of Equation (C-1) is the energy emitted from the cover-glass-cell-stack. The energy emitted is given by

$$Q_{rad} = \epsilon\sigma T^4 \tag{C-3}$$

when the thermal sink is considered to be absolute zero. The above equation implies that the emissivity is a constant; however, it is preferable to express the emissivity as a function of temperature in the final equation.

The emissivity is measured monochromatically and a wavelength-temperature transformation can be accomplished by using Plank's law for normal black body radiation. A polynominal can be fitted to the $\epsilon(T)$ data; thus,

$$\epsilon\sigma T^4 = (A_{o_\epsilon} + A_{1_\epsilon} T + \ldots\ldots A_{n_\epsilon} T^n)\sigma T^4 \tag{C-4}$$

Considering the ratio of active cell area to total cell area ($A_A/A_T$), the power generated by the solar cell can be expressed as

$$P = \left(\frac{A_A}{A_T}\right) \eta \, NS \tag{C-5}$$

where $\eta$ is an over-all efficiency accounting for various parameters. Following the development of Cobb (Reference 8) $\eta$ is separated into its composite parts which allows appropriate functional representation.

The cell response, filter transmittance, and solar radiation can be represented as functions of wavelength. The "filter effectiveness" is thus expressed as

$$\eta_{FB} = \frac{\int_0^\infty \tau_\lambda r_\lambda s_\lambda d_\lambda}{\int_0^\infty r_\lambda s_\lambda d_\lambda} \tag{C-6}$$

The increase in effective transmittance which results from the presence of the adhesive has been omitted; however, this effect can be accounted for by adjusting the transmissivity. Utilizing the ideal filter approximation as an optimum filter type, the optimization analysis assumes constant values

of transmittance in the bandpass region and zero transmittance in the rejection region. The "filter effectiveness" is then simplified and the cut-on and cut-off wavelengths are included as follows:

$$\eta_{FB} = \frac{\tau \int_{\lambda_1}^{\lambda_2} r_\lambda s_\lambda d_\lambda}{\sum_0^\infty r_\lambda s_\lambda \Delta_\lambda} \qquad \text{(C-7)}$$

The bare cell efficiency $N_B$ is a product of the standard cell conversion efficiency and the temperature dependence. The temperature dependence is essentially linear; however, at low temperatures basic data indicated a deviation from the linear relationship. The bare cell efficiency was then represented by the following function relation:

$$\eta_B = (A_{o_T} + A_{1_T} T + \ldots\ldots A_{n_T} T^n)\, \eta_o \qquad \text{(C-8)}$$

Substituting Equations (C-7) and (C-8) into Equation (C-5) yields

$$P = (A_{o_T} + A_{1_T} T + \ldots\ldots A_{n_T} T^n)\, \eta_o\, NS\, \frac{\tau \int_{\lambda_1}^{\lambda^\infty} r_\lambda s_\lambda d_\lambda}{\sum_0^\infty r_\lambda s_\lambda d_\lambda} \qquad \text{(C-9)}$$

Available data was used to determine the quantity $r_\lambda s_\lambda$ as a function of wavelength. These data were approximated by a "least squares" curve fit to an $n^{th}$ order polynomial as follows:

$$r_\lambda s_\lambda = A_{o_r} + A_{1_r} \lambda + \ldots\ldots A_{n_r} \lambda^n \qquad \text{(C-10)}$$

The order of the polynomial used is based upon a tolerance comparison of the polynomial and the numerical integrals between $\lambda_{r_1}$ and $\lambda_{r_2}$. A maximum value of the order of the polynomial was also imposed on the calculational procedure.

The procedure described above was used for the determination of the optimum filter for a particular isolation. This analysis also allows for the optimization of a filter when used with an area fraction of reflective coating.

# APPENDIX D
# OPTIMIZATION PROCEDURE

The optimization analysis assumes that the optimum interference filter would be one that closely approximates the ideal filter. The concept of the ideal filter implies that specification of the cut-on and cut-off wavelengths completely defines the filter. The power and energy balance equations presented in Appendix B are the equations used to determine the cut-on and cut-off wavelengths. The wavelengths to be determined are those which maximize the power at a particular insolation. The energy balance is a constraint which must also be satisfied. If these equations were linear the optimum power parameters could be directly solved by the use of the Lagrange multiplier method. However, the nonlinearity of these equations required use of the Runge-Kutta-Gill method of solving N first order differential equations by integration.

A computer program previously developed by Philco was used for the solution of these equations. This program maximizes the function F(X) subject to the constraint G(X) = 0, where X is an N dimensional vector. F(X) is maximized when the projection of $\nabla F(X)$ on the hypersurface G(X) = 0. The basic differential equation which solves for the projection (P) is given by

$$P = \nabla F - \left( \frac{\nabla F \cdot \nabla G}{\nabla G \cdot \nabla G} \right) \nabla G \qquad \text{(D-1)}$$

When the normal of P is smaller than a given value (the calculation tolerance) or when the integrating step size reaches a minimum limit the values of X, and F(X) are considered optimum. In the optimization analysis F(X) and G(X) are the power and energy balance equations respectively. The program provides the optimum values of the components of the N dimensional vector (i.e., cut-on and cut-off wavelength, area fraction of coating, etc.) for the particular case considered.

# APPENDIX E

## TRANSIENT TIME RESPONSE

The purpose of this appendix is to describe the method employed in the determination of the transient time response of the solar cell, and specifically, the time required of the various systems to reach the quasi-steady-state operating temperatures. The transient response can be characterized by the following equation:

$$\omega c \frac{dT}{d\theta} = - \epsilon A \sigma T^4 + A\alpha\bar{Q} \qquad \text{(E-1)}$$

where

$\omega c$ = the system thermal capacity joules/$^{o}$K

$A$ = the geometric area meter$^2$

$\bar{Q}$ = average heat flux to system watts/meter$^2$

$\epsilon$ = solar cell emissivity - dimensionless

$\alpha$ = solar cell absorptivity - dimensionless

Assuming the system to be at some initial temperature $T_o$ at time zero provides the initial boundary conditions necessary to solve the above equation for $\theta$ as a function of the system temperature. Thus,

$$\theta = \frac{1}{A}\left(\tanh^{-1}\frac{T}{T_\infty} - \tanh^{-1}\frac{T_o}{T_\infty} + \tan^{-1}\frac{T}{T_\infty} - \tan\frac{T_o}{T_\infty}\right) \qquad \text{(E-2)}$$

where

$$A = \frac{2 \epsilon A \sigma T_\infty^{\,3}}{\omega c}$$

It is observed that at an infinitely long time, the system is in a quasi steady state and then $\frac{dT}{d\theta}$ equals zero. Thus, from equation (E1), when $T_\infty$ is defined as the steady state temperature

$$T_{\infty} = \left( \frac{\alpha \bar{Q}}{\epsilon \sigma} \right)^{\frac{1}{4}} \qquad \text{(E-3)}$$

It is now observed that the quantity A is a system parameter and will remain constant for a particular problem. Thus, it is apparent that if the system temperature can be determined for any time greater than zero, the solution for the quantity A follows. For the solar cell/filter systems herein considered, the quantity A can, however, be approximated with some degree of certainty.

Examination of equation (E-2) reveals that an infinitely long time would be required to reach steady state; however, it is also obvious that the calculation of the time required to approach steady state within some specified interval is routine.

# APPENDIX F
# EQUILIBRIUM TEMPERATURE ANALYSIS

The initial estimate of the solar cell mean operating temperature is of prime concern in establishing the necessary experimental fixtures and measuring equipment. This analysis will also be used for several initial approximations concerning estimated solar cell performance.

Subsequent transient temperature analyses will illustrate that in the range of variables herein considered the temperature variations resulting from rotation are small; hence, the equilibrium analysis does predict the mean quasi-steady-state temperature. Therefore, this analysis is applicable to the evaluation of the actual rotating solar cell performance.

At equilibrium conditions the following energy balance governs the system temperature

$$Q_{ave_{in}} = Q_{ave_{out}} \tag{F-1}$$

The average energy into a rotating system irradiated on one side only can be expressed as:

$$Q_{ave_{in}} = \frac{\alpha\, q \int_0^{\pi} \cos\theta\, d\theta}{2\pi} \tag{F-2}$$

where

$\theta$ = angle of incidence
Q = source intensity - heat input
$\alpha$ = absorptivity

Simplifying equation (F-2)

$$Q_{ave_{in}} = \frac{\alpha\, Q_{in}}{\pi} \tag{F-3}$$

The average energy out of the rotating system can be expressed (assuming constant temperature and an absolute zero sink) as follows:

$$Q_{ave_{out}} = \epsilon \sigma T^4 + Q_e + Q_{cond} \qquad \text{(F-4)}$$

where

$\epsilon$ = cell emissivity
$\sigma$ = Stefan Boltzmann constant
$T$ = cell temperature
$Q_e$ = electrical output
$Q_{cond}$ = conduction losses

Assuming the solar cell is perfectly insulated from the mounting:

$$Q_{cond} = 0 \qquad \text{(F-5)}$$

Now $Q_e$ is a function of $Q_{ave_{in}}$ and load resistance, and when $Q_e$ is a maximum it is in the order of 10 percent of $Q_{ave_{in}}$. It is also obvious that $Q_e$ can be accounted for by modifying the $\alpha$ such that the effective absorptivity reflects the electrical loss. Hence,

$$\alpha_{eff} = \alpha(1 - \eta) \qquad \text{(F-6)}$$

where

$\eta$ is the solar cell efficiency

Thus equation (F-1) becomes

$$\frac{\alpha_{eff} Q_{in}}{\pi} = \epsilon \sigma T^4 \qquad \text{(F-7)}$$

Solving for T

$$T = \left[\left(\frac{\alpha_{eff}}{\epsilon}\right)\left(\frac{1}{\sigma}\right)\left(\frac{Q_{in}}{\pi}\right)\right]^{\frac{1}{4}} \qquad \text{(F-8)}$$

which thus provides the approximation of quasi-steady-state cell temperature as a function of the effective ($\alpha/\epsilon$) and solar insolance.

Figure F-1 presents the results of calculations using equation (F-8). For example, consider a solar cell with a cover glass having an effective $\alpha/\epsilon$ equal to 0.8. Figure F-1 shows that the equilibrium temperature is 168°C at six suns. The above analysis then states that if the temperature variations during rotation are small, this temperature should be the mean operating temperature.

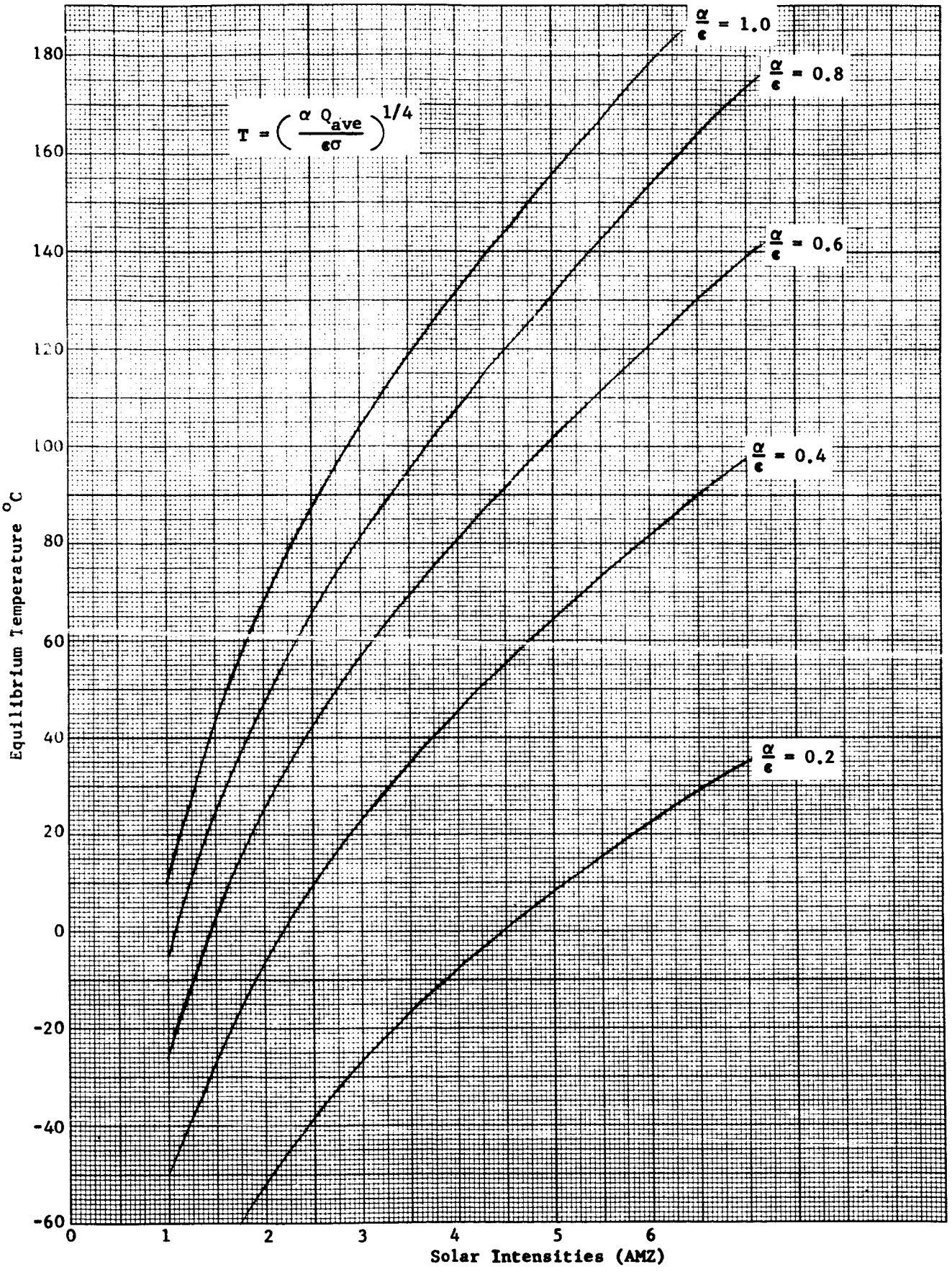


Figure F-1 Quasi Steady State Equilibrium Temperatures as a Function of Solar Intensity for Various $\alpha/\epsilon$ Ratios

# APPENDIX G

## SOLAR CELL COVER ENVIRONMENTAL TESTING

All solar cell covers supplied by Optical Coating Laboratory, Incorporated are subjected to the following environmental testing:

### Humidity

The filter shall withstand being exposed for a continuous period of 72 hours to a thermostatically controlled environment of $120^{\circ}F$ F $\pm$ $2^{\circ}F$ and 98% + 2% relative humidity. (Ref. Military Specification MIL-C-675, Para. 4.6.9.)

### Solubility

The filter shall withstand being immersed in boiling distilled water for a continuous period of 15 minutes.

### Abrasion Resistance

Immediately after removing the filter from the environmental test chamber, the filter shall be subjected to an eraser abrasion resistance test of 20 complete strokes with a pressure of 2 to 2 1/2 pounds. (Ref. MIL-C-675, Para. 4.6.11.)

### Temperature Cycle

The filter shall withstand being cooled to the temperature of liquid nitrogen, be retained at this temperature for one hour, and subsequently heated to $350^{\circ}F$ $\pm$ $10^{\circ}F$ and retained at this elevated temperature for a period of one hour. The rate of temperature change shall not exceed $30^{\circ}F$ per minute.

### Adhesion

The filter shall not separate from the substrate or delaminate when a strip of cellulose tape, which has been pressed firmly in contact with the filter, is removed with a "snap" action.

# APPENDIX H

## SPECTROPHOTOMETRIC MEASUREMENTS

Appendix H presents the spectrophotometric measurements made on the filters and coatings used in this study. The curves presented are typical for each filter type; no attempt was made to include all the measurements made during the progress of this study. The curves are presented in three sections as follows:

1. Transmittance as a function of Incident Angle (also calculated values for typical filter (Reference 6)).

2. Transmittance as a function of Temperature.

3. Reflectance of Filter-Cell-Stock Assemblies (also reflectance of sample coating).

OCLI THEORETICAL CALCULATIONS
TYPICAL FILTER

SAMPLE DESCRIPTION _____ SUBMITTED BY _____ CURVE NO. _____

OPERATOR _____ SLIT WIDTH, AUTOMATIC _____ CONSTANT _____ M.M. AT _____ MICRONS. SLIT SERVO GAIN _____ SCAN SPEED _____

INSTRUMENT MODE, TRANSMISSION - T-1 ___ T-5 ___ T-10 ___ T-20 ___ T-50 ___ ABSORPTANCE. _____ DIFFUSE TRANS. _____ SPECULAR REFLECTANCE _____ DIFFUSE REFL. _____

REFERENCE, AIR ___ $MgCO_3$ ___ OTHER _____ PEN RESPONSE _____ SOLVENT _____ CELL PATH (THICKNESS) _____ CONCENTRATION _____

REMARKS _____

PERKIN-ELMER MODEL NO
SPECTROPHOTOMETER

SPECTRUM ANALYSIS-(NEAR INFRARED)

TRANSMITTANCE-REFLECTANCE

1.0 .90 .80 .70 .60 .50 .40 .30 .20 .10

.6 .7 .8 .9 1.0 1.1 1.2 1.3 1.4 1.5 1.6 1.7 1.8 1.9 2.0 2.1 2.2 2.3 2.4 2.5 2.6 2.7

WAVELENGTH MICRONS

102

WDL-TR2949

OCLI THEORETICAL CALCULATIONS
TYPICAL FILTER

SAMPLE DESCRIPTION _____ SUBMITTED BY _____ CURVE NO. _____

OPERATOR _____ SLIT WIDTH, AUTOMATIC _____ CONSTANT _____ M.M. AT _____ MICRONS. SLIT SERVO GAIN _____ SCAN SPEED _____

INSTRUMENT MODE, TRANSMISSION - T-1 ____ T-5 ____ T-10 ____ T-20 ____ T-50 ____ ABSORTANCE _____ DIFFUSE TRANS. _____ SPECULAR REFLECTANCE _____ DIFFUSE REFL. _____

REFERENCE, AIR ____ $MgCO_3$ ____ OTHER _____ PEN RESPONSE ____ SOLVENT _____ CELL PATH (THICKNESS) _____ CONCENTRATION _____

REMARKS _____

PERKIN-ELMER MODEL NO. 50
SPECTROPHOTOMETER

SPECTRUM ANAL. SIS - (VISIBLE)

TRANSMITTANCE - REFLECTANCE

1.0 .90 .80 .70 .60 .50 .40 .30 .20 .10

350 360 370 380 390 400 425 450 475 500 525 550 575 600 650 700 790

WAVELENGTH

MILLIMICRONS

103

2

WDL-TR7949

FILTER NO. 1

SAMPLE DESCRIPTION SC FILTER PART 10 SUBMITTED BY D BRIGGS CURVE NO. 2215 - 2218

OPERATOR VC LITTLE SLIT WIDTH, AUTOMATIC ____ CONSTANT ____ M.M. AT ____ MICRONS. SLIT SERVO GAIN ____ SCAN SPEED ____

INSTRUMENT MODE, TRANSMISSION - T-1 ____ T-5 ____ T-10 ____ T-20 ____ T-50 ____ ABSORPTANCE ____ DIFFUSE TRANS. ____ SPECULAR REFLECTANCE ____ DIFFUSE REFL. ____

REFERENCE, AIR ____ $MgCO_3$ ____ OTHER ____ PEN RESPONSE ____ SOLVENT ____ CELL PATH (THICKNESS) ____ CONCENTRATION ____

REMARKS ____

PERKIN-ELMER MODEL NO 30
SPECTROPHOTOMETER

SPE RUM ANAL SIS - (VISIBL

TRANSMITTANCE - REFLECTANCE

1.0 .90 .80 .70 .60 .50 .40 .30 .20 .10

0 5 30 45 15 30 0 15

15 30 0 15

350 360 370 380 390 400 42

WAVELENGTH

450 475 500 525 550 575 600 650 700

MILLIMICRONS

104

3

WIL-TR2949

FILTER NO. 1

SAMPLE DESCRIPTION SC FILTER 1B — SUBMITTED BY D BRIGGS — CURVE NO. 2749-2802

OPERATOR SC LITTLE — SLIT WIDTH, AUTOMATIC ____ CONSTANT ____ ____ M.M. AT ____ MICRONS. SLIT SERVO GAIN ____ SCAN SPEED ____

INSTRUMENT MODE, TRANSMISSION - T-1 ____ T-5 ____ T-10 ____ T-20 ____ T-50 ____ ABSORPTANCE ____ DIFFUSE TRANS. ____ SPECULAR REFLECTANCE ____ DIFFUSE REFL. ____

REFERENCE, AIR ____ $MgCO_3$ ____ OTHER ____ PEN RESPONSE ____ SOLVENT ____ CELL PATH (THICKNESS) ____ CONCENTRATION ____

REMARKS ____

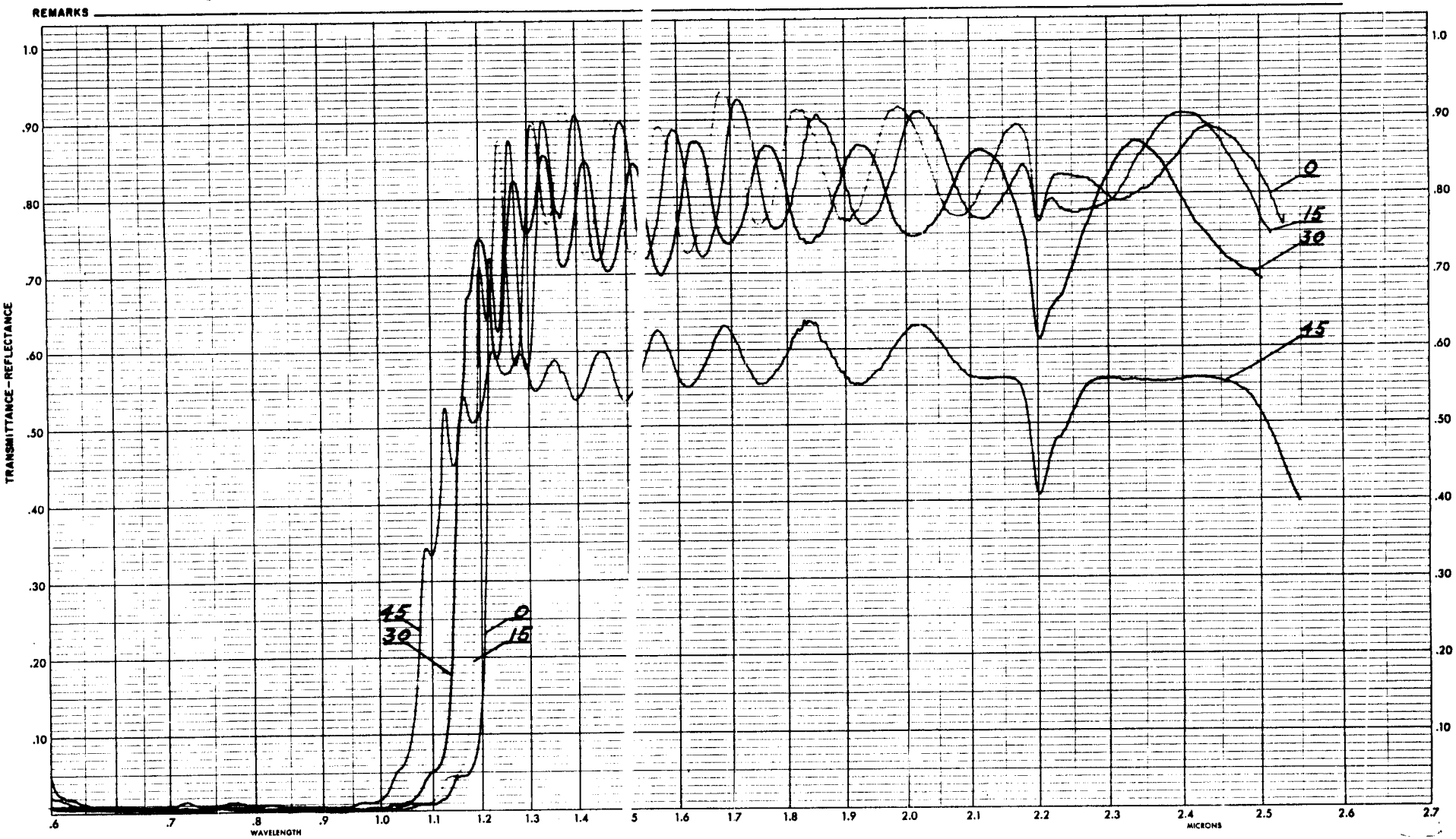


SPECTRUM ANAL. IS-(NEAR INFRARED) PERKIN-ELMER MODEL NO SPECTROPHOTOMETER

TRANSMITTANCE-REFLECTANCE

105

WDL-TR2949

4

FILTER NO. 2

SAMPLE DESCRIPTION SC FILTER PART 2 C SUBMITTED BY D BRIGGS CURVE NO. 2731-2734

OPERATOR JC LITTLE SLIT WIDTH, AUTOMATIC ____ CONSTANT ____ M.M. AT ____ MICRONS. SLIT SERVO GAIN ____ SCAN SPEED ____

INSTRUMENT MODE, TRANSMISSION - T-1 ____ T-5 ____ T-10 ____ T-20 ____ T-50 ____ ABSORPTANCE ____ DIFFUSE TRANS. ____ SPECULAR REFLECTANCE ____ DIFFUSE REFL. ____

REFERENCE, AIR ____ $MgCO_3$ ____ OTHER ____ PEN RESPONSE ____ SOLVENT ____ CELL PATH (THICKNESS) ____ CONCENTRATION ____

REMARKS

PERKIN-ELMER MODEL NO. 350
SPECTROPHOTOMETER

SPECTRUM ANALYSIS-(VISIBLE)

TRANSMITTANCE-REFLECTANCE

1.0 .90 .80 .70 .60 .50 .40 .30 .20 .10

WAVELENGTH

MILLIMICRONS

45 30 0 15

106

VDL-TR2949

FILTER NO.2

SAMPLE DESCRIPTION SC FILTER PART 2 Q SUBMITTED BY D BRIGGS CURVE NO. 2811 - 2814

OPERATOR JC LITTLE SLIT WIDTH, AUTOMATIC ____ CONSTANT ____ M.M. AT ____ MICRONS. SLIT SERVO GAIN ____ SCAN SPEED ____

INSTRUMENT MODE, TRANSMISSION - T-1 ____ T-5 ____ T-10 ____ T-20 ____ T-50 ____ ABSORPTANC ____ DIFFUSE TRANS. ____ SPECULAR REFLECTANCE ____ DIFFUSE REFL. ____

REFERENCE, AIR ____ $MgCO_3$ ____ OTHER ____ PEN RESPONSE ____ SOLVENT ____ CELL PATH (THICKNESS) ____ CONCENTRATION ____

REMARKS ____

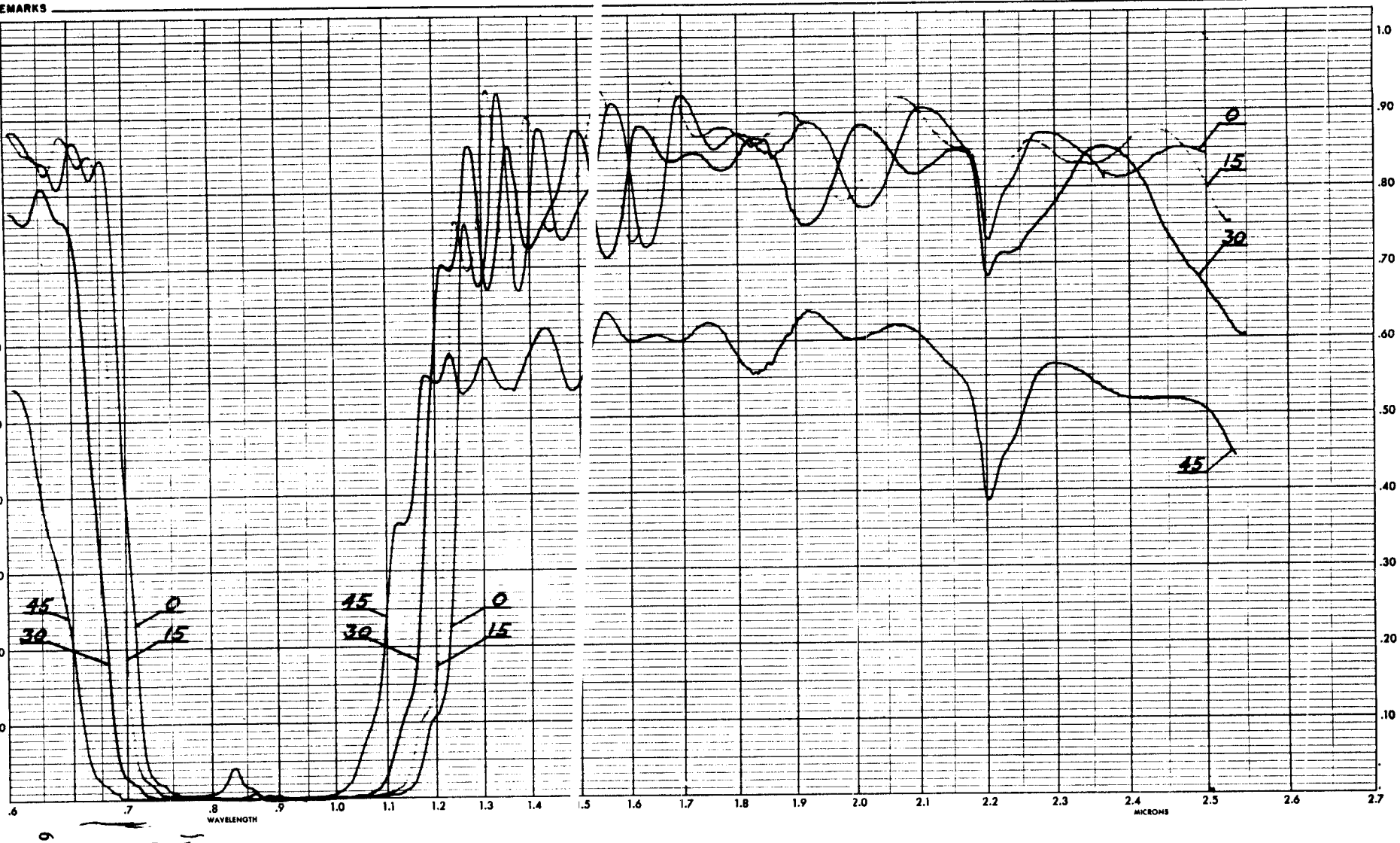


SPECTRUM ANAL · IS-(NEAR INFRARED) PERKIN-ELMER MODEL NO SPECTROPHOTOMETER

TRANSMITTANCE-REFLECTANCE

107

WIL-TR2949

FILTER NO. 3

SAMPLE DESCRIPTION "C" FILTER PART 3 IV SUBMITTED BY D BRIGGS CURVE NO. 2751 - 2754

OPERATOR JC LITTLE SLIT WIDTH, AUTOMATIC ____ CONSTANT ____ M.M. AT ____ MICRONS. SLIT SERVO GAIN ____ SCAN SPEED ____

INSTRUMENT MODE, TRANSMISSION - T-1 ____ T-5 ____ T-10 ____ T-20 ____ T-50 ____ ABSORPTANC ____ DIFFUSE TRANS. ____ SPECULAR REFLECTANCE ____ DIFFUSE REFL. ____

REFERENCE, AIR ____ $MgCO_3$ ____ OTHER ____ PEN RESPONSE ____ SOLVENT ____ CELL PATH (THICKNESS) ____ CONCENTRATION ____

REMARKS ____

PERKIN-ELMER MODEL NO
SPECTROPHOTOMETER

SPE RUM ANAL; SIS - (VISIBL

TRANSMITTANCE-REFLECTANCE

1.0 .90 .80 .70 .60 .50 .40 .30 .20 .10

330 360 370 380 390 400 WAVELENGTH

425 450 475 500 525 550 575 600 650 700 750 MILLIMICRONS

45 30 0 15

45

108

WDL-TR2949

FILTER NO. 3

SAMPLE DESCRIPTION SC FILTER PART 3N SUBMITTED BY D BRIGGS CURVE NO. 2831-2837

OPERATOR VC LITTLE SLIT WIDTH, AUTOMATIC ____ CONSTANT ____ M.M. AT ____ MICRONS. SLIT SERVO GAIN ____ SCAN SPEED ____

INSTRUMENT MODE, TRANSMISSION - T-1 ____ T-5 ____ T-10 ____ T-20 ____ T-50 ____ ABSORPTANCE ____ DIFFUSE TRANS. ____ SPECULAR REFLECTANCE ____ DIFFUSE REFL. ____

REFERENCE, AIR ____ $MgCO_3$ ____ OTHER ____ PEN RESPONSE ____ SOLVENT ____ CELL PATH (THICKNESS) ____ CONCENTRATION ____

REMARKS ____

SPECTRUM ANAL IS - (NEAR INFRARED) PERKIN-ELMER MODEL NO SPECTROPHOTOMETER

TRANSMITTANCE-REFLECTANCE

1.0 .90 .80 .70 .60 .50 .40 .30 .20 .10

45 30 0 15 30 45 0 15 0 30 45 15

.6 .7 .8 .9 1.0 1.1 1.2 1.3 1.4 1.5 1.6 1.7 1.8 1.9 2.0 2.1 2.2 2.3 2.4 2.5 2.6 2.7

WAVELENGTH MICRONS

109

WIL-TR2949

FILTER NO. 4

SAMPLE DESCRIPTION SC FILTER PART 4 N SUBMITTED BY D BRIGGS CURVE NO. 2847-2850

OPERATOR JC LITTLE SLIT WIDTH, AUTOMATIC CONSTANT M.M. AT MICRONS. SLIT SERVO GAIN SCAN SPEED

INSTRUMENT MODE, TRANSMISSION - T-1 T-5 T-10 T-20 T-50 ABSORPTANCE DIFFUSE TRANS. SPECULAR REFLECTANCE DIFFUSE REFL.

REFERENCE, AIR $MgCO_3$ OTHER PEN RESPONSE SOLVENT CELL PATH (THICKNESS) CONCENTRATION

REMARKS

SPECTRUM ANALYSIS-(NEAR INFRARED) PERKIN-ELMER MODEL NO. 112 SPECTROPHOTOMETER

TRANSMITTANCE-REFLECTANCE

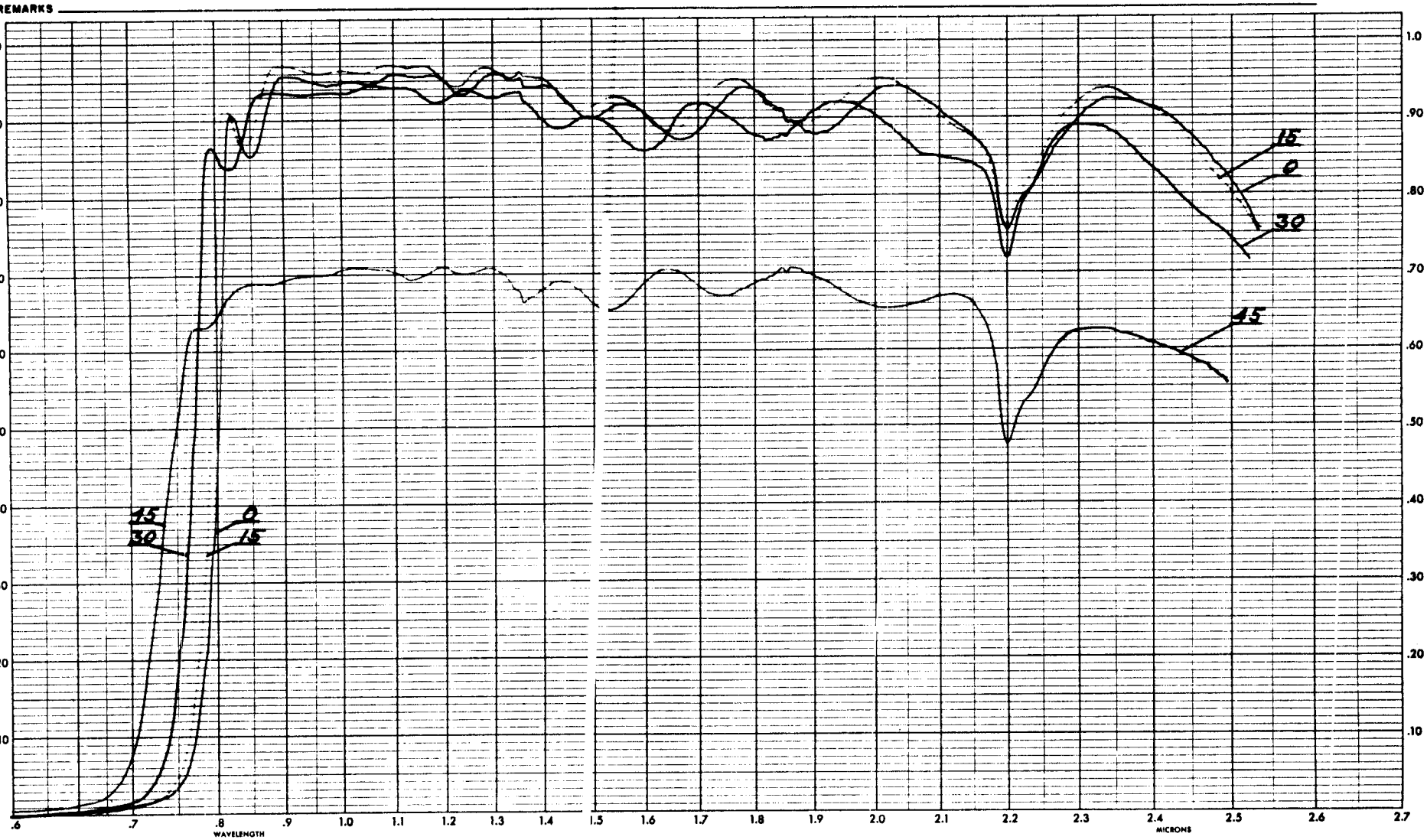


WDL-TR2949

FILTER NO. 4

SAMPLE DESCRIPTION SC FILTER PART 4 W SUBMITTED BY D BRIGGS CURVE NO. 2851-2854

OPERATOR JC LITTLE SLIT WIDTH, AUTOMATIC CONSTANT M.M. AT MICRONS. SLIT SERVO GAIN SCAN SPEED

INSTRUMENT MODE, TRANSMISSION - T-1 T-5 T-10 T-20 T-50 ABSORPTANCE DIFFUSE TRANS. SPECULAR REFLECTANCE DIFFUSE REFL.

REFERENCE, AIR $MgCO_3$ OTHER PEN RESPONSE SOLVENT CELL PATH (THICKNESS) CONCENTRATION

REMARKS

SPECTRUM ANALYSIS-(NEAR INFRARED) PERKIN-ELMER MODEL NO SPECTROPHOTOMETER

TRANSMITTANCE-REFLECTANCE

1.0 .90 .80 .70 .60 .50 .40 .30 .20 .10

0 15 30 45

.6 .7 .8 .9 1.0 1.1 1.2 1.3 1.4 1.5 1.6 1.7 1.8 1.9 2.0 2.1 2.2 2.3 2.4 2.5 2.6 2.7

WAVELENGTH MICRONS

MIL-TR2949

FILTER NO. 5

SAMPLE DESCRIPTION SC FILTER PART SI — SUBMITTED BY D BRIGGS — CURVE NO. 2947-2950

OPERATOR JC LIMLE — SLIT WIDTH, AUTOMATIC ✓ — CONSTANT — — M.M. AT 750MUL MICRONS. SLIT SERVO GAIN .05 — SCAN SPEED 2P

INSTRUMENT MODE, TRANSMISSION - T-1 ✓ T-5 ___ T-10 ___ T-20 ___ T-50 ___ ABSORPTANCE ___ DIFFUSE TRANS. ___ SPECULAR REFLECTANCE ___ DIFFUSE REFL. ___

REFERENCE, AIR ✓ $MgCO_3$ ___ OTHER ___ PEN RESPONSE 1 — SOLVENT ___ CELL PATH (THICKNESS) ___ CONCENTRATION ___

REMARKS ___

PERKIN-ELMER MODEL NO 50
SPECTROPHOTOMETER

SPECTRUM ANALYSIS-(VISIBL

TRANSMITTANCE-REFLECTANCE

1.0 .90 .80 .70 .60 .50 .40 .30 .20 .10

30 0 15 15

15 30 15 0

350 360 370 380 390 400 425 450 475 500 525 550 575 600 650 700 750

WAVELENGTH — MILLIMICRONS

112

11

WIL-TR2949

FILTER NO. 5

SAMPLE DESCRIPTION SC FILTER PART 5 SUBMITTED BY D BRIGGS CURVE NO. 2855 - 2853

OPERATOR JC LITTLE SLIT WIDTH, AUTOMATIC ____ CONSTANT ____ M.M. AT ____ MICRONS. SLIT SERVO GAIN ____ SCAN SPEED ____

INSTRUMENT MODE, TRANSMISSION - T-1 ____ T-5 ____ T-10 ____ T-20 ____ T-50 ____ ABSORPTANCE ____ DIFFUSE TRANS. ____ SPECULAR REFLECTANCE ____ DIFFUSE REFL. ____

REFERENCE, AIR ____ $MgCO_3$ ____ OTHER ____ PEN RESPONSE ____ SOLVENT ____ CELL PATH (THICKNESS) ____ CONCENTRATION ____

REMARKS ____

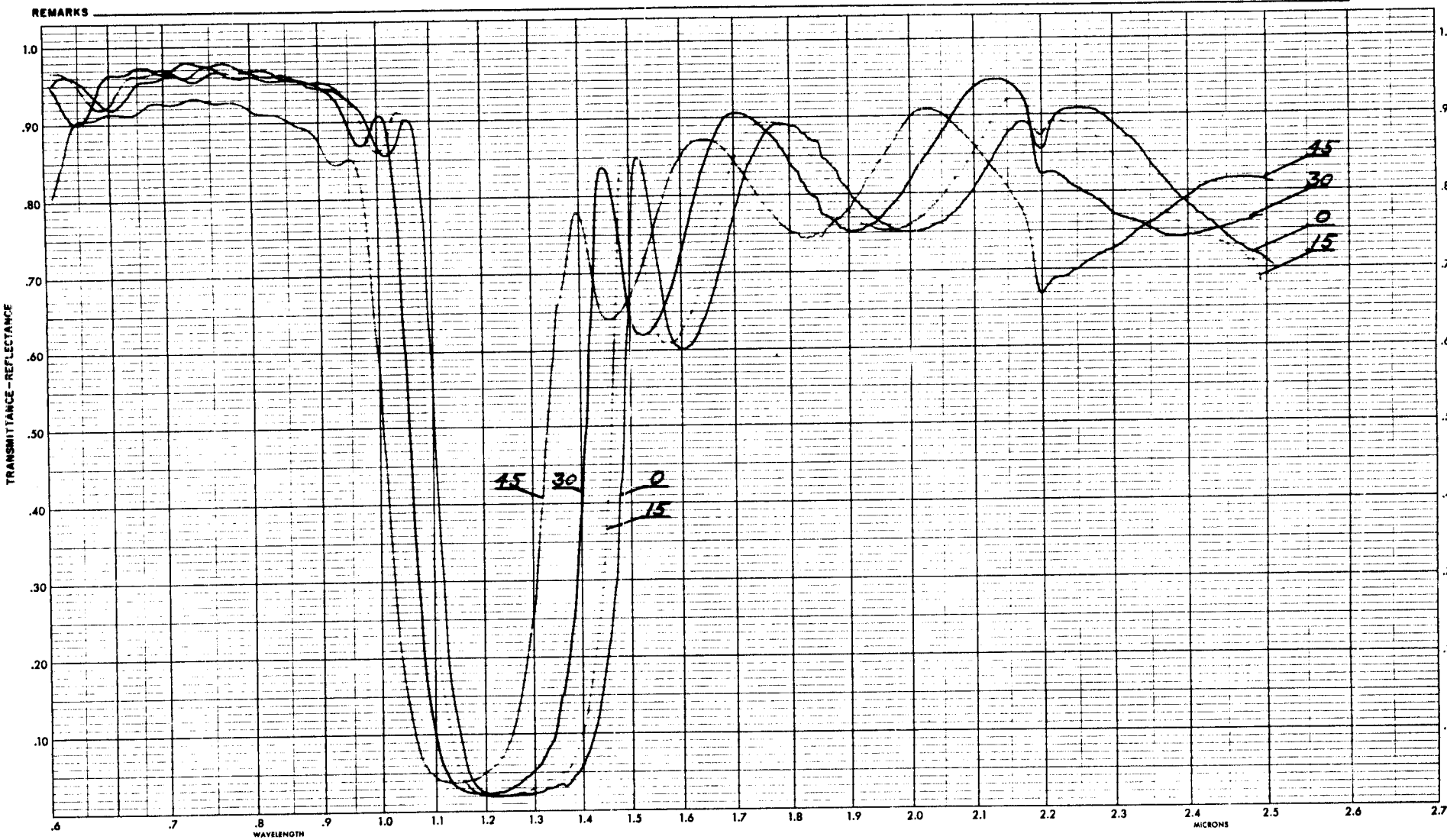


PERKIN-ELMER MODEL NC SPECTROPHOTOMETER

SPECTRUM ANALYSIS-(NEAR INFRARED)

TRANSMITTANCE-REFLECTANCE

113

12

WDL-TR2949

FILTER NO. 6

SAMPLE DESCRIPTION SC FILTER PART 6 VIII SUBMITTED BY DORIGO CURVE NO. 2927-2930

OPERATOR JC LITTLE SLIT WIDTH, AUTOMATIC CONSTANT 0.05 M.M. AT 700 MILL MICRONS. SLIT SERVO GAIN .5 SCAN SPEED 2F

INSTRUMENT MODE, TRANSMISSION - T-1 T-5 T-10 T-20 T-50 ABSORPTANCE DIFFUSE TRANS. SPECULAR REFLECTANCE DIFFUSE REFL.

REFERENCE, AIR $MgCO_3$ OTHER PEN RESPONSE SOLVENT CELL PATH (THICKNESS) CONCENTRATION

REMARKS

PERKIN-ELMER MODEL NO. 0 SPECTROPHOTOMETER

SPECTRUM ANALYSIS-(VISIBL

TRANSMITTANCE-REFLECTANCE

1.0 .90 .80 .70 .60 .50 .40 .30 .20 .10

0 15 30 45

350 360 370 380 390 400 425 450 475 500 525 550 575 600 650 700 750

WAVELENGTH MILLIMICRONS

114

13

WDL-TR2969

FILTER NO. 6

SAMPLE DESCRIPTION S'C FILTER PART 6 VIII SUBMITTED BY D BRIGGS CURVE NO. 2875-2878

OPERATOR ____ SLIT WIDTH, AUTOMATIC ____ CONSTANT ____ M.M. AT ____ MICRONS. SLIT SERVO GAIN ____ SCAN SPEED ____

INSTRUMENT MODE, TRANSMISSION - T-1 ____ T-5 ____ T-10 ____ T-20 ____ T-50 ____ ABSORPTANCE ____ DIFFUSE TRANS. ____ SPECULAR REFLECTANCE ____ DIFFUSE REFL. ____

REFERENCE, AIR ____ $MgCO_3$ ____ OTHER ____ PEN RESPONSE ____ SOLVENT ____ CELL PATH (THICKNESS) ____ CONCENTRATION ____

REMARKS ____

SPECTRUM ANAL IS - (NEAR INFRARED) PERKIN-ELMER MODEL NO SPECTROPHOTOMETER

TRANSMITTANCE - REFLECTANCE

1.0 .90 .80 .70 .60 .50 .40 .30 .20 .10

0 15 30 45 15 30 0 15

.6 .7 .8 .9 1.0 1.1 1.2 1.3 1.4 1.5 1.6 1.7 1.8 1.9 2.0 2.1 2.2 2.3 2.4 2.5 2.6 2.7

WAVELENGTH MICRONS

WDL-TR2949

TRANSMITTANCE AS A FUNCTION OF TEMPERATURE
(Normal Incidence)

FILTER NO. 1

SAMPLE DESCRIPTION SX FILTER PART 1A SUBMITTED BY D BRIGGS CURVE NO. —

OPERATOR JC LITTLE SLIT WIDTH, AUTOMATIC ✓ CONSTANT — 0.5 M.M. AT 730 MILL MICRONS. SLIT SERVO GAIN 1.0 SCAN SPEED 65

INSTRUMENT MODE, TRANSMISSION - T-1 ✓ T-5 — T-10 — T-20 — T-50 — ABSORPTANCE — DIFFUSE TRANS. — SPECULAR REFLECTANCE — DIFFUSE REFL. —

REFERENCE, AIR ✓ $MgCO_3$ — OTHER — PEN RESPONSE 1 SOLVENT — CELL PATH (THICKNESS) — CONCENTRATION —

REMARKS Red 80°F, Green 150°F, Purple 250°F

PERKIN-ELMER MODEL NO. 350 SPECTROPHOTOMETER

SPECTRUM ANALYSIS - (VISIBLE)

TRANSMITTANCE - REFLECTANCE

1.0 .90 .80 .70 .60 .50 .40 .30 .20 .10

80 150 250

250 80 150

350 360 370 380 390 400 425 450 475 500 525 550 575 600 650 700 750

WAVELENGTH MILLIMICRONS

117

15

WDL-TR2949

FILTER NO. 1

SAMPLE DESCRIPTION SC FILTER PART 1A SUBMITTED BY D BRIGGS CURVE NO. 2974, 85, 86

OPERATOR JC LITTLE SLIT WIDTH, AUTOMATIC ✓ CONSTANT — 1.0 M.M. AT 2.0 MICRONS. SLIT SERVO GAIN 5 SCAN SPEED 16E

INSTRUMENT MODE, TRANSMISSION - T-1 ✓ T-5 ___ T-10 ___ T-20 ___ T-50 ___ ABSORPTANCE ___ DIFFUSE TRANS. ___ SPECULAR REFLECTANCE ___ DIFFUSE REFL. ___

REFERENCE, AIR ✓ $MgCO_3$ ___ OTHER ___ PEN RESPONSE 1 SOLVENT ___ CELL PATH (THICKNESS) ___ CONCENTRATION ___

REMARKS Bd 80°F, Beam 170°F, Purge 250°F

PERKIN-ELMER MODEL NO. 90 SPECTROPHOTOMETER

SPECTRUM ANAL. JIS-(NEAR INFRARED)

TRANSMITTANCE-REFLECTANCE

1.0 .90 .80 .70 .60 .50 .40 .30 .20 .10

.6 .7 .8 .9 1.0 1.1 1.2 1.3 1.4 1.5 1.6 1.7 1.8 1.9 2.0 2.1 2.2 2.3 2.4 2.5 2.6 2.7

WAVELENGTH MICRONS

118

16

WIL-TR2949

FILTER NO. 2

SAMPLE DESCRIPTION SC FILTER PAR 2 A SUBMITTED BY DBRIGGS CURVE NO. —

OPERATOR JC LITTLE SLIT WIDTH, AUTOMATIC ✓ CONSTANT — 015 M.M. AT 750 MILL MICRONS. SLIT SERVO GAIN 1.0 SCAN SPEED 4TF

INSTRUMENT MODE, TRANSMISSION – T-1 ✓ T-5 — T-10 — T-20 — T-50 — ABSORPTANCE — DIFFUSE TRANS. — SPECULAR REFLECTANCE — DIFFUSE REFL. —

REFERENCE, AIR ✓ $MgCO_3$ — OTHER — PEN RESPONSE 1 SOLVENT — CELL PATH (THICKNESS) — CONCENTRATION —

REMARKS Red 80°F Green 150°, Purple 250°

PERKIN-ELMER MODEL NO. 3 SPECTROPHOTOMETER

SPECTRUM ANALYSIS – (VISIBLE)

TRANSMITTANCE-REFLECTANCE

80
150
250

1.0 .90 .80 .70 .60 .50 .40 .30 .20 .10

350 360 370 380 390 400 425 450 475 500 525 550 575 600 650 700 750

WAVELENGTH MILLIMICRONS

119

17

WDL-TR2949

FILTER NO. 2

SAMPLE DESCRIPTION SC FILTER PART 2A SUBMITTED BY D BRIGGS CURVE NO. 2987, 86 2989

OPERATOR J C LITTLE SLIT WIDTH, AUTOMATIC ✓ CONSTANT — 4.0 M.M. AT 2.0 MICRONS. SLIT SERVO GAIN 5 SCAN SPEED 1.5

INSTRUMENT MODE, TRANSMISSION - T-1 ✓ T-5 ___ T-10 ___ T-20 ___ T-50 ___ ABSORPTANCE ___ DIFFUSE TRANS. ___ SPECULAR REFLECTANCE ___ DIFFUSE REFL. ___

REFERENCE, AIR ✓ MgCO3 ___ OTHER ___ PEN RESPONSE ___ SOLVENT ___ CELL PATH (THICKNESS) ___ CONCENTRATION ___

REMARKS Bed 80°F, Green 150°F, Purple 250°F

PERKIN-ELMER MODEL NO. 120
SPECTROPHOTOMETER

SPECTRUM ANAL. -IS-(NEAR INFRARED)

TRANSMITTANCE-REFLECTANCE

1.0 .90 .80 .70 .60 .50 .40 .30 .20 .10

.6 .7 .8 .9 1.0 1.1 1.2 1.3 1.4 1.5 1.6 1.7 1.8 1.9 2.0 2.1 2.2 2.3 2.4 2.5 2.6 2.7

WAVELENGTH MICRONS

18

WL-TR2949

FILTER NO. 3

SAMPLE DESCRIPTION SC FILTER PART 3A #3 SUBMITTED BY P BRIGGS CURVE NO. _____

OPERATOR JC LITTLE SLIT WIDTH, AUTOMATIC ✓ CONSTANT 0.5 M.M. AT 750 mμ MICRONS. SLIT SERVO GAIN 4.0 SCAN SPEED 4.5

INSTRUMENT MODE, TRANSMISSION - T-1 ✓ T-5 ___ T-10 ___ T-20 ___ T-50 ___ ABSORPTANCE ___ DIFFUSE TRANS. ___ SPECULAR REFLECTANCE ___ DIFFUSE REFL. ___

REFERENCE, AIR ✓ $MgCO_3$ ___ OTHER ___ PEN RESPONSE 1 SOLVENT ___ CELL PATH (THICKNESS) ___ CONCENTRATION ___

REMARKS Red 80°F, Green 150°F, Purple 250°F

PERKIN-ELMER MODEL NO. 350
SPECTROPHOTOMETER

SPECTRUM ANALYSIS - (VISIBLE)
TRANSMITTANCE-REFLECTANCE

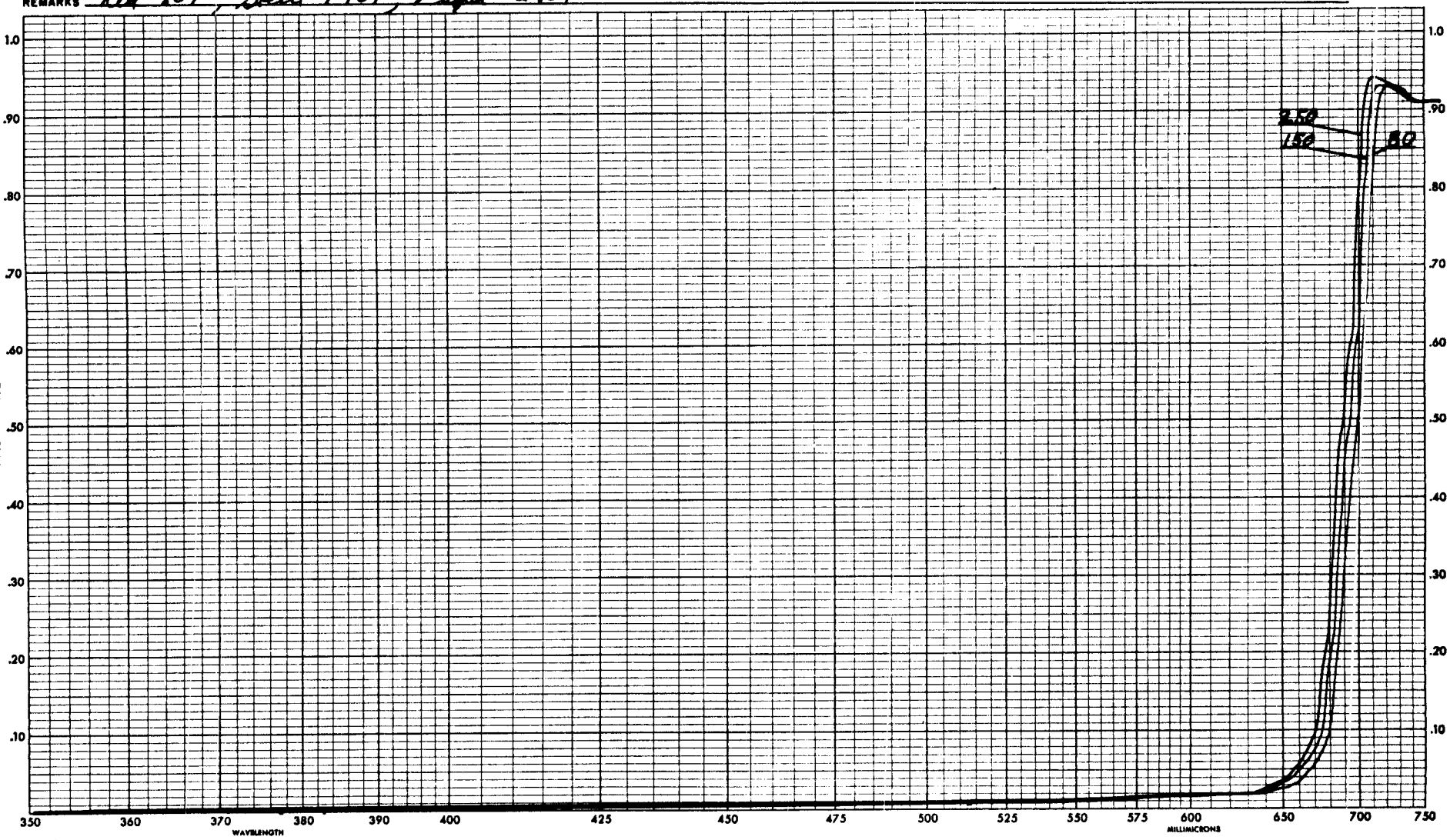


121

19

WDL-TR2949

FILTER NO. 3

SAMPLE DESCRIPTION SC FILTER PART 3A SUBMITTED BY D BRIGGS CURVE NO. 2990 91, 92

OPERATOR JC LITTLE SLIT WIDTH, AUTOMATIC ✓ CONSTANT 10 M.M. AT 2.0 MICRONS. SLIT SERVO GAIN 5 SCAN SPEED 1 1/2 E

INSTRUMENT MODE, TRANSMISSION - T-1 ✓ T-5 ___ T-10 ___ T-20 ___ T-50 ___ ABSORPTANCE ___ DIFFUSE TRANS. ___ SPECULAR REFLECTANCE ___ DIFFUSE REFL. ___

REFERENCE, AIR ✓ $MgCO_3$ ___ OTHER ___ PEN RESPONSE 1 SOLVENT ___ CELL PATH (THICKNESS) ___ CONCENTRATION ___

REMARKS Red - 80°F, Green 150°F Purple 250°F

122

SPECTRUM ANAL: IS - (NEAR INFRARED) PERKIN-ELMER MODEL NO SPECTROPHOTOMETER

TRANSMITTANCE-REFLECTANCE

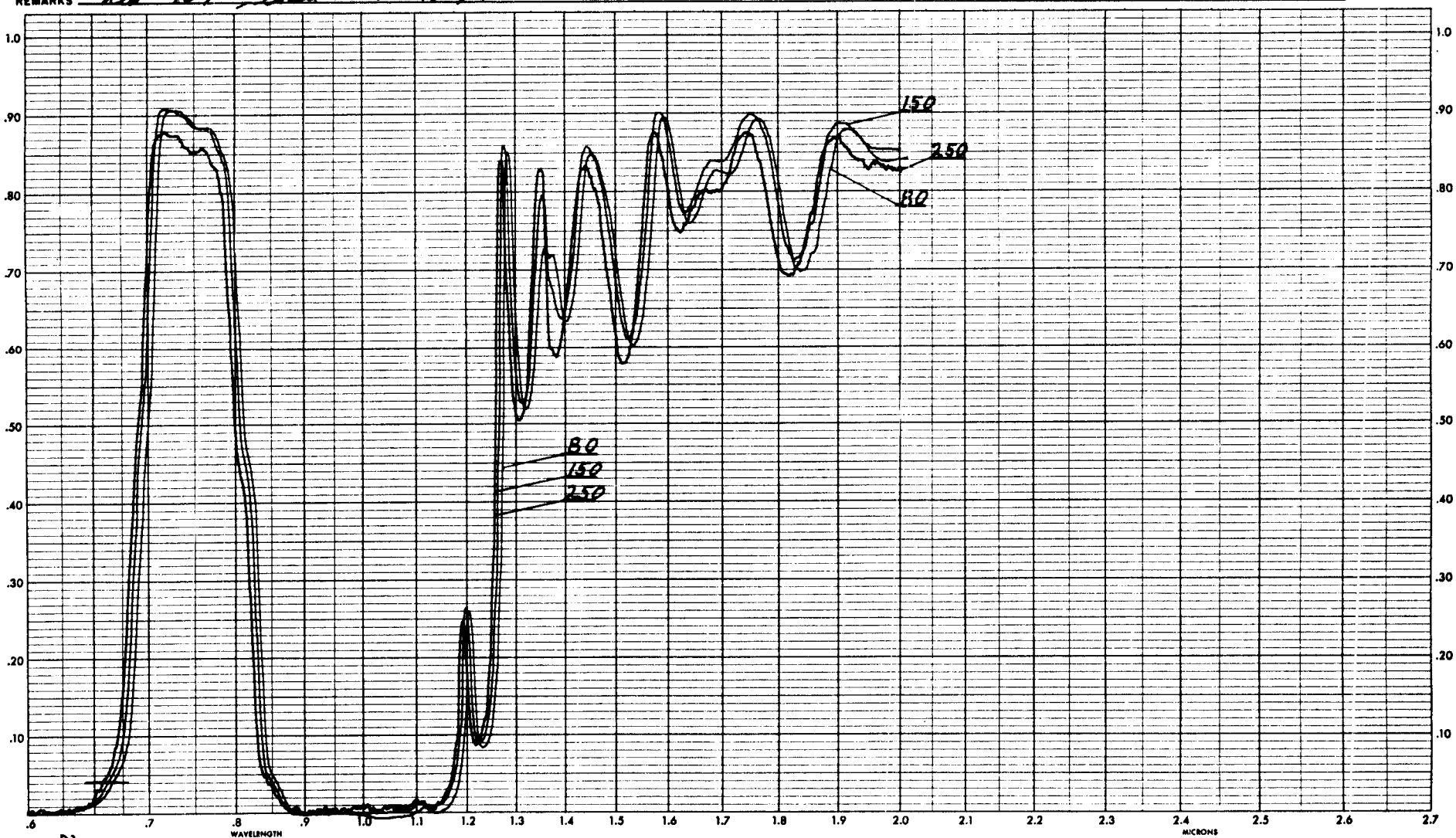


20

WIL-TR2949

FILTER NO. 4

SAMPLE DESCRIPTION GC FILTER PART 4A SUBMITTED BY D BRIGGS CURVE NO.

OPERATOR VC LITTLE SLIT WIDTH, AUTOMATIC ✓ CONSTANT — .05 M.M. AT 750 MILLI MICRONS. SLIT SERVO GAIN 60 SCAN SPEED 1/2

INSTRUMENT MODE, TRANSMISSION - T-1 ✓ T-5 ___ T-10 ___ T-20 ___ T-50 ___ ABSORPTANCE — DIFFUSE TRANS. — SPECULAR REFLECTANCE — DIFFUSE REFL.

REFERENCE, AIR ✓ $MgCO_3$ ___ OTHER ___ PEN RESPONSE 1 SOLVENT — CELL PATH (THICKNESS) — CONCENTRATION —

REMARKS

PERKIN-ELMER MODEL NO. 350
SPECTROPHOTOMETER

SPECTRUM ANALYSIS - (VISIBLE)
TRANSMITTANCE-REFLECTANCE

123

1.0 .90 .80 .70 .60 .50 .40 .30 .20 .10

350 360 370 380 390 400 425 450 475 500 525 550 575 600 650 700 750

WAVELENGTH MILLIMICRONS

21

WDL-TR2949

FILTER NO. 4

SAMPLE DESCRIPTION SC FILTER PART 4A SUBMITTED BY D BRIGGS CURVE NO. 2993, 94, 95

OPERATOR JC LITTLE SLIT WIDTH, AUTOMATIC ✓ CONSTANT — 1.0 M.M. AT 2.0 MICRONS. SLIT SERVO GAIN 5 SCAN SPEED 1.5

INSTRUMENT MODE, TRANSMISSION - T-1 ✓ T-5 ___ T-10 ___ T-20 ___ T-50 ___ ABSORPTANCE — DIFFUSE TRANS. — SPECULAR REFLECTANCE — DIFFUSE REFL. —

REFERENCE, AIR ✓ $MgCO_3$ ___ OTHER ___ PEN RESPONSE 1 SOLVENT — CELL PATH (THICKNESS) — CONCENTRATION —

REMARKS Red 80°F, Green 150°F, Purple 250°F


SPECTRUM ANAL. /IS-(NEAR INFRARED) PERKIN-ELMER MODEL NO SPECTROPHOTOMETER

TRANSMITTANCE-REFLECTANCE

124

22

WDL-TR2949

FILTER NO. 5

SAMPLE DESCRIPTION SY FILTER PART SI SUBMITTED BY D BRIGGS CURVE NO. 3008 OR 3010

OPERATOR _____ SLIT WIDTH, AUTOMATIC K CONSTANT — .05 M.M. AT >370 MILL MICRONS. SLIT SERVO GAIN 1.0 SCAN SPEED 1.5F

INSTRUMENT MODE, TRANSMISSION - T-1 K T-5 ___ T-10 ___ T-20 ___ T-50 ___ ABSORPTANCE ___ DIFFUSE TRANS. ___ SPECULAR REFLECTANCE ___ DIFFUSE REFL. ___

REFERENCE, AIR K $MgCO_3$ ___ OTHER ___ PEN RESPONSE 1 SOLVENT ___ CELL PATH (THICKNESS) ___ CONCENTRATION ___

REMARKS Red 80°F, [redacted] Green 150°F, Purple 250°F

PERKIN-ELMER MODEL NO. 350 SPECTROPHOTOMETER

SPECTRUM ANALYSIS-(VISIBLE)

TRANSMITTANCE-REFLECTANCE

1.0 .90 .80 .70 .60 .50 .40 .30 .20 .10

250 80 150

350 360 370 380 390 400 425 450 475 500 525 550 575 600 650 700 750

WAVELENGTH MILLIMICRONS

125

23

WDL-TR2949

FILTER NO. 5

SAMPLE DESCRIPTION SC FILTER PART 51 SUBMITTED BY D BRIGGS CURVE NO. 2996, 97, 98

OPERATOR JC KITTLE SLIT WIDTH, AUTOMATIC ✓ CONSTANT — 40 M.M. AT 2.0 MICRONS. SLIT SERVO GAIN 5 SCAN SPEED 15C

INSTRUMENT MODE, TRANSMISSION - T-1 ✓ T-5 ___ T-10 ___ T-20 ___ T-50 ___ ABSORPTANCE ___ DIFFUSE TRANS. ___ SPECULAR REFLECTANCE ___ DIFFUSE REFL. ___

REFERENCE, AIR ✓ $MgCO_3$ ___ OTHER ___ PEN RESPONSE ✓ SOLVENT ___ CELL PATH (THICKNESS) ___ CONCENTRATION ___

REMARKS Ad 80°F, Intern 150°F, Purple 250°F

SPECTRUM ANAL. IS-(NEAR INFRARED) PERKIN-ELMER MODEL NO SPECTROPHOTOMETER

TRANSMITTANCE-REFLECTANCE

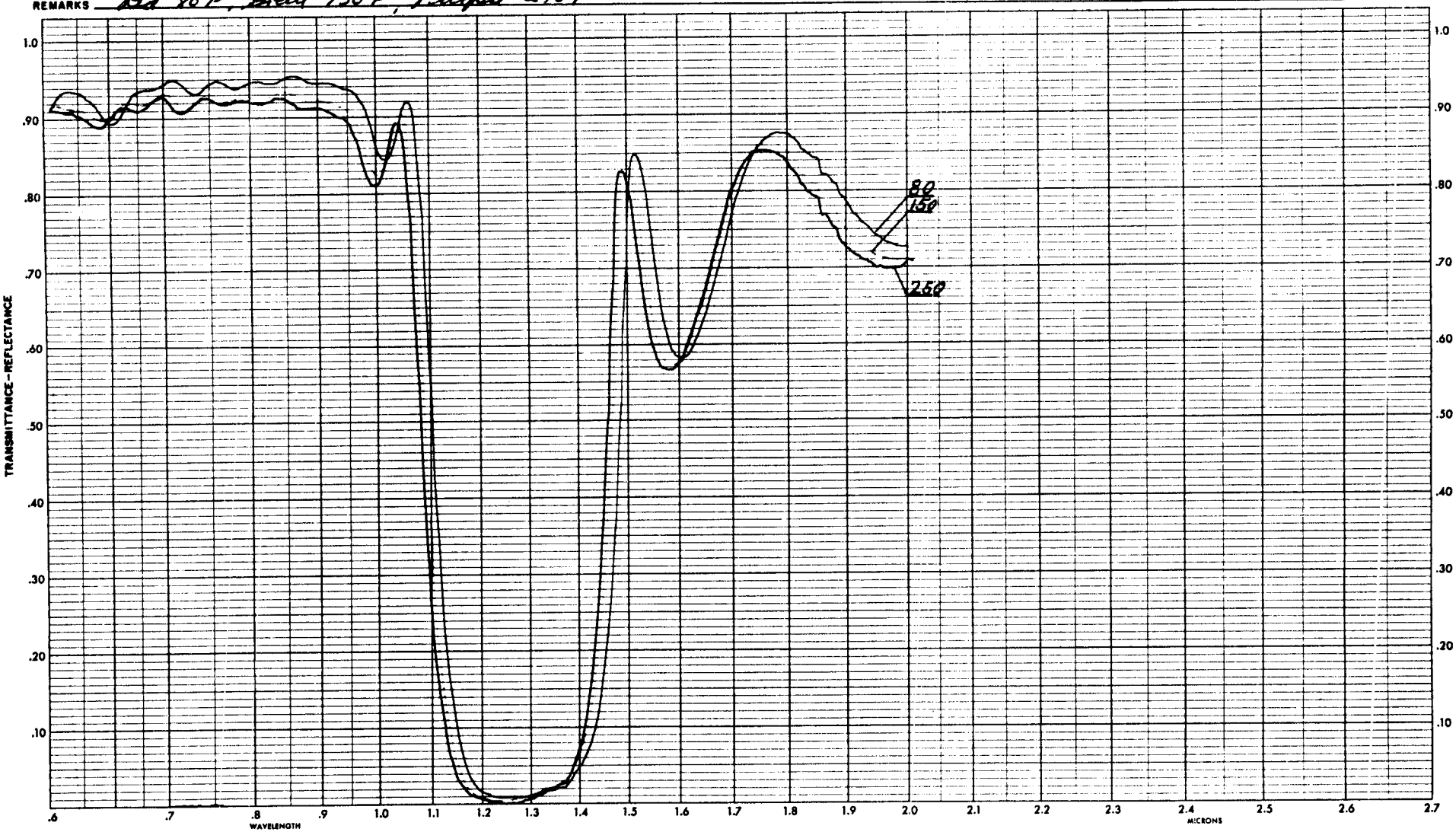


126

24

WDL-TR2949

FILTER NO. 6

SAMPLE DESCRIPTION SC FILTER PART 6 II SUBMITTED BY D BRIGGS CURVE NO. 3005, 06, 07

OPERATOR JC LITTLE SLIT WIDTH, AUTOMATIC ✓ CONSTANT — 0.5 M.M. AT 750 MU MICRONS. SLIT SERVO GAIN LO SCAN SPEED 15E

INSTRUMENT MODE, TRANSMISSION - T-1 ✓ T-5 ___ T-10 ___ T-20 ___ T-50 ___ ABSORPTANCE ___ DIFFUSE TRANS. ___ SPECULAR REFLECTANCE ___ DIFFUSE REFL. ___

REFERENCE, AIR ✓ $MgCO_3$ ___ OTHER ___ PEN RESPONSE 1 SOLVENT ___ CELL PATH (THICKNESS) ___ CONCENTRATION ___

REMARKS Red 80°F, [redacted] green 150°F, Purple 250°F

PERKIN-ELMER MODEL NO. 350
SPECTROPHOTOMETER

SPECTRUM ANALYSIS - (VISIBLE)
TRANSMITTANCE - REFLECTANCE

80
150
250

1.0 .90 .80 .70 .60 .50 .40 .30 .20 .10

350 360 370 380 390 400 425 450 475 500 525 550 575 600 650 700 750

WAVELENGTH MILLIMICRONS

127

25

WDL-TR2949

FILTER NO. 6

SAMPLE DESCRIPTION SC FILTER PART 6 II SUBMITTED BY D BRIGGS CURVE NO. 2994, 3000 3001

OPERATOR JC LITTLE SLIT WIDTH, AUTOMATIC ✓ CONSTANT — 1.0 M.M. AT 2.0 MICRONS. SLIT SERVO GAIN 5 SCAN SPEED 1.5F

INSTRUMENT MODE, TRANSMISSION - T-1 ✓ T-5 ___ T-10 ___ T-20 ___ T-50 ___ ABSORPTANCE ___ DIFFUSE TRANS. ___ SPECULAR REFLECTANCE ___ DIFFUSE REFL. ___

REFERENCE, AIR ✓ $MgCO_3$ ___ OTHER ___ PEN RESPONSE 1 SOLVENT ___ CELL PATH (THICKNESS) ___ CONCENTRATION ___

REMARKS Red 80°F, Green 150°F, Purple 250°F

PERKIN-ELMER MODEL NC SPECTROPHOTOMETER

SPECTRUM ANAL · IS - (NEAR INFRARED)

TRANSMITTANCE - REFLECTANCE

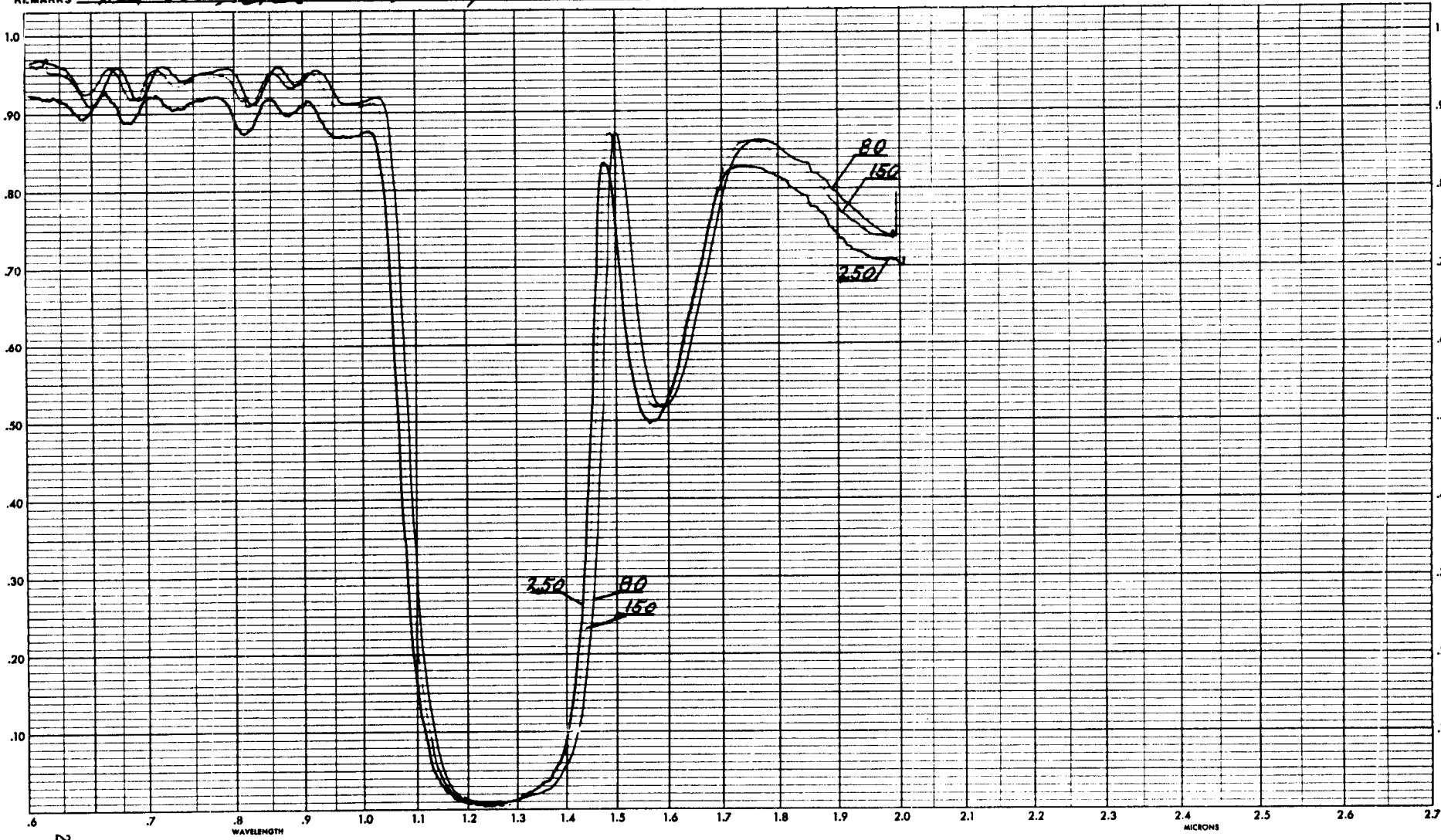


128

26

WIL-TR2949

THERMAL CONTROL BOX

SAMPLE DESCRIPTION SPECTROMETER SHIFT DUE TO TEMPERATURE CH SUBMITTED BY D. HIGGS CURVE NO. 2991, 92, 93

OPERATOR JC LITTLE SLIT WIDTH, AUTOMATIC ✓ CONSTANT — 20 M.M. AT 2.5 MICRONS SLIT SERVO GAIN 60 SCAN SPEED 1.5 F

INSTRUMENT MODE, TRANSMISSION - T-1 ✓ T-5 ___ T-10 ___ T-20 ___ T-50 ___ ABSORPTANCE — DIFFUSE TRANS. — SPECULAR REFLECTANCE — DIFFUSE REFL. —

REFERENCE, AIR ✓ $MgCO_3$ ___ OTHER ___ PEN RESPONSE 1 SOLVENT — CELL PATH (THICKNESS) — CONCENTRATION —

REMARKS Red - 100% line at 80°F, Green - 100% line at 150°F, Purple - 100% line at 250°F

PERKIN-ELMER MODEL NO SPECTROPHOTOMETER

SPECTRUM ANAL. IS - (NEAR INFRARED)

TRANSMITTANCE-REFLECTANCE

1.0 .90 .80 .70 .60 .50 .40 .30 .20 .10

.6 .7 .8 .9 1.0 1.1 1.2 1.3 1.4 1.5 1.6 1.7 1.8 1.9 2.0 2.1 2.2 2.3 2.4 2.5 2.6 2.7

WAVELENGTH MICRONS

129

27

WDL-TR2949

BARE FUSED SILICA
COVER GLASS

SAMPLE DESCRIPTION SC FILTER PART 91 SUBMITTED BY D BRIGGS CURVE NO. 2907-2910

OPERATOR JC LITTLE SLIT WIDTH, AUTOMATIC ✓ CONSTANT — 10 M.M. AT 750 mμ MICRONS. SLIT SERVO GAIN 0 SCAN SPEED 2

INSTRUMENT MODE, TRANSMISSION - T-1 ✓ T-5 — T-10 — T-20 — T-50 — ABSORPTANCE — DIFFUSE TRANS. — SPECULAR REFLECTANCE — DIFFUSE REFL. —

REFERENCE, AIR ✓ $MgCO_3$ — OTHER — PEN RESPONSE ✓ SOLVENT — CELL PATH (THICKNESS) — CONCENTRATION —

REMARKS

PERKIN-ELMER MODEL NO 350
SPECTROPHOTOMETER

SPECTRUM ANALYSIS-(VISIBL

TRANSMITTANCE-REFLECTANCE

0 15 30 45

1.0 .90 .80 .70 .60 .50 .40 .30 .20 .10

350 360 370 380 390 400 425 450 475 500 525 550 575 600 650 700 750

WAVELENGTH MILLIMICRONS

130

28

WDL-TR2949

BARE FUSED SILICA
COVER GLASS

SAMPLE DESCRIPTION SC FILTER PART 9E SUBMITTED BY D BRIGGS CURVE NO. 2995-2999

OPERATOR _____ SLIT WIDTH, AUTOMATIC _____ CONSTANT _____ M.M. AT _____ MICRONS. SLIT SERVO GAIN _____ SCAN SPEED _____

INSTRUMENT MODE, TRANSMISSION - T-1 ___ T-5 ___ T-10 ___ T-20 ___ T-50 ___ ABSORPTANCE _____ DIFFUSE TRANS. _____ SPECULAR REFLECTANCE _____ DIFFUSE REFL. _____

REFERENCE, AIR ___ $MgCO_3$ ___ OTHER _____ PEN RESPONSE _____ SOLVENT _____ CELL PATH (THICKNESS) _____ CONCENTRATION _____

REMARKS _____

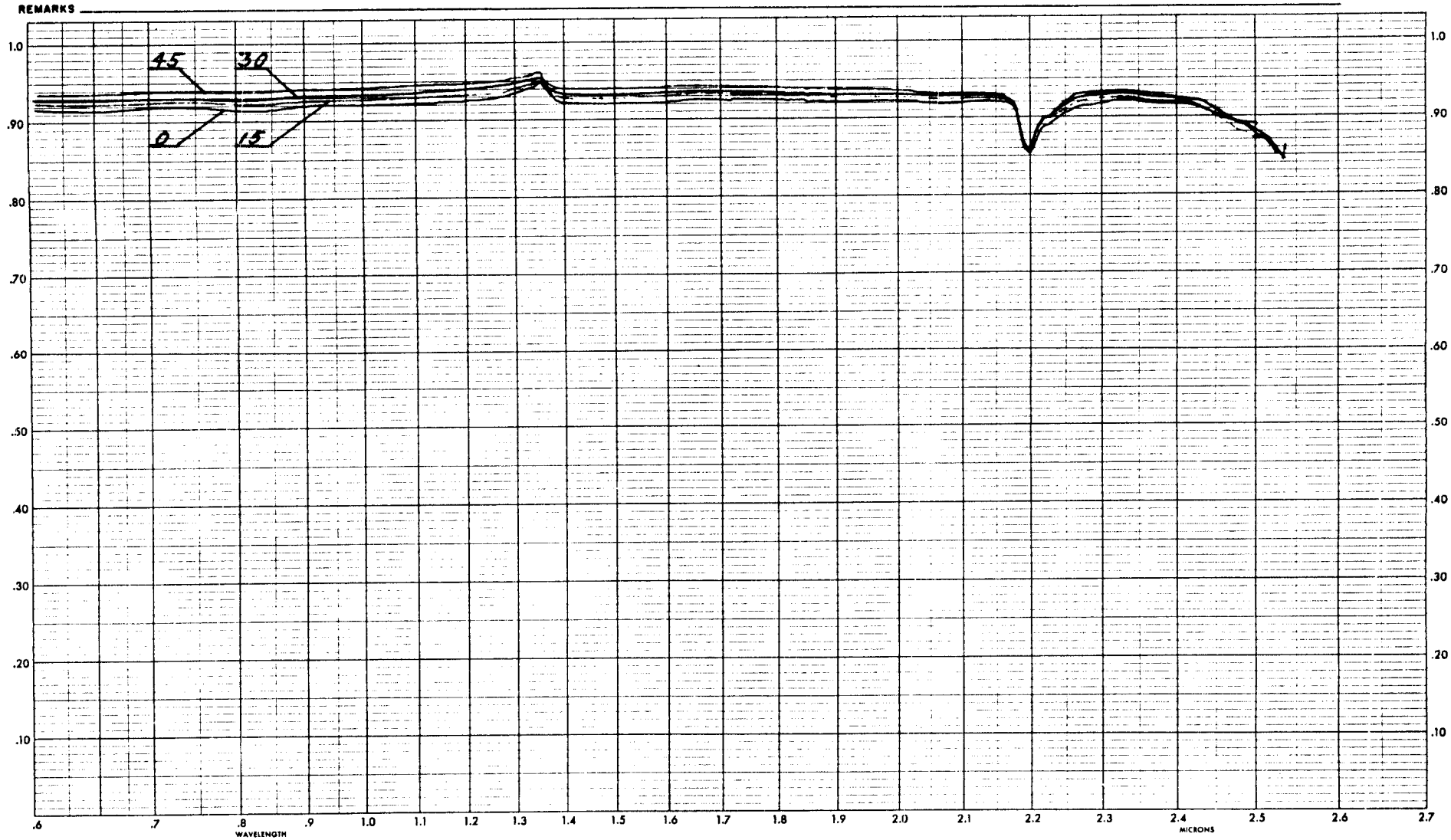


PERKIN-ELMER MODEL NO. 0
SPECTROPHOTOMETER

SPECTRUM ANAL · IS-(NEAR I"FRARED)

TRANSMITTANCE-REFLECTANCE

131

29

WIL-TR2949

BARE FUSED SILICA COVER GLASS
WITH A.R. COATING

SAMPLE DESCRIPTION SC FILTER PART 101 SUBMITTED BY D BRIGGS CURVE NO. 2803-2846
OPERATOR VC LITTLE SLIT WIDTH, AUTOMATIC ✓ CONSTANT 10 M.M. AT 750 milli MICRONS. SLIT SERVO GAIN 0 SCAN SPEED 2F
INSTRUMENT MODE, TRANSMISSION - T-1 ✓ T-5 ___ T-10 ___ T-20 ___ T-50 ___ ABSORPTANCE ___ DIFFUSE TRANS. ___ SPECULAR REFLECTANCE ___ DIFFUSE REFL. ___
REFERENCE, AIR ✓ $MgCO_3$ ___ OTHER ___ PEN RESPONSE ✓ SOLVENT ___ CELL PATH (THICKNESS) ___ CONCENTRATION ___
REMARKS Red 0°, Green 15°, Purple 30°, Blue 45°

PERKIN-ELMER MODEL NO. 350
SPECTROPHOTOMETER

SPECTRUM ANALYSIS-(VISIBL

TRANSMITTANCE-REFLECTANCE

0 15 30 45

1.0 .90 .80 .70 .60 .50 .40 .30 .20 .10

350 360 370 380 390 400 425 450 475 500 525 550 575 600 650 700 750

WAVELENGTH MILLIMICRONS

132

30

WDL-TR2949

BARE FUSED SILICA COVER GLASS
WITH A.R. COATING

SAMPLE DESCRIPTION SCFILTER PART 107 SUBMITTED BY D BRIGGS CURVE NO. 2899-2902

OPERATOR JE LITTLE SLIT WIDTH, AUTOMATIC ____ CONSTANT ____ M.M. AT ____ MICRONS. SLIT SERVO GAIN ____ SCAN SPEED ____

INSTRUMENT MODE, TRANSMISSION - T-1 ____ T-5 ____ T-10 ____ T-20 ____ T-50 ____ ABSORPTANCE ____ DIFFUSE TRANS. ____ SPECULAR REFLECTANCE ____ DIFFUSE REFL. ____

REFERENCE, AIR ____ $MgCO_3$ ____ OTHER ____ PEN RESPONSE ____ SOLVENT ____ CELL PATH (THICKNESS) ____ CONCENTRATION ____

REMARKS ____

SPECTRUM ANALYSIS-(NEAR INFRARED) PERKIN-ELMER MODEL NO SPECTROPHOTOMETER

TRANSMITTANCE-REFLECTANCE

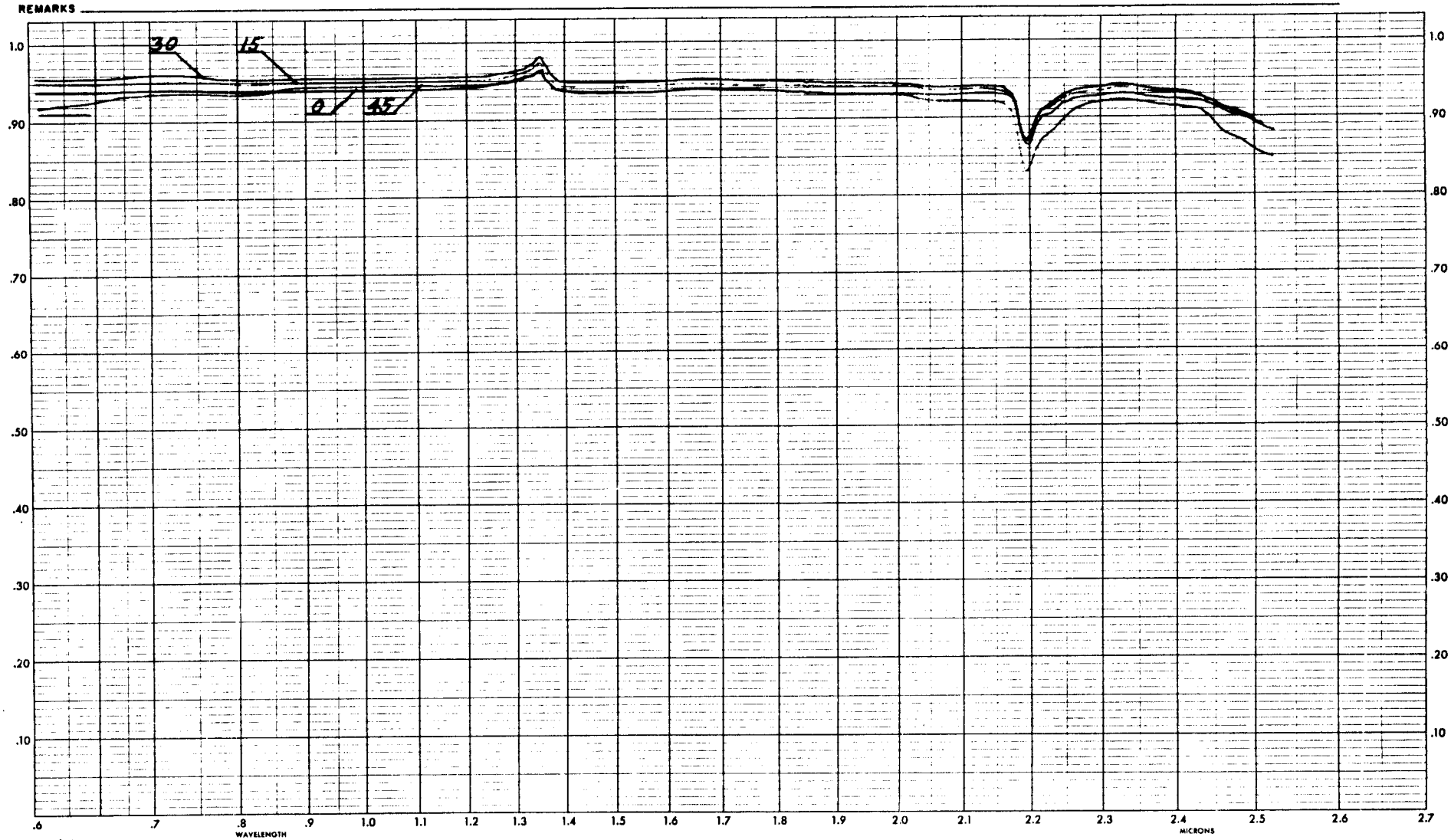


133

31

WDL-TR2949

# REFLECTANCE OF FILTER-CELL-STACK ASSEMBLIES

FILTER NO. 1

SAMPLE DESCRIPTION S/C FILTER PART #1 SUBMITTED BY D BRIGGS CURVE NO. 2967

OPERATOR JC LITTLE SLIT WIDTH, AUTOMATIC ✓ CONSTANT — .05 M.M. AT 750 MIL MICRONS. SLIT SERVO GAIN 1.2 SCAN SPEED 1.5F

INSTRUMENT MODE, TRANSMISSION - T-1 ✓ T-5 ___ T-10 ___ T-20 ___ T-50 ___ ABSORPTANCE ___ DIFFUSE TRANS. ___ SPECULAR REFLECTANCE ✓ DIFFUSE REFL. ✓

REFERENCE, AIR ___ $MgCO_3$ ✓ OTHER ___ PEN RESPONSE 1 SOLVENT — CELL PATH (THICKNESS) — CONCENTRATION —

REMARKS

PERKIN-ELMER MODEL 350 SPECTROPHOTOMETER

SPECTRUM ANALYSIS-(VISIBLE)

[redacted]-REFLECTANCE

1.0 .90 .80 .70 .60 .50 .40 .30 .20 .10

350 360 370 380 390 400 425 450 475 500 525 550 575 600 650 700 750

WAVELENGTH MILLIMICRONS

135

32

WDL-TR2949

FILTER NO. 1

SAMPLE DESCRIPTION SC FILTER PART #1 SUBMITTED BY R. BRIGGS CURVE NO. 2981

OPERATOR J.C. LITTLE SLIT WIDTH, AUTOMATIC ✓ CONSTANT ____ M.M. AT ____ MICRONS. SLIT SERVO GAIN 8.0 SCAN SPEED 1.5F

INSTRUMENT MODE, TRANSMISSION - T-1 ✓ T-5 ____ T-10 ____ T-20 ____ T-50 ____ ABSORPTANCE ____ DIFFUSE TRANS. ____ SPECULAR REFLECTANCE ✓ DIFFUSE REFL. ✓

REFERENCE, AIR ____ $MgCO_3$ ✓ OTHER ____ PEN RESPONSE 1 SOLVENT ____ CELL PATH (THICKNESS) ____ CONCENTRATION ____

REMARKS ____

50

PERKIN-ELMER MODEL 136 SPECTROPHOTOMETER

SPECTRUM ANALYSIS - (NEAR FRARED)

TRANSMITTANCE-REFLECTANCE

1.0 .90 .80 .70 .60 .50 .40 .30 .20 .10

.6 .7 .8 .9 1.0 1.1 1.2 1.3 1.4 1.5 1.6 1.7 1.8 1.9 2.0 2.1 2.2 2.3 2.4 2.5 2.6 2.7

WAVELENGTH MICRONS

33

WDL-TR2949

FILTER NO. 2

SAMPLE DESCRIPTION 5°C FILTER PART #2 SUBMITTED BY D BLIGGS CURVE NO. 2968

OPERATOR JC LITTLE SLIT WIDTH, AUTOMATIC ✓ CONSTANT — .05 M.M. AT 750MIL MICRONS. SLIT SERVO GAIN 1.2 ✓ SCAN SPEED 4.5F

INSTRUMENT MODE, TRANSMISSION - T-1 ✓ T-5 ___ T-10 ___ T-20 ___ T-50 ___ ABSORPTANCE — DIFFUSE TRANS. — SPECULAR REFLECTANCE ✓ DIFFUSE REFL. ✓

REFERENCE, AIR — $MgCO_3$ ✓ OTHER — PEN RESPONSE 1 SOLVENT — CELL PATH (THICKNESS) — CONCENTRATION —

REMARKS

PERKIN-ELMER MODEL 350 SPECTROPHOTOMETER

SPECTRUM ANALYSIS-(VISIBLE)

TRANSMITTANCE-REFLECTANCE

1.0 .90 .80 .70 .60 .50 .40 .30 .20 .10

350 360 370 380 390 400 425 450 475 500 525 550 575 600 650 700 750

WAVELENGTH MILLIMICRONS

137

34

WIL-TR2949

FILTER NO. 2

SAMPLE DESCRIPTION SC FILTER PART #2 SUBMITTED BY DBRIGGS CURVE NO. 2980

OPERATOR JC LITTLE SLIT WIDTH, AUTOMATIC ✓ CONSTANT ✓ 3.0 M.M. AT 2.5 MICRONS. SLIT SERVO GAIN 800 SCAN SPEED 15F

INSTRUMENT MODE, TRANSMISSION - T-1 ✓ T-5 ___ T-10 ___ T-20 ___ T-50 ___ ABSORPTANCE ___ DIFFUSE TRANS. ___ SPECULAR REFLECTANCE ✓ DIFFUSE REFL. ___

REFERENCE, AIR ___ $MgCO_3$ ✓ OTHER ___ PEN RESPONSE / SOLVENT ___ CELL PATH (THICKNESS) ___ CONCENTRATION ___

REMARKS ___

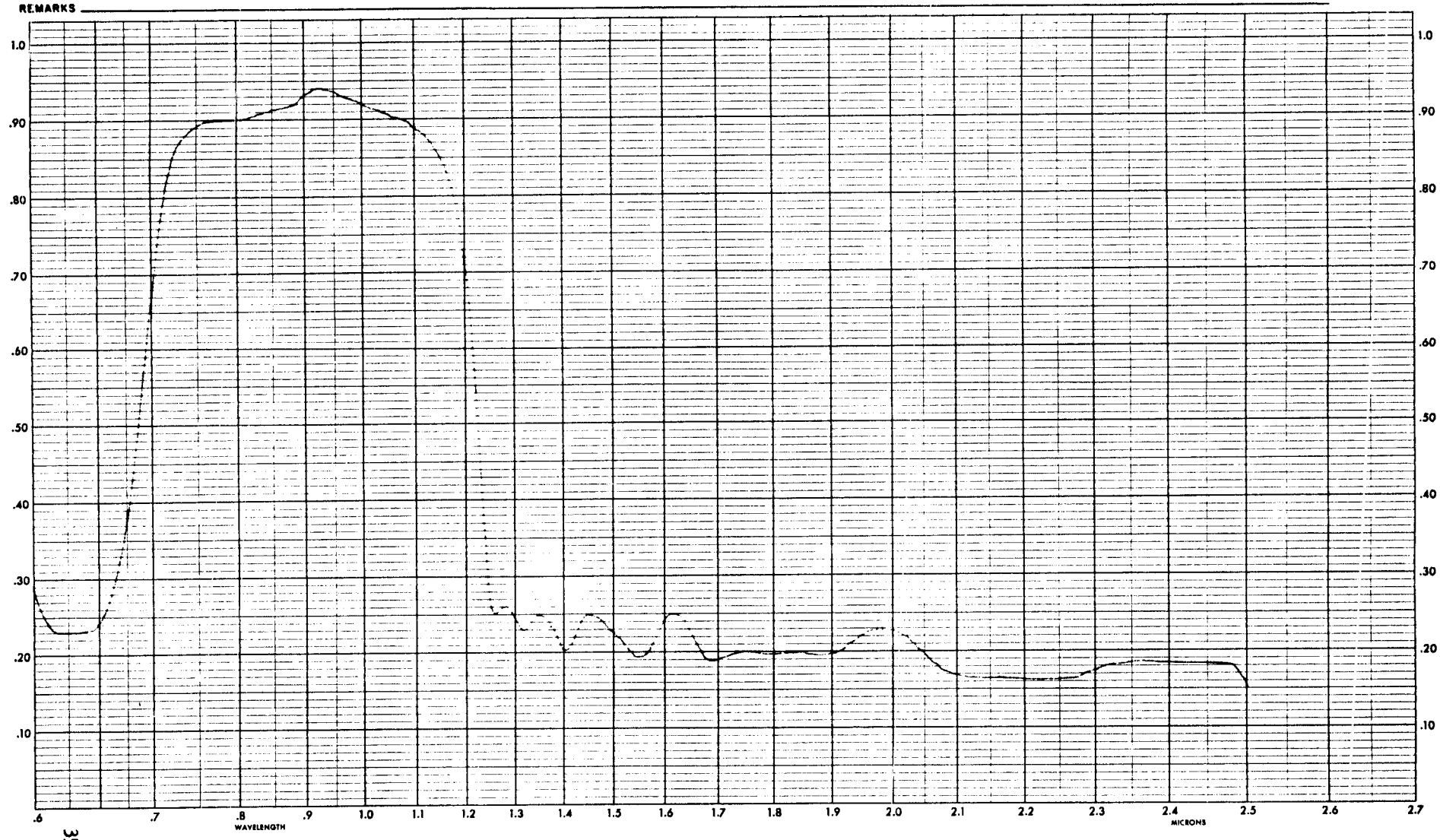


SPECTRUM ANALYSIS-(NEAR INFRARED) PERKIN-ELMER MODEL 90 SPECTROPHOTOMETER

138

35

WDL-TR2949

FILTER NO. 3

SAMPLE DESCRIPTION S'C FILTER PART #3 SUBMITTED BY D BRIGGS CURVE NO. ~~49~~ 2949

OPERATOR JC LITTLE SLIT WIDTH, AUTOMATIC ✓ CONSTANT — 0.5 M.M. AT 750 MILL MICRONS. SLIT SERVO GAIN 1/2 SCAN SPEED 1.5F

INSTRUMENT MODE, TRANSMISSION - T-1 ✓ T-5 ___ T-10 ___ T-20 ___ T-50 ___ ABSORPTANCE ___ DIFFUSE TRANS. ___ SPECULAR REFLECTANCE ✓ DIFFUSE REFL. ✓

REFERENCE, AIR ___ $MgCO_3$ ✓ OTHER ___ PEN RESPONSE 1 SOLVENT — CELL PATH (THICKNESS) — CONCENTRATION —

REMARKS

PERKIN-ELMER MODEL 350 SPECTROPHOTOMETER

SPECTRUM ANALYSIS - (VISIBLE)

TRANSMITTANCE-REFLECTANCE

1.0 .90 .80 .70 .60 .50 .40 .30 .20 .10

350 360 370 380 390 400 425 450 475 500 525 550 575 600 650 700 750

WAVELENGTH MILLIMICRONS

139

36

WDL-TR2949

FILTER NO. 3

SAMPLE DESCRIPTION SC FILTER PART [redacted] #3 SUBMITTED BY D.BRIGGS CURVE NO. 2979

OPERATOR JC LITTLE SLIT WIDTH, AUTOMATIC ✓ CONSTANT — 3.0 M.M. AT 2.5 MICRONS. SLIT SERVO GAIN 8.0 SCAN SPEED 1.5F

INSTRUMENT MODE, TRANSMISSION -- T-1 ✓ T-5 ___ T-10 ___ T-20 ___ T-50 ___ ABSORPTANCE — DIFFUSE TRANS. — SPECULAR REFLECTANCE ✓ DIFFUSE REFL. ✓

REFERENCE, AIR ___ $MgCO_3$ ✓ OTHER ___ PEN RESPONSE 1 SOLVENT — CELL PATH (THICKNESS) — CONCENTRATION —

REMARKS

50

SPE RUM ANAL JIS-(NEAR [redacted] RARED) PERKIN-ELMER MODE SPECTROPHOTOMETER

TRANSMITTANCE-REFLECTANCE

1.0 .90 .80 .70 .60 .50 .40 .30 .20 .10

.6 .7 .8 .9 1.0 1.1 1.2 1.3 1.4 1.5 1.6 1.7 1.8 1.9 2.0 2.1 2.2 2.3 2.4 2.5 2.6 2.7

WAVELENGTH MICRONS

140

37

WDL-TR2949

FILTER NO. 4

SAMPLE DESCRIPTION SC FILTER PART # 4 SUBMITTED BY D. BRIGGS CURVE NO. 2970

OPERATOR JC LITTLE SLIT WIDTH, AUTOMATIC ✓ CONSTANT — 0.5 M.M. AT 750 MILL MICRONS SLIT SERVO GAIN 1.2 SCAN SPEED 1.5F

INSTRUMENT MODE, TRANSMISSION - T-1 ✓ T-5 ___ T-10 ___ T-20 ___ T-50 ___ ABSORPTANCE ___ DIFFUSE TRANS. ___ SPECULAR REFLECTANCE ✓ DIFFUSE REFL. ___

REFERENCE, AIR ___ $MgCO_3$ ✓ OTHER ___ PEN RESPONSE ✓ SOLVENT ___ CELL PATH (THICKNESS) ___ CONCENTRATION ___

REMARKS ___

PERKIN-ELMER MODE 350 SPECTROPHOTOMETER

SPECTRUM ANALYSIS - (VISIBLE)

TRANSMITTANCE - REFLECTANCE

1.0 .90 .80 .70 .60 .50 .40 .30 .20 .10

350 360 370 380 390 400 425 450 475 500 525 550 575 600 650 700 750

WAVELENGTH MILLIMICRONS

141

38

WDL-TR2949

FILTER NO. 4

SAMPLE DESCRIPTION SC FILTER PART #4 SUBMITTED BY D BRIGGS CURVE NO. 2978

OPERATOR JC LITTLE SLIT WIDTH, AUTOMATIC ✓ CONSTANT — 3.0 M.M. AT 2.5 MICRONS, SLIT SERVO GAIN 8.0 SCAN SPEED 45P

INSTRUMENT MODE, TRANSMISSION - T-1 ✓ T-5 ___ T-10 ___ T-20 ___ T-50 ___ ABSORPTANCE ___ DIFFUSE TRANS. ___ SPECULAR REFLECTANCE ✓ DIFFUSE REFL. ✓

REFERENCE, AIR ___ $MgCO_3$ ✓ OTHER ___ PEN RESPONSE 1 SOLVENT — CELL PATH (THICKNESS) — CONCENTRATION —

REMARKS

50

SPECTRUM ANALYSIS-(NEAR INFRARED) PERKIN-ELMER MODEL SPECTROPHOTOMETER

TRANSMITTANCE-REFLECTANCE

1.0 .90 .80 .70 .60 .50 .40 .30 .20 .10

.6 .7 .8 .9 1.0 1.1 1.2 1.3 1.4 1.5 1.6 1.7 1.8 1.9 2.0 2.1 2.2 2.3 2.4 2.5 2.6 2.7

WAVELENGTH MICRONS

142

39

WDL-TR2949

FILTER NO. 5

SAMPLE DESCRIPTION SC FILTER PART #5 SUBMITTED BY D. BRIGGS CURVE NO. 2977

OPERATOR JC LIME SLIT WIDTH, AUTOMATIC ← CONSTANT — .05 M.M. AT 750 MILLI MICRONS. SLIT SERVO GAIN 1/2 SCAN SPEED 4.5

INSTRUMENT MODE, TRANSMISSION - T-1 ___ T-5 ___ T-10 ___ T-20 ___ T-50 ___ ABSORPTANCE ___ DIFFUSE TRANS. ___ SPECULAR REFLECTANCE ← DIFFUSE REFL. ←

REFERENCE, AIR ___ $MgCO_3$ ← OTHER — PEN RESPONSE / SOLVENT — CELL PATH (THICKNESS) — CONCENTRATION —

REMARKS

PERKIN-ELMER MODEL ... 350 SPECTROPHOTOMETER

SPECTRUM ANALYSIS - (VISIBLE)

TRANSMITTANCE - REFLECTANCE

1.0 .90 .80 .70 .60 .50 .40 .30 .20 .10

350 360 370 380 390 400 425 450 475 500 525 550 575 600 650 700 750

WAVELENGTH MILLIMICRONS

1.43

40

WDL-TR2949

FILTER NO. 5

SAMPLE DESCRIPTION SC FILTER PART #5 SUBMITTED BY D BRIGGS CURVE NO. 2977

OPERATOR JC LITTLE SLIT WIDTH, AUTOMATIC ✓ CONSTANT — 3.0 M.M. AT 2.5 MICRONS. SLIT SERVO GAIN 8.0 SCAN SPEED 45E

INSTRUMENT MODE, TRANSMISSION - T-1 ✓ T-5 ___ T-10 ___ T-20 ___ T-50 ___ ABSORPTANCE ___ DIFFUSE TRANS. ___ SPECULAR REFLECTANCE ___ DIFFUSE REFL. ✓

REFERENCE, AIR ___ $MgCO_3$ ✓ OTHER ___ PEN RESPONSE 1 SOLVENT ___ CELL PATH (THICKNESS) ___ CONCENTRATION ___

REMARKS ___

SPECTRUM ANALYSIS - (NEAR INFRARED) PERKIN-ELMER MODEL SPECTROPHOTOMETER

REFLECTANCE - REFLECTANCE

1.0 .90 .80 .70 .60 .50 .40 .30 .20 .10

.6 .7 .8 .9 1.0 1.1 1.2 1.3 1.4 1.5 1.6 1.7 1.8 1.9 2.0 2.1 2.2 2.3 2.4 2.5 2.6 2.7

WAVELENGTH MICRONS

1444

WDL-TR2969

FILTER NO. 6

SAMPLE DESCRIPTION SP. FILTER PART #6 SUBMITTED BY P. BRIGGS CURVE NO. 1972

OPERATOR JC LITTLE SLIT WIDTH, AUTOMATIC ✓ CONSTANT — .05 M.M. AT 750 mμ MICRONS. SLIT SERVO GAIN 1.2 SCAN SPEED 1.5

INSTRUMENT MODE, TRANSMISSION - T-1 ✓ T-5 ___ T-10 ___ T-20 ___ T-50 ___ ABSORPTANCE ___ DIFFUSE TRANS. ___ SPECULAR REFLECTANCE ✓ DIFFUSE REFL. ✓

REFERENCE, AIR ___ $MgCO_3$ ✓ OTHER ___ PEN RESPONSE 1 SOLVENT ___ CELL PATH (THICKNESS) ___ CONCENTRATION ___

REMARKS

PERKIN-ELMER MODEL No. 350 SPECTROPHOTOMETER

SPECTRUM ANALYSIS - (VISIBLE)

TRANSMITTANCE-REFLECTANCE

1.0 .90 .80 .70 .60 .50 .40 .30 .20 .10

350 360 370 380 390 400 425 450 475 500 525 550 575 600 650 700 750

WAVELENGTH MILLIMICRONS

145

42

WDL-TR2949

FILTER NO. 6

SAMPLE DESCRIPTION SC FILTER PART #6 SUBMITTED BY DISRIGG CURVE NO. 2976

OPERATOR JC LITTLE SLIT WIDTH, AUTOMATIC ✓ CONSTANT — 30 M.M. AT 2.5 MICRONS SLIT SERVO GAIN ✓ SCAN SPEED 4cm

INSTRUMENT MODE, TRANSMISSION - T-1 ✓ T-5 ___ T-10 ___ T-20 ___ T-50 ___ ABSORPTANCE — DIFFUSE TRANS. — SPECULAR REFLECTANCE ✓ DIFFUSE REFL. ✓

REFERENCE, AIR ___ $MgCO_3$ ✓ OTHER ___ PEN RESPONSE / SOLVENT — CELL PATH (THICKNESS) — CONCENTRATION —

REMARKS

SPECTRUM ANALYSIS - (NEAR INFRARED) PERKIN-ELMER MODEL 50 SPECTROPHOTOMETER

TRANSMITTANCE - REFLECTANCE

1.0 .90 .80 .70 .60 .50 .40 .30 .20 .10

.6 .7 .8 .9 1.0 1.1 1.2 1.3 1.4 1.5 1.6 1.7 1.8 1.9 2.0 2.1 2.2 2.3 2.4 2.5 2.6 2.7

WAVELENGTH MICRONS

1446

WDL-TR2949

43

BARE FUSED SILICA
COVER GLASS

SAMPLE DESCRIPTION SC FILTER PART #9 SUBMITTED BY D BRIGGS CURVE NO 2974

OPERATOR JC LITTLE SLIT WIDTH, AUTOMATIC ✓ CONSTANT — 0.5 M.M. AT 750 MU MICRONS. SLIT SERVO GAIN 1.2 SCAN SPEED 4.5

INSTRUMENT MODE, TRANSMISSION - T-1 ✓ T-5 — T-10 — T-20 — T-50 — ABSORPTANCE — DIFFUSE TRANS. — SPECULAR REFLECTANCE ✓ DIFFUSE REFL. —

REFERENCE, AIR — $MgCO_3$ ✓ OTHER — PEN RESPONSE 1 SOLVENT — CELL PATH (THICKNESS) ✓ CONCENTRATION —

REMARKS

PERKIN-ELMER MODEL NO. 350
SPECTROPHOTOMETER

SPECTRUM ANALYSIS - (VISIBLE)

TRANSMITTANCE - REFLECTANCE

1.0 .90 .80 .70 .60 .50 .40 .30 .20 .10

350 360 370 380 390 400 425 450 475 500 525 550 575 600 650 700 750

WAVELENGTH MILLIMICRONS

147

44

WIL-TR2949

BARE FUSED SILICA
COVER GLASS

SAMPLE DESCRIPTION S'C FILTER PART #9 SUBMITTED BY D BRIGGS CURVE NO 2975

OPERATOR VC LITTLE SLIT WIDTH, AUTOMATIC ✓ CONSTANT — 3.0 M.M. AT 2.5 MICRONS. SLIT SERVO GAIN 5.0 SCAN SPEED 1.0

INSTRUMENT MODE, TRANSMISSION - T-1 ___ T-5 ___ T-10 ___ T-20 ___ T-50 ___ ABSORPTANCE ___ DIFFUSE TRANS. ___ SPECULAR REFLECTANCE ✓ DIFFUSE REFL ✓

REFERENCE, AIR ___ $MgCO_3$ ✓ OTHER ___ PEN RESPONSE 1 SOLVENT ___ CELL PATH (THICKNESS) ___ CONCENTRATION ___

REMARKS ___

SPECTRUM ANALYSIS - (NEAR INFRARED) PERKIN-ELMER MODEL 350 SPECTROPHOTOMETER - REFLECTANCE

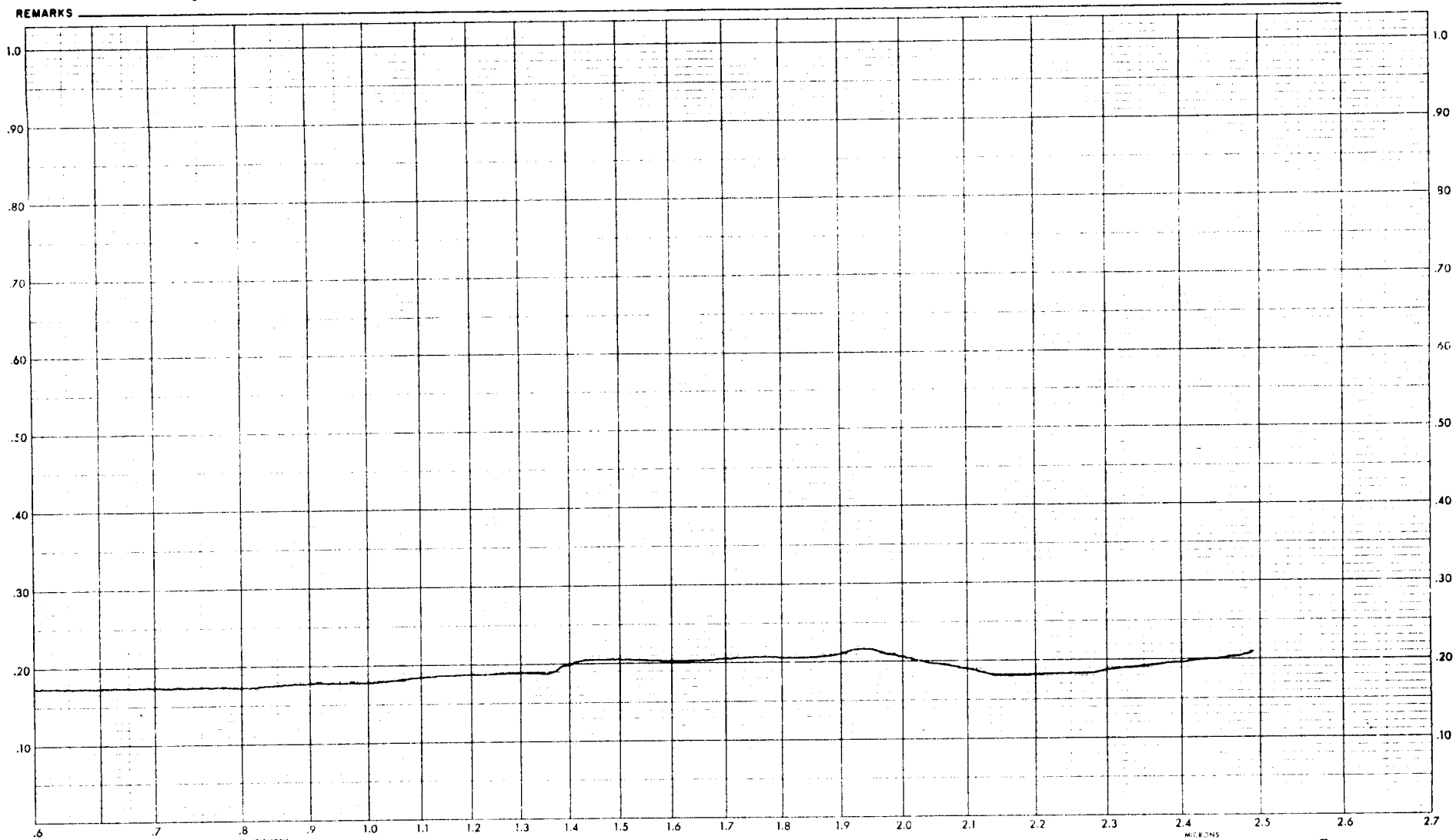


148

45

WDL-TR2949

SILVER COATING SAMPLE

SAMPLE DESCRIPTION S.C. REFLECTIVE FILTER 1" DIA SUBMITTED BY D.B. CURVE NO. 2041

OPERATOR V.C. LITTLE SLIT WIDTH, AUTOMATIC ✓ CONSTANT — 3.2 M.M. AT 350 MILLIMICRONS. SLIT SERVO GAIN 2.0 SCAN SPEED 2F

INSTRUMENT MODE, TRANSMISSION - T-1 ✓ T-5 ___ T-10 ___ T-20 ___ T-50 ___ ABSORPTANCE ___ DIFFUSE TRANS. ___ SPECULAR REFLECTANCE ___ DIFFUSE REFL. ___

REFERENCE, AIR ___ $MgCO_3$ ✓ OTHER ___ PEN RESPONSE 1 SOLVENT ___ CELL PATH (THICKNESS) ___ CONCENTRATION ___

REMARKS ___

PERKIN-ELMER MODEL 350 SPECTROPHOTOMETER

SPECTRUM ANALYSIS - (VISIBLE) TRANSMITTANCE - REFLECTANCE

1.0 .90 .80 .70 .60 .50 .40 .30 .20 .10

350 360 370 380 390 400 425 450 475 500 525 550 575 600 650 700 750

WAVELENGTH MILLIMICRONS

149

46

WDL-TR2969

SILVER COATING SAMPLE

SAMPLE DESCRIPTION SC Reflectance Filter 1" dia. SUBMITTED BY Don Briggs CURVE NO. 3042

OPERATOR JC Little SLIT WIDTH, AUTOMATIC ✓ CONSTANT — 30 M.M. AT 2.5 MICRONS. SLIT SERVO GAIN 8.5 SCAN SPEED 2E

INSTRUMENT MODE, TRANSMISSION - T-1 ✓ T-5 ___ T-10 ___ T-20 ___ T-50 ___ ABSORPTANCE ___ DIFFUSE TRANS. ___ SPECULAR REFLECTANCE ✓ DIFFUSE REFL. ___

REFERENCE, AIR ___ $MgCO_3$ ✓ OTHER ___ PEN RESPONSE / SOLVENT ___ CELL PATH (THICKNESS) ___ CONCENTRATION ___

REMARKS ___

SPECTRUM ANALYSIS-(NEAR INFRARED) PERKIN-ELMER MODEL 350 SPECTROPHOTOMETER

TRANSMITTANCE-REFLECTANCE

1.0 .90 .80 .70 .60 .50 .40 .30 .20 .10

.6 .7 .8 .9 1.0 1.1 1.2 1.3 1.4 1.5 1.6 1.7 1.8 1.9 2.0 2.1 2.2 2.3 2.4 2.5 2.6 2.7

WAVELENGTH MICRONS

150

47

WDL-TR2949